University of Alberta

Development of a "Flow-Through" Cell to Measure the Electrophoretic Mobility of Small Gas Bubbles

by

Shulamit Kuttner

A thesis
submitted to the Faculty of Graduate Studies and Research
in partial fulfillment of the requirements for the degree of
Master of Science

Department of Chemical and Materials Engineering

Edmonton, Alberta
Fall 1997

National Library of Canada
Acquisitions and Bibliographic Services
395 Wellington Street
Ottawa ON K1A 0N4
Canada

Bibliothèque nationale du Canada
Acquisitions et services bibliographiques
395, rue Wellington
Ottawa ON K1A 0N4
Canada

Your file Votre référence

Our file Notre référence

The author has granted a non-exclusive licence allowing the National Library of Canada to reproduce, loan, distribute or sell copies of this thesis in microform, paper or electronic formats.

The author retains ownership of the copyright in this thesis. Neither the thesis nor substantial extracts from it may be printed or otherwise reproduced without the author's permission.

L'auteur a accordé une licence non exclusive permettant à la Bibliothèque nationale du Canada de reproduire, prêter, distribuer ou vendre des copies de cette thèse sous la forme de microfiche/film, de reproduction sur papier ou sur format électronique.

L'auteur conserve la propriété du droit d'auteur qui protège cette thèse. Ni la thèse ni des extraits substantiels de celle-ci ne doivent être imprimés ou autrement reproduits sans son autorisation.

0-612-22620-4

Canada

University of Alberta

Library Release Form

Name of Author: Shulamit Kuttner

Title of Thesis: Development of a "Flow-Through" Cell to Measure the Electrophoretic Mobility of Small Gas Bubbles

Degree: Master of Science

Year this Degree Granted: 1997

Permission is hereby granted to the University of Alberta to reproduce single copies of this thesis and to lend or sell such copies for private, scholarly, or scientific research purposes only.

The author reserves all other publication and other rights in association with the copyright in the thesis, and except as hereinbefore provided, neither the thesis nor any substantial portion thereof may be printed or otherwise reproduced in any material form whatever without the author's prior written permission.

Shulamit Kuttner

August 28, 1997

#202 626-57 Avenue SW.,
Calgary, Alberta
T2V 0H4

University of Alberta

Faculty of Graduate Studies and Research

The undersigned certify that they have read, and recommend to the Faculty of Graduate Studies and Research for acceptance, a thesis entitled *Development of a "Flow-Through" Cell to Measure the Electrophoretic Mobility of Small Gas Bubbles* by Shulamit Kuttner in partial fulfillment of the requirements for the degree of Master of Science.

Dr. J.H. Masliyah (Supervisor)

Dr. S.E. Wanke

Dr. D. Li

Date: August 27, 1997

Dedicated to my family Eldad, Mina, Amos, and Chantal

and to my beloved husband, Corneil

ABSTRACT

A "Flow-Through" cell was developed to measure the electrophoretic mobility of gas bubbles in aqueous solutions. Electrophoretic measurement of gas bubbles is usually difficult to perform, owing to the inherent buoyancy of the bubbles. As a result, bubbles often rise too quickly to measure their electrophoretic mobility in conventional cells. The "Flow-Through" cell was designed to circumvent this difficulty in three ways:

1. Very small bubbles were generated electrolytically on the tip of a 30 μm diameter platinum wire.
2. The bubbles were formed in water that had been previously treated to partially remove dissolved gases. The unsaturated water induced bubbles to shrink, thus producing bubbles ranging from 7 to 15 μm in diameter.
3. The cell liquid was slowly drained such that rising bubbles were effectively trapped at one height, thus allowing electrophoretic measurements to be taken.

A prototype "Flow-Through" cell was built and tested using aqueous solutions of potassium chloride and sodium sulphate. No surfactants were added to the solutions. The measured electrophoretic mobilities were in the same order of magnitude as the results from a similar study by Brandon et al. (1985b). However, the scatter of the data in this study was large, indicating the need for improvements to be made.

ACKNOWLEDGEMENTS

I'd like to thank Syncrude Canada Ltd. for the financial assistance that made this project possible. The successful completion of this thesis could not have been achieved without assistance of many persons. I'd like to extend my thanks to my advisor, Dr. Jacob Masliyah, for his support and the sharing of his wisdom. Many thanks are also due to Dr. S. Basu, Dr. Tadeusz Dabros and Dr. Qi Dai of CANMET, and especially to Ross Chow of the Alberta Research Council (ARC) for their advice in the field of electrokinetics and the generous lending of equipment.

I'd like to thank Dr. Steve Bergens and Dr. James Plambeck from the Department of Chemistry at the University of Alberta for their time and assistance with the electrochemical aspects of this project. Dr. Sigurdson from the Department of Mechanical Engineering and Brian Lowry were very helpful in sharing information on video cassette recorders. David Sloan from Leica provided a wealth of information on the optical components. Their help is much appreciated.

I owe much appreciation to the skilled persons who actually built the electrophoresis cell and its multifaceted components. To this end, I'd like to thank Murray P. Connors and his associates at the glass blowing shop, and Keith Fauldar, Bob Scott, and Ron Van Den Heuvel at the machine shop. I'd also like to extend thanks to Walter Boddez and Richard Cooper for their very enthusiastic help in all matters related

to instrumentation and electrical circuitry. Special thanks are also extended to Kevin Dorma, Samir Kayande, and Bemal Mehta for patiently coaching me in the use of FLOW3D simulation software.

There were many persons who provided practical ideas, advice, or feedback: Alison Miller, Artin Afacan, Sean Sanders, Harvey Yarranton, and Andree Koenig. To them, I extend my warmest gratitude. Finally, I'd like to thank my friend Susan Miller, my family, and my husband, Corneil, without whose unwavering love and support I would not have had the courage to complete this endeavour.

Shulamit Kuttner

Calgary, Alberta, Canada

TABLE OF CONTENTS

CHAPTER 1	**INTRODUCTION**	1
1.1	Electokinetic Phenomena	1
1.2	Literature Survey	2
1.3	Summary	8
CHAPTER 2	**ELECTROKINETIC THEORY**	10
2.1	The Zeta Potential	10
2.2	Electrophoresis	12
2.2.1	The Hückel and Helmholtz-Smulochowski Equations	13
2.2.2	Complex Models of Electrophoretic Velocity	13
2.2.2.1	Henry's Equation	14
2.2.2.2	O'Brien and White Model	16
2.3	Effect of Electroosmosis on Electrophoresis	18
2.4	Summary	21

TABLE OF CONTENTS (CONTINUED)

CHAPTER 3	**THE BUBBLE-PRODUCING SYSTEM**	22
3.1	Background	22
3.2	Literature Review of Bubble-Producing Methods	25
3.3	Experimental Work	26
3.4	Summary	34
CHAPTER 4	**THE ELECTROPHORESIS CELL**	35
4.1	Scope of the Problem	35
4.2	Preliminary Cell Design	35
4.3	The "Flow-Through" Cell	41
4.3.1	Cell Design	41
4.3.2	Computer Simulations of Flow Patterns	44
4.3.3	Cell Construction	52
4.5	Summary	55

TABLE OF CONTENTS (CONTINUED)

CHAPTER 5	**THE ELECTRIC FIELD-PRODUCING SYSTEM**	56
5.1	Purpose and Operating Criteria	56
5.2	Description of System Components	56
5.2.1	Power Supply	56
5.2.2	Ammeter	56
5.2.3	Switch Box	56
5.2.4	Voltmeter	58
5.2.5	Electrodes	58
5.3	Palladium-Hydrogen Electrodes	59
5.3.1	Background	59
5.3.2	Development of Preparatory and Testing Procedures	60
5.3.3	Electrode Performance Tests	62
5.3.3.1	Estimation of Required Electric Field Magnitude	62
5.3.3.2	Experimental Set-up and Method	66
5.3.3.3	Preliminary Electrode Tests (Test Group 1)	68
5.3.3.4	Tests of Electric Field Stability Within a Specified Time Period (Group 2)	73
5.3.3.5	Variation of Electrode Performance With Different Solutions (Test Group 3)	83
5.4	Summary and Recommendations	88

TABLE OF CONTENTS (CONTINUED)

CHAPTER 6	**THE OPTICAL SYSTEM**	90
6.1	Equipment Criteria	90
6.2	Equipment Configuration	90
6.3	Measurement of Cell Depth	95
6.4	Calibration of Magnification	97
6.5	Image Distortion Due to Screen Curvature	97
6.6	Summary	102
CHAPTER 7	**PROCEDURES (ELECTROPHORESIS TESTS)**	103
7.1	Preparatory Procedures	103
7.1.1	Preparation of Electrolyte Solution	103
7.1.2	Preparation and Mounting of the Electrophoresis Cell	103
7.1.3	Preparation of the Electric Field Generating System	105
7.1.4	Measurement of the Local Cell Depth and Location of the Stationary Planes	105
7.2	Electrophoresis Experiments	106
7.2.1	Procedure	106
7.2.2	Collection of Data	109
7.2.2.1	Local Depth of the Cell	109
7.2.2.2	Electric Current	109

TABLE OF CONTENTS (CONTINUED)

CHAPTER 7 (CONTINUED)

7.2.2.3	Height of Solution in the Electrophoresis Cell	109
7.2.2.4	Horizontal Velocity of the Bubble	109
7.2.2.5	Conductivity of the Solution	110
7.3	Summary	110
CHAPTER 8	**RESULTS AND DISCUSSION**	111
8.1	Organization of Data	111
8.2	Analysis of Data	111
8.3	Results	115
8.4	Recommendations	122
8.4.1	Methods of Improving the Reproducibility and Accuracy of the Data	122
8.4.2	Methods of Easing the Operation of the Cell	124
8.5	Summary	124
LITERATURE CITED		125

TABLE OF CONTENTS (CONTINUED)

APPENDICES

APPENDIX 2-1	Electrical Potential Distribution Near a Flat, Stationary Surface	129
APPENDIX 2-2	Electroosmotic Flow in a Closed Rectangular Duct	133
APPENDIX 3-1	Calculation of a Bubble's Terminal Velocity and Electrophoretic Velocity	137
APPENDIX 3-2	Shrinking Sphere Model of Gas Transfer from a Bubble to its Surrounding Liquid	139
APPENDIX 5-1	Estimation of Required Electric Field Strength	144

LIST OF TABLES

TABLE	TITLE	PAGE
4.1	Calculation of Inlet Velocity Range for Computer Simulations	44
4.2	Summary of Simulations Depicted in Figures 4.5 to 4.10	51
5.1	Typical Experimentally Determined Electrophoretic Mobilities Found by Various Researchers	64
5.2	Electrode Tests, Group 1: Summary of Results	72
5.3	Electrode Tests, Group 2: Experimental Design	74
5.4	Electrode Tests, Group 2: Electrode Preparation	75
5.5	Electrode Tests, Group 2: Summary of Results	77
5.6	Electrode Tests, Group 2: Calculated Cell Constants	81
5.7	Electrode Tests, Group 3: Electrode Preparation	83
5.8	Electrode Tests, Group 3: Experimental Design	85
5.9	Electrode Tests, Group 3: Summary of Test Results	86
6.1	Precision Testing of Dial Indicator Readings	95
6.2	Calibration of Magnification	97
8.1	Calculated κa values for Aqueous KCl and Na_2SO_4 Solutions and Various Bubble Radii	114
8.2	Results From Tests Conducted with KCl Solutions	116
8.3	Results From Tests Conducted with Na_2SO_4 Solutions	118

LIST OF TABLES (CONTINUED)

TABLE	TITLE	PAGE
A-5-1.1	Electric Field Strength Required to Give $U_{obs}=4.17\times10^{-4}$ m/s	144
A-5-1.2	Electric Field Strength Required to Give $U_{obs}=8.33\times10^{-4}$ m/s	145
A-5-1.3	Electric Field Strength Required to Give $U_{obs}=1.67\times10^{-3}$ m/s	145

LIST OF FIGURES

FIGURE	TITLE	PAGE
2.1	The Helmholtz and Gouy-Chapman Models	11
2.2	The Stern Model for Distribution of Charge at an Interface	11
2.3	Electrophoresis of a Spherical Particle	12
2.4	Variation of Henry's Function with κa	15
2.5	O'Brien and White's Solutions for the Electromobility of a Solid, Nonconducting Spherical Particle in KCl with $\kappa a<3$ and $\kappa a>3$.	17
2.6a	Calculated Electroosmotic Flow Profile in a Closed Rectangular Duct, with Depth=2×10^{-3} m, Assuming Negatively Charged Walls	20
2.6b	Coordinate System for Closed Rectangular Duct	20
3.1	Comparison of Calculated Terminal and Electrokinetic Velocities of an Air Bubble in Water at 298 K	23
3.2	Variation of Laplace Pressure with Bubble Diameter for an Oxygen Bubble at 298 K	24
3.3	Okada's Apparatus for Electrophoresis of Bubbles	25
3.4	Fukui and Yuu's Apparatus for Producing Micron-Sized Bubbles by Electrolysis	27
3.5	Equipment Used to Form Bubbles by Pressurized Dissolution of Air In Water, Followed by Incremental Pressure Release	28
3.6	Bubble-Producing Platinum Wire Electrode	29
3.7	Calculated Shrinkage of Oxygen and Hydrogen Bubbles in Partially Degassed Water	31

LIST OF FIGURES (CONTINUED)

FIGURE	TITLE	PAGE
3.8	Calculated Terminal Velocities of Hydrogen and Oxygen Bubbles in Partially Degassed Water	32
3.9	Calculated Height Gain of Hydrogen and Oxygen Bubbles in Partially Degassed Water	33
4.1	Rudimentary Electrophoresis Cell and Bubble Manifold	36
4.2	Preliminary Cell Mounted onto Adjustable Motorized Stand	39
4.3	Illustration of the "Flow-Through" Concept	40
4.4	Coordinate System Used for Computer Flow Simulations	42
4.5	Sample FLOW 3D Output File: m44fc (Cutaway View of the Central Plane (y=0)	45
4.6	Sample FLOW 3D Output File: m45fc (Cutaway View of the Central Plane (y=0)	46
4.7	Sample FLOW 3D Output File: m46fc (Cutaway View of the Central Plane (y=0)	47
4.8	Sample FLOW 3D Output File: m60fc (Cutaway View of the Central Plane (y=0)	48
4.9	Sample FLOW 3D Output File: m48fc (Cutaway View of the Central Plane (y=0)	49
4.10	Sample FLOW 3D Output File: m47fc (Cutaway View of the Central Plane (y=0)	50
4.11	The "Flow-Through" Cell	53
4.12	The Liquid Flow Control Network	54
5.1	Schematic Layout of the Electric Field-Producing System	57

LIST OF FIGURES (CONTINUED)

FIGURE	TITLE	PAGE
5.2	Circuit Diagram for Electrolytic Charging of Palladium Wires	61
5.3	Electric Field Strengths Required to Produce the Electrophoretic Mobilities in Table 5.1	65
5.4	Configuration of Test Apparatus	67
5.5	Effect of Electrolyte Concentration on the Zeta-Potential in Aqueous Surfactant-free Solutions of Na_2SO_4, $NaClO_4$, and $NaNO_3$	69
5.6	Re-Designed Electrolysis Chamber	71
5.7	Results from Preliminary Electrode Tests (Test Group 1)	72
5.8	Sample Current-Time Plot Derived from Test Group 2, Set 2 (Test Number 2)	76
5.9	Sample Current-Time Plot Derived from Test Group 2, Set 2 (Test Number 3)	76
5.10	Test Group 2: Variation of Current Range with Liquid Height for Voltage Drops of 25 V and 50 V	79
5.11	Test Group 2: Variation of Current Range with Voltage Drop for Liquid Heights of 0.15 m and 0.25 m	80
5.12	Test Group 2: Variation of Current Median with Voltage Drop and Liquid Height	82
5.13	Test Group 3: Variation of Current Range with Solution Conductivity	87
5.14	Test Group 3: Variation of Current Median with Solution Conductivity	87
6.1	Schematic Arrangement of Optical Components	91

LIST OF FIGURES (CONTINUED)

FIGURE	TITLE	PAGE
6.2	Arrangement of Microscope and CCTV Camera	92
6.3	Front View of Microscope Mounting Assembly	93
6.4	Detailed View of Camera Support Trough	94
6.5	Top View of Dial Indicator Configuration	96
6.6	Variation of Magnification with Vertical Position of Video Image on Video Screen (y-coordinate)	99
6.7	Variation of Magnification with Horizontal Position of Video Image on Video Screen (x-coordinate)	100
6.8	Uncertainty of Magnification as a Function of Line Segment Length	101
7.1	Expected Direction of Bubble Motion Resulting from the Configuration of the Electric Field-Producing Circuit	108
8.1	Variation of Drift Velocity with Solution Conductivity	113
8.2	Comparison of Data from this Work to Results from Brandon et al. (1985): Effect of pH on the Electrophoretic Mobility of Chlorine Bubbles in Aqueous 0.001 M KCl Solution (Surfactant-Free)	120
8.3	Effect of Bubble Diameter on the Electrophoretic Mobility of Chlorine Bubbles (Same System as Figure 8.2)	120
8.4	Comparison of Data from this Work to Results from Brandon et al. (1985): Effect of pH on the Electrophoretic Mobility of Oxygen Bubbles in Aqueous 0.001 M Na_2SO_4 Solution (Surfactant-Free)	121
8.5	Effect of Bubble Diameter on the Electrophoretic Mobility of Oxygen Bubbles (Same System as Figure 8.4)	121

LIST OF FIGURES (CONTINUED)

FIGURE	TITLE	PAGE
A-2-1.1	Geometry for Distribution of Electrical Potential for Two Parallel, Flat Stationary Surfaces in Contact with an Electrolyte Solution	130
A-2-2.1	Geometry of a Closed Rectangular Duct (Top View)	136

NOMENCLATURE

A_{xy}	cross-sectional area of the cell, defined by the x and y unit vectors (m)
a	radius of a spherical particle (m)
b_1	dimensionless constant, defined in Equation A-3-2.7
C_1	integration constant, defined by Equation A-2-1.12
C_2	integration constant, defined by Equation A-2-1.12
$C_{G,S}$	molar concentration of gas at the bubble surface ($kmol/m^3$)
$C_{G,B}$	molar concentration of gas in the bulk solution ($kmol/m^3$)
$\mathcal{D}_{G/W}$	diffusivity of a gas in water (m^2/s)
$\mathcal{D}_{H/W}$	diffusivity of hydrogen in water (m^2/s)
$\mathcal{D}_{O/W}$	diffusivity of oxygen in water (m^2/s)
d_B	diameter of a bubble (m, unless stated otherwise)
$d_{B,t}$	diameter of a bubble at time, t (m)
E	electric field (V/m or N/C)
E_∞	electric field, far from a particle or stationary surface (V/m or N/C)
e	elementary charge (1.602×10^{-19} C)
f	function (defined by Equation 2-4)
g	gravitational constant ($9.81\ m/s^2$)
H	height of the liquid in the cell (m, unless stated otherwise)
H_B	height traversed by a gas bubble (m, unless stated otherwise)
He	Henry's constant (atm/mol fraction)

NOMENCLATURE (CONTINUED)

He_H	Henry's constant for hydrogen in water (atm/mol fraction)
He_O	Henry's constant for oxygen in water (atm/mol fraction)
k	Boltzmann constant (1.381×10^{-23} J K^{-1})
k_L	mass transfer coefficient (m/s)
L	horizontal distance [of a bubble], traversed across the video monitor (m)
M_G	molar mass of a gas (kg/kmol)
M_H	molar mass of hydrogen (kg/kmol)
M_O	molar mass of oxygen (kg/kmol)
M_w	molar mass of water (kg/kmol)
MF	magnification factor (dimensionless)
m'	rate of mole transfer (kmol/s)
N_A	Avagadro's number (6.022×10^{23} mol^{-1})
n_k	ionic number concentration of the k'$_{th}$ species (m^{-3})
n_∞	bulk ionic number concentration (m^{-3})
P	pressure (kPa, unless stated otherwise)
P_{Atm}	atmospheric pressure (kPa, unless stated otherwise)
$P_{Laplace}$	Laplace pressure (kPa, unless stated otherwise)
P_s	Pressure at a particle surface, as defined by Equation A-3-2.5 (kPa unless stated otherwise)
P_w	pressure gradient in the w direction, defined by Equation A-2-2.6 (kPa/m)

NOMENCLATURE (CONTINUED)

Q_{liquid}	liquid flowrate (m^3/s),
Re	Reynolds number, defined by Equation A-3-2.8 (dimensionless)
RO	(abbr.) "reverse osmosis"
Sc	Schmidt Number, defined by Equation A-3-2.10 (dimensionless)
Sh	Sherwood Number, defined by Equation A-3-2.7 (dimensionless)
T	temperature (K)
t	time (s)
Δt	time step (s)
U_E	electroosmotic velocity (m/s)
U_{obs}	observed velocity of a particle [on the video monitor] (m/s)
U_M	Electrophoretic mobility, defined by Equation 5.4 ($m^2/V\ s$)
U_P	actual electrophoretic velocity of a particle (m/s)
U^*_P	dimensionless electrophoretic velocity (defined by Equations 2-5 to 2-7)
$U_{T,\ bubble}$	terminal velocity of the bubble (m/s),
$U_{T,\ liquid}$	vertical velocity of the liquid (m/s),
$U_{T,\ Avg}$	average vertical liquid velocity (m/s),
u	dummy variable
$V_{B,t}$	volume of a bubble at time, t (m^3)
V_W	volume of water or solution (m^3)

NOMENCLATURE (CONTINUED)

W	half the cell width, as shown in Figure 4.4 (m, unless stated otherwise)
w	distance along the cell width, measured from the centre (m, unless stated otherwise)
X	half the cell height, as shown in Figure 4.4 (m, unless stated otherwise)
x	distance along the cell height, as measured from the centre (m, unless stated otherwise)
Y	half the cell depth, as shown in Figure 4.4 (m, unless stated otherwise)
y	distance along the cell depth, as measured from the centre (m, unless stated otherwise)
z	net absolute valence of ions in solution (dimensionless)
z_k	valence of the k'$_{th}$ species (dimensionless)
β^*	dimensionless group (defined by Equation 2-9)
$\gamma_{G/W}$	surface tension between the gas/liquid interface (N/m)
ε	dielectric constant (dimensionless)
ε_o	permittivity of a vacuum (8.854×10^{-12} C/Vm)
κ	inverse Debye length (m^{-1})
κ^{-1}	Debye length (m)
μ	viscosity (Pa s)
μ_w	viscosity of water (Pa s)
π	3.14 (dimensionless)

NOMENCLATURE (CONTINUED)

ρ_G	density of a gas (kg/m^3)
ρ_H	density of hydrogen (kg/m^3)
ρ_O	density of oxygen (kg/m^3)
ρ_w	density of water (kg/m^3)
$\rho^{(f)}$	free charge density (C/m^3)
σ	solution conductivity ($\Omega^{-1}m^{-1}$)
ϕ	total electrical potential (V)
ψ	electrical potential due to the double layer (V)
ψ_d	electrical potential at the Stern plane (V)
ψ_s	electrical potential at a surface (V)
ζ	zeta-potential of a particle or bubble (V)
ζ_s	zeta-potential of a stationary surface (V)
ζ^*	dimensionless zeta-potential (defined by Equation 2-8)

CHAPTER 1 INTRODUCTION

1.1 ELECTROKINETIC PHENOMENA

When a material is placed in contact with an aqueous solution, a redistribution of charge takes place, causing a net electrical potential to form at the interface. Such a phenomenon occurs at solid-liquid, liquid-liquid, and gas-liquid interfaces. The existence of this surface potential forms the fundamental basis for many naturally occurring processes. For example, the transport behaviour of red blood cells is affected by the electrical potential they carry on their surface (Seaman, 1975).

The occurrence of a surface potential can also be utilized for industrial purposes. Processes that involve adsorption, flocculation, ion exchange, and flotation, can all be modeled, in part, by electrostatic principles. Such processes include removal of heavy metal ions from aqueous solutions by ion exchange resins and flotation of oil droplets and fine particles by froth flotation. In view of the numerous applications, it is of value to better our understanding of surface charge interactions, so that we can improve our process operations.

The surface potential of a material cannot be measured directly. Rather, the surface potential is inferred by studying the electrokinetic behaviour of the system, and applying fundamental theory. Four electrokinetic transport phenomena have been identified: electrophoresis, electroosmosis, streaming potential, and Dorn potential.

Particle electrophoresis occurs when a small particle, immersed in an electrolyte solution, is subjected to an electric field. As a result of its own surface potential, the particle is attracted toward the electrode of opposite charge. In contrast, electroosmosis is defined as a fluid's movement due to its proximity to a charged stationary surface. For example, consider an electrolyte solution adjacent to a glass wall. Because the glass wall is in contact with the solution, an excess electrical charge forms at the interface. When a uniform electric field is applied parallel to the wall, the ions near the glass are attracted to the pole of opposite charge. As the ions move, they drag the liquid with them. If a particle is immersed in this solution, it too will be dragged along with the liquid. Both electrophoresis and electroosmosis are explained in detail in Chapter 2 (Electrokinetic Theory).

Streaming potential is caused by the flow of charged particles under a pressure gradient between two electrodes. The motion causes a measurable electrical current, (the "streaming current"), that can be back-calculated to determine the surface potential of the particles. The Dorn potential is similarly defined, except that the flow is caused by gravimetric settling of particles. Often the terms, streaming potential and Dorn potential, are used interchangeably in the literature.

Of the four of these phenomena, electrophoresis is the most commonly used to measure the surface potential of small particles in liquids. Several commercial devices are available, such as the Rank Brothers' Mark II apparatus, to name but one. The devices often consist of a glass or quartz container that is called the cell. The cell can be either cylindrical or rectangular and is usually mounted with its broad side horizontal. It is filled with the solution of choice and particles whose surface potential is to be determined. Two electrodes are placed on either side. A potential is applied between the electrodes, causing an electric field to form between the gap. The objects then migrate horizontally to the electrode of opposite charge. Their resultant velocity is determined by timing their movement over a fixed distance. Because this velocity is often very small (on the order of 10^{-8} m/s per V/m of electric field), the motion must be observed through a microscope.

As the particles are also subject to gravity, they travel vertically as well as horizontally. In certain cases, the settling velocity is much greater than the electrokinetic velocity. For this reason, is very difficult to apply electrophoresis to large, dense objects or very buoyant objects (such as bubbles).

1.2 LITERATURE SURVEY

While electrokinetic studies on small solid particles in liquids has been abundant, similar studies of gas bubbles has been quite limited. The principle reason for this trend is that electrophoresis of bubbles is very difficult to perform. Unless the bubbles are very small, they rise too quickly to allow time for an adequate measurement of their horizontal velocity. Recently, electrokinetic studies of bubbles have been revived, since it has been shown that the charge of the bubbles is an important factor governing flotation processes.

Sirois and Millar (1973) developed a very large electrophoresis device, consisting of a Lucite tank of dimensions 10 × 10 x 10 cm. The tank was painted black, except for a narrow strip along the front, that allowed the bubbles to be photographed against the dark background. A stroboscope lamp was mounted beneath the tank. The stroboscope was set to 600 flashes per minute, thus providing ten bubble images per second of rise time. The air bubbles themselves were delivered from a stainless steel tube (35 gauge). Typical bubble diameters ranged between 0.15 and 0.40 mm. The electric field was supplied by two flat palladium surfaces, placed 5 cm apart. Electrophoretic measurements were made for dodecylamine hydrochloride (DAH) and sodium alkylarylsulphonate systems at pH levels of 6 and 10.

The main difficulty with Sirois and Millar's apparatus was that power dissipation caused convective currents in the cell. In consequence, the solution temperature had to be maintained at 277 K, and measurements could only be taken within three to five seconds of applying the power. The authors thus concluded that their device was best used for qualitative estimations (Sirois and Millar, 1973).

Dibbs et al. (1974) researched the streaming potential of bubbles in basic solutions of DAH, over the pH range 6.3 to 11. The bubbles were prepared by forcing high purity nitrogen through a porous glass frit, and the streaming current was measured by two silver/silver chloride electrodes. In the absence of DAH, the streaming current of bubbles in pure water was determined to be negative.

The magnitude of the streaming current increased with increasing pH, and decreased as the bubbles "aged". The addition of DAH caused the streaming potential to increase, and even become positive at high concentrations. The results from the streaming current measurements were compared to the flotation recovery of quartz from the same solutions, under the same conditions. Optimum recovery was achieved for conditions in which the quartz and the bubbles displayed oppositely charged potentials.

Usui and Sasaki (1978) utilized the streaming potential method in their study of argon bubbles in aqueous solutions of anionic sodium hexadecyl sulphate (SHS) and cationic hexadecyltrimethylammonium bromide (HTAB). The zeta potentials of bubbles were determined to increase in magnitude as the concentration of the surfactants was increased. The results were attributed to the adsorption of surfactant at the gas-liquid interface, with the cationic surfactant producing a positive charge, and the anionic surfactant producing a negative charge. The magnitudes of the zeta-potentials from the SHS system were larger than those for equal concentrations of HTAB. Furthermore, the addition of 1-butanol to both solutions substantially raised the magnitude of the zeta-potentials. These two results were shown to be related to the degree of surfactant adsorption onto the bubbles' surface. The SHS was adsorbed more easily that the HTAB, and butanol was found to enhance the adsorption of both surfactants.

Usui et al. (1981) also determined that the zeta-potential of bubbles, as determined by the Dorn potential method, was dependent on the bubble size. This result was not predicted by classical theory. The apparatus and method of this study were similar to those of the earlier study (Usui and Sasaki, 1978). In this study, SHS was added to water at concentrations of 1×10^{-5} and 1×10^{-6} M. The argon bubbles in question had diameters ranging from 200 to 800 μm. The magnitude of the zeta-potentials decreased in magnitude as the mean bubble diameter was increased. In comparison, the same experiment performed with solid glass beads of comparable diameters, exhibited no dependency of zeta-potential on the bead diameter. This deviation from the classical theory was attributed to slippage of ions on the mobile gas-liquid interface. This theory predicts that the bubbles' electrokinetic behaviour would approach that of solid spheres as the bubble diameters approach zero.

Somasundaran et al. (1983), studied the attachment of alumina particles onto air bubbles, and proposed that the attachment was in part, a function of the electrical double layer forces between the particles and the bubbles. The alumina particles were suspended in solutions containing sodium dodecyl sulphonate (NaDDS), sodium chloride(NaCl), and

sodium hydroxide (NaOH) or hydrochloric acid (HCl), depending on the desired pH. The zeta-potentials of the particles were measured by a Lazer Zee Meter, while the zeta-potentials of the bubbles had to be estimated from surface tension data (see reference for details).

In later studies, Li and Somasundaran (1991, 1992) found that certain electrolytes could reverse the surface charge of nitrogen bubbles in solution. The bubbles were produced by injecting nitrogen through a porous glass frit (2 - 2.5 μm porosity) at the bottom of a Buchner funnel filled with the desired salt solution. The solution was circulated by a peristaltic pump to keep the bubbles from coalescing. The diameter of the bubbles was estimated to be 5 μm or smaller. Just prior to making measurements, the pump was turned off, and a sample was injected into the Lazer Zee Meter. It was found that bubbles exhibited a negative charge in sodium chloride (NaCl) solutions. In magnesium chloride ($MgCl_2$) solutions, the charge became positive in the pH range 9 to 11 (Li and Somasundaran, 1991). The same effect was observed in trivalent aluminum chloride ($AlCl_3$) solutions (Li and Somasundaran, 1992). The charge reversal was attributed to the adsorption of metal cations onto the bubble surface.

Collins and Jameson (1976, 1977) investigated the flotation of small polystyrene particles, and concluded that the surface potentials of the particles and bubbles were both pertinent factors. The chemical system they studied consisted of sodium sulphate (Na_2SO_4) solutions, with concentrations ranging from 5×10^{-4} to 1×10^{-2} M. The system also contained 5×10^{-5} M of the cationic surfactant, cetyltrimethylammonium bromide (CTAB), as well as a frothing agent (5% v/v ethanol). The surface potentials of the bubbles were measured in a modified Rank Brothers Mark II electrophoresis cell, with cross sectional area of 1×10 mm (Collins et al., 1978). The cell was mounted horizontally with the broadest side vertical. The bubbles were generated electrolytically on the tip of a fine platinum wire. This wire was sealed into the narrow edge at the bottom of the cell (a second wire was sealed into the top to act as a counter electrode). The motion of these bubbles was followed by racking the microscope assembly up with a micrometer adjustment screw. The largest bubbles that could be tracked in this manner had diameters of about 35 μm. Larger bubbles rose too quickly, and much smaller bubbles tended to dissolve.

Collins et al. (1978) reported that their device was troublesome to operate, which resulted in some inconsistent results. However, the electrophoretic mobility of the bubbles and polystyrene particles were determined to have the same sign and be in the same order of magnitude. Both mobilities were observed to decrease was the concentration of Na_2SO_4 was increased, while the collection efficiency was observed to increase accordingly. Collins et al. concluded that the flotation efficiency was a function of the product of the mobilities of the bubbles and the particles.

Fukui and Yuu (1979) performed similar studies on the flotation of polystyrene, using the same chemical system as Collins et al. (1978), except that aluminum chloride ($AlCl_3$) replaced the Na_2SO_4. Their apparatus differed slightly from Collins et al.'s, in that their bubbles were produced electrolytically in a separate container, and then manually poured into the electrophoresis cell. The bubble and particle mobilities were nearly identical to those determined from the Na_2SO_4 system. Similarly, the effect of the mobilities on the flotation efficiency concurred with Collins et al.'s study, leading Fukui and Yuu to the same conclusions.

In a later study, Fukui and Yuu (1982) adopted the method of Collins et al. They improved the procedure in the following ways. Firstly, they introduced the use of a video camera and recorder to track the motion of the bubbles. Supposedly, the new technology allowed them to keep track of bubbles as large as 75 μm in diameter. Secondly, the cell they used had a larger ratio of width to depth, thus reducing errors caused by end effects near the sides of the cell. Finally, they took mobility measurements at the front and back stationary planes and then averaged the results. Consequently, Fukui and Yuu took more measurements for any given condition, and claimed that their results had greater accuracy than Collins et al.

Brandon et al. (1985a, b) performed a detailed study of the electrophoretic mobilities of oxygen, hydrogen, and chlorine bubbles in electrolyte solutions. Mobility measurements were made in a cylindrical electrophoresis cell, mounted horizontally. The electric field was provided by platinum/palladium-hydrogen or silver/silver chloride electrodes. The bubbles were generated electrolytically at the tip of fine silver or platinum wires. The bubbles were quite large, ranging from 30 to 200 μm in diameter. The rise velocity of these was correspondingly large, and it is unclear how the authors were able to circumvent this difficulty.

Brandon et al.'s team (1985b) was one of the few who researched electrolyte systems both with and without surfactants. Several chemical systems were investigated in this study, including electrolyte solutions of Na_2SO_4, sodium chlorate ($NaClO_4$), and sodium nitrate ($NaNO_3$) under varying conditions of pH, salt concentration, and with or without the surfactants: dodecyltrimethylammonium bromide (DoTAB) and sodium dodecylsulphate (SDS). Two unusual results were obtained. Firstly the magnitude of the bubble mobility appeared to be a linear function of the size of the bubbles. Secondly, the electrophoretic mobility did not vary linearly with the electric field strength. Both observations were contrary to traditional theory. The dependence of zeta-potential on bubble size was also reported by Usui et al. (1981), but in Usui et al.'s results, the magnitude of the zeta-potential decreased as the bubble diameter increased.

Yoon and Yordan (1986) examined the effect of anionic, cationic, and nonionic surfactants on the zeta-potentials of air bubbles in potassium chloride (KCl) solutions under various pH conditions. The bubbles they studied had diameters ranging from

40 μm to 80 μm. These bubbles were formed by forcing air into solution through a modified glass aspirator (Sebba, 1971). Electrophoresis tests were conducted in a Rank Brothers Mark II cell. The cell was modified by attaching small glass tubes into the side-arms. The tubes provided an inlet and outlet by which the solution was circulated through the cell. When the microscope was focused, the circulation was stopped, and measurements were taken. Readings were taken at the front and back stationary levels, in the manner of Fukui and Yuu (1982). The authors did not provide details on how they managed to keep the bubbles within the microscope's field of view.

Yoon and Yordan (1986) determined that the bubbles could be charged negatively or positively, according to the type of surfactant that was used. Not surprisingly, anionic and cationic surfactants respectively produced negative and positive surface potentials, while nonionic surfactants had very little effect at all. The magnitude of the surface potentials increased as the concentration of ionic surfactants increased, and tapered off near the critical micelle concentration.

In later years, Yoon and Yordan joined with Laskowski (1989) to study the electrokinetic potentials of bubbles in "weak electrolyte type" surfactants. Experimental details were essentially the same as those in their earlier work (1986). The reagents investigated DAH, lauric acid, sodium oleate, SDS, and sodium dodecane sulphonate. It was found that for strong electrolyte type surfactants, the bubble zeta-potential was almost entirely determined by the type of the surfactant. In comparison, the zeta-potential in weak electrolyte type surfactants was determined by the solution pH.

Kubota et al. (1983) examined the effects of the three surfactants, sodium benzenesulphonate, SDS, and cetylpyridinium chloride on the surface potentials of air bubbles in water. The bubbles were produced as follows. Air was dissolved into water a pressure of 0.5 MPa. The pressure was then reduced to atmospheric conditions, causing air bubbles to form in the water. The largest bubbles were allowed to rise to the surface, leaving a "slightly turbid" suspension of very tiny bubbles, suitable for electrophoresis (the average diameter of the bubbles was not specified). Electrophoresis measurements were made in a standard Briggs rectangular quartz cell with internal dimensions 1.036 × 22.4 × 70 mm. The results indicated that the sign of the bubble zeta-potentials were dependent on the type of surfactant, and the magnitude was dependent on the concentration. It was also shown that the magnitude depended on the degree to which the surfactant was adsorbed on the bubble surface.

Kubota later teamed up with Jameson (1993) to continue electrophoretic studies of gas bubbles. The "dissolved air" technique (Kubota et al., 1983) was modified slightly. Air was replaced by nitrogen gas, and bubble nucleation was aided by a beam of low intensity light. Electrophoresis was performed in a flat rectangular cell. The details of the procedure were otherwise the same as described in an earlier study (Kubota et al., 1983). The mobility of the bubbles was found to be depressed by increasing the concentration of

the electrolytes, NaCl and magnesium sulphate ($MgSO_4$). Further studies with $AlCl_3$ and aluminum sulphate ($Al_2(SO_4)_3$) systems demonstrated a reversal of the bubbles' surface charge. This supported the results of Li and Somasundaran (1991, 1992). The effect of chain length was examined for aqueous systems of n-alkyltrimethylammonium bromides (n = 10, 12, 14, 16) in various concentrations of CTAB at a pH of 5.6. It was shown that as the chain length was increased, the isoelectric point of the bubble mobility was shifted increasingly towards lower CTAB concentrations. (The isoelectric point is the point at which the electrophoretic mobility reverses sign). Finally, the effect of pH on bubble electromobility was tested in the absence of any electrolytes or surfactants. At very low pH, the mobility was positively charged. As the pH was raised, the mobility became increasingly negative, reaching a plateau at about pH 9.

Okada and Akagi (1987) used the same "dissolved air" method developed by Kubota et al. (1983). The bubbles they generated had diameters between 20 μm and 40 μm. Some slight improvements were made to the procedure. For example, the bubbles were introduced via a vertical glass tube drilled into the base of the rectangular cell. The tube contained a nozzle that helped to suppress the introduction of undesirable large bubbles or other disturbances. In comparison, Kubota et al. simply poured the solution directly into the cell. Okada and Akagi adapted a video camera to follow the path of the bubbles, so that the experiments could be played back in slow time for analysis. The cell stage could be moved downward keep the bubbles in the field of view. It is unclear from Kubota et al.'s report whether they too made use of video technology. Okada and Akagi's results for a system with 5×10^{-5} M CTAB and varying concentrations of Na_2SO_4 coincided closely with the results from Collins et al. (1978) for the same given system.

Okada et al. (1988) furthermore tested the zeta-potentials in systems of SDS (1×10^{-5} M) for varying concentrations of NaCl, calcium chloride ($CaCl_2$), and $Al_2(SO_4)_3$. As expected, bubbles' zeta-potentials were negative, and the concentration of electrolyte depressed the magnitude. Moreover, a sign reversal from negative to positive, was observed for the $Al_2(SO_4)_3$ system. The zeta-potentials of oil particles in the same electrolyte solutions were also measured and compared to those of the bubbles. The oil particles carried the same sign as the bubbles in the NaCl and $CaCl_2$ systems, but carried the opposite sign in the $Al_2(SO_4)_3$ system. Photographs were taken of the oil droplets in the proximity of air bubbles. The oil particles were repelled by the bubbles in the NaCl and $CaCl_2$ systems, but attached readily to bubbles in aqueous $Al_2(SO_4)_3$. Oil flotation experiments on these same three electrolyte systems confirmed that recovery from the $Al_2(SO_4)_3$ system far surpassed that of the other two electrolytes.

In a separate study, Okada et al. (1990) extended the research into the flotation of latex particles in KCl and $AlCl_3$ solutions, in the presence of SDS (1×10^{-5} M). Within the investigated range of concentrations, the $AlCl_3$ did not produce a charge reversal as it did for the $Al_2(SO_4)_3$ system. It did, however, reduce the bubbles' zeta-potential nearly to

zero. The zeta-potentials of the latex particles remained negative also, but they were reduced as the salt concentration was raised. An improvement in the flotation efficiency was observed to coincide with this decrease of both zeta-potentials. In contrast, the flotation efficiency remained low and stayed nearly constant over the range of potassium chloride concentrations that was used. The zeta-potentials of the bubbles and the latex particles in this system remained negative, and nearly coincided with each other over the entire range of electrolyte concentrations.

Finally, Okada et al. (1990) researched the behaviour of zeta-potentials of bubbles in solutions of the surfactants, DAH, SDS, and polyoxyethylene ether (POE). The ionic surfactants strongly influenced the zeta-potential over the entire range of pH that was studied, and the results correlated well with the results from Yoon and Yordan (1986). The nonionic surfactant had little effect of the zeta-potential.

1.3 SUMMARY

Electrophoresis and streaming potential were the two most prevalent methods used to study the electrokinetic behaviour of bubbles. Most attempts at electrophoresis aimed at circumventing the problem of the bubbles' quick rate of ascent. Researchers generally focused their efforts on making bubbles very small so as to reduce their inherent buoyancy. It was often also necessary to either move the entire cell downwards (or the microscope upward) so as to keep the bubbles within the field of view.

In this work, a unique "Flow-through" electrophoresis cell was designed and built, which incorporated the three following methods:

1. the bubbles were produced by electrolysis using a 30 μm diameter platinum wire,
2. bubble shrinkage was enhanced by partially removing gas from the electrolyte solution, and
3. the bubbles' rise velocity was reduced by having the solution flow downward through the cell.

This thesis outlines the design and problem solving processes that were undertaken to complete and test this cell. Chapter 2 outlines the relevant electrokinetic theory and the manner in which it affects the design and operation of the apparatus. Chapters 3 to 6 respectively, describe the design processes as related to the major components of the apparatus: the bubble-producing devices, the actual electrophoresis cell and liquid flow control system, the electric-field producing system, and the optical units. In Chapters 7 and 8, all the individual components are all brought together to perform preliminary electrophoresis experiments. Chapter 7 describes the experimental and preparatory procedures, and is, in essence, a manual for the operation of the cell. In Chapter 8, the results of these experiments are presented. Evaluations are made with the objective of

assessing the cell's performance, and illuminating areas that need further development. The chapter and thesis is completed with a list of recommendations for improvements.

CHAPTER 2 ELECTROKINETIC THEORY

2.1 ZETA-POTENTIAL

Most materials attain a surface charge when placed in contact with aqueous solutions. This occurrence takes place at the boundary between solids and liquids, gases and liquids, and even two immiscible liquids. The charged surface causes a redistribution of ions to occur in the aqueous phase. Ions of opposite charge (counterions) are attracted to the boundary, while ions of like charge (coions) are repelled.

Several models have been devised to describe the phenomenon. The Helmholtz theory describes the interface as two distinct parallel layers ions. The term "double layer" was coined to describe the appearance of this charge aggregation. The double layer concept was supplanted by the Gouy-Chapman theory. In this model, the charges are portrayed by point sources whose distribution is formed by a balance of attraction forces and Brownian motion. These two models are compared in Figure 2.1.

The Gouy-Chapman theory breaks down when the concentration of ions in the medium becomes large enough that the their finite size becomes significant. Stern proposed a model in which the inner boundary is approximated by one hydrated ion radius (Hunter, 1988). This concept is illustrated in Figure 2.2. The ions between the surface and the Stern plane are thought to be immobile and form the inner portion of the double layer. The potentials at the surface and the Stern plane are designated ψ_s and ψ_d respectively. Neither ψ_s nor ψ_d can be measured directly. Beyond the Stern plane, the potential drops exponentially as the ion density gradually thins. The thickness of the double layer is defined by the Debye length, κ^{-1}. For a symmetrical electrolyte, κ^{-1} is described by Equation 2-1:

$$\kappa^{-1} = \left[\frac{\varepsilon\varepsilon_o kT}{2e^2 z^2 n_\infty}\right]^{\frac{1}{2}} \qquad \textbf{(2-1)}$$

where ε is the dielectric constant of the medium,
ε_o is the permittivity of a vacuum (8.854×10^{-12} C/Vm),
k is the Boltzmann constant (1.381×10^{-23} J/K),
e is the fundamental charge (1.602×10^{-19} C),
z is the net valence of the ions, and
n_∞ represents the bulk ionic number concentration (m^{-3}).

As κ increases, the layer becomes increasingly compact. For a spherical object with radius, a (m), a very thin double layer occurs when $\kappa a \gg 1$. Conversely, a very thick layer relative to the particle diameter occurs when $\kappa a \ll 1$.

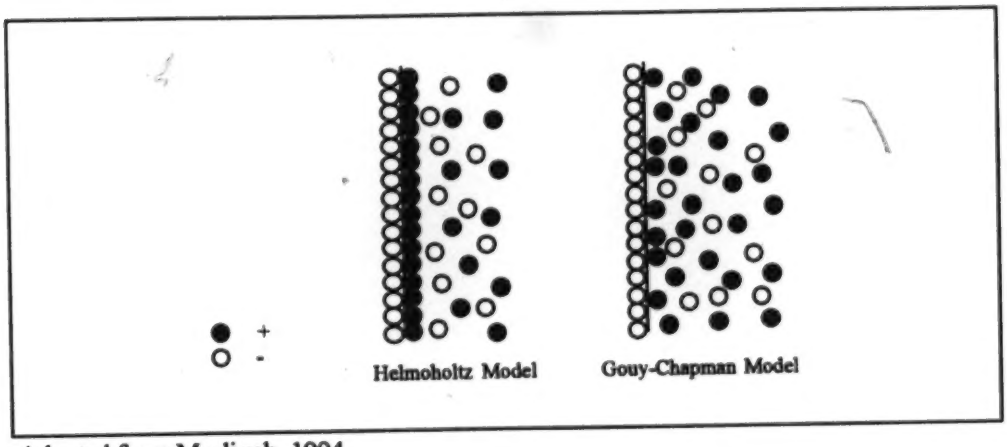

Adapted from Masliyah, 1994

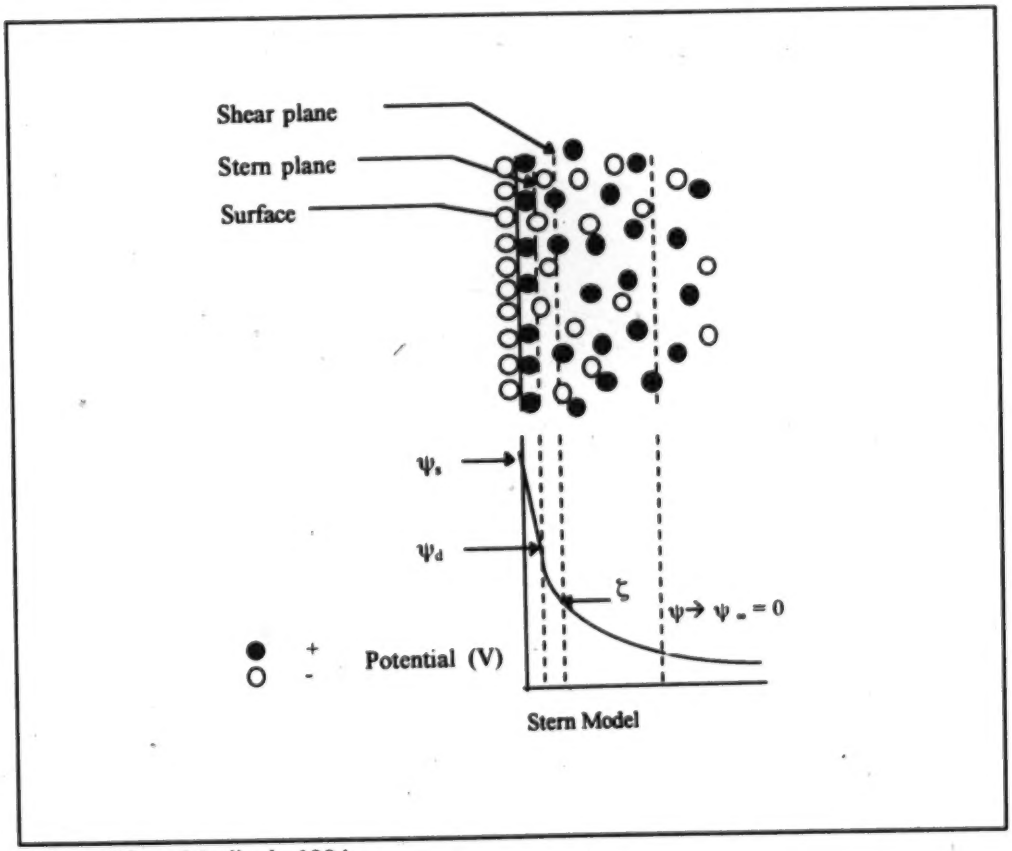

Adapted from Masliyah, 1994

Figure 2.1 (above) **The Helmholtz and Gouy-Chapman Models**
Figure 2.2 (below) **The Stern Model for Distribution of Charge at an Interface**

Just outside the Stern plane, there exists a region, one to two ion radii in thickness, in which the ions are thought to be mobile. The outer boundary of this region is referred to as the shear plane, at which the no-slip boundary condition applies. The corresponding potential at this boundary is called the electrokinetic or zeta–potential (ζ). The electrokinetic potential is only slightly different from the Stern potential. Thus, ζ is often used to approximate ψ_d.

The zeta–potential cannot be measured directly, but it can be deduced by observing the electrokinetic behaviour of the object in question. In this work, the electrokinetic phenomena of importance are electrophoresis and electroosmosis. These are described in detail in the next sections.

2.2 ELECTROPHORESIS

Electrophoresis is defined as the motion of a charged surface plus attached material relative to a stationary fluid resulting from an applied electric field (Hunter, 1988). Figure 2.3 illustrates the electrophoresis of a spherical particle with negative charge. The particle is suspended in an electrolytic medium. A uniform electric field is established by the two electrodes placed at either end of the electrophoresis container, or "cell". Due to its surface electric charge, the sphere then moves toward the appropriate terminal.

Electrophoresis is a popular method of obtaining information on the zeta-potential of a particle. The zeta-potential can be calculated from the measured electrophoretic velocity with the aid of theoretical models.

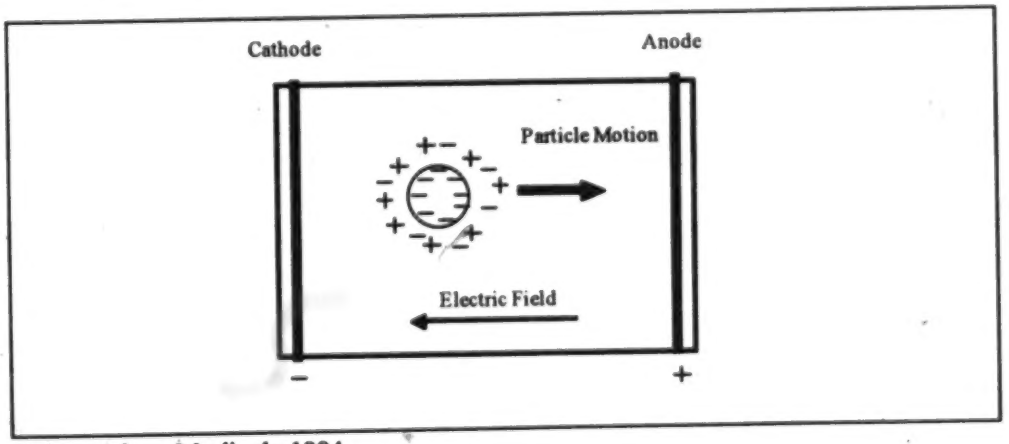

Adapted from Masliyah, 1994

Figure 2.3 Electrophoresis of a Spherical Particle

2.2.1 The Hückel and Helmholtz-Smulochowski Equations

The Hückel expression gives the electrophoretic velocity, U_p, of a sphere in a uniform electric field to be given by:

$$U_p = \frac{2\,\varepsilon\varepsilon_o\zeta}{3\quad\mu}E_\infty \tag{2-2}$$

where U_p is the electrophoretic velocity of the particle,
ζ is the zeta-potential (V),
E_∞ represents the electric field far from the influence of the particle (V/m), and
μ is the viscosity of the liquid (Pa s).

The Hückel model applies to a single rigid, non-conducting sphere in which $\kappa a \ll 1$. In practice, this situation frequently arises in non-electrolyte systems. The condition of non-conductivity is imposed because conductors are usually polarized by the electric field and so inhibit the passage of current.

The Helmholtz-Smulochowski Equation is given by:

$$U_p = \frac{\varepsilon\varepsilon_o\zeta}{\mu}E_\infty \tag{2-3}$$

The Helmholtz-Smulochowski equation applies to spherical objects with double layers that are very small relative to their radii ($\kappa a \gg 1$). This situation is prevalent in aqueous systems. As with the Hückel Equation, the condition of non-conductivity is imposed,. A detailed treatise of both these models is provided in Hiemenz (1986).

2.2.2 Complex Models of Electrophoretic Velocity

The simplest models treat the limiting cases of a rigid spherical object with either a very large double layer ($\kappa a \ll 1$) or a very small double layer ($\kappa a \gg 1$). More complex treatises, such as Henry's equation, are required for Debye lengths of intermediate range. In this region, several additional effects need consideration. These effects are electrophoretic retardation, relaxation, and surface conductance.

Electrophoretic retardation occurs due to the attraction of anions to the anode, and the cations to the cathode. As the ions move, they pull the neutral electrolyte molecules with them. This action inhibits the motion of the particle.

Relaxation refers to the drag force resulting from initial asymmetry of the surrounding double layer. When the electric field is applied, the particle moves relative

to the ions in the mobile part of the double layer. A relaxation interval is needed for the ions in the double layer to return to their usual arrangement through diffusion and convection (Hiemenz, 1986).

Surface conductance takes place because the ions in the mobile part of the double layer have a higher conductivity than the ions in the bulk solution. This effect is most prevalent when κa and ζ are large. The conductivity distorts the surrounding electric field lines, and thus alters the magnitude of ζ.

2.2.2.1 Henry's Equation

Henry analyzed the electrophoretic velocity of a single spherical particle to include intermediate values of κa in addition to the extreme cases already mentioned. The treatise assumes that the sphere is a non-conductor, and that the total potential of the sphere is a linear combination of the electrical double layer and the potential due to the electric field. The model further assumes that $\zeta << 0.025$ V. Thus, ζ is small enough that the Debye approximation applies (see Appendix 2-1). Furthermore, the electrophoretic velocity is assumed to be in the creeping flow regime, and relaxation effects are ignored.

With these conditions satisfied, the steady state electrophoretic velocity is given by Equation 2-4.

(2-4)
$$U_P = \left[\frac{2\zeta\varepsilon\varepsilon_0 E_\infty}{3\mu}\right] f(\kappa a)$$

where

$$f(\kappa a) = 1+\frac{1}{16}(\kappa a)^2-\frac{5}{48}(\kappa a)^3-\frac{1}{96}(\kappa a)^4+\frac{1}{96}(\kappa a)^5-\frac{1}{8}(\kappa a)^4 e^{\kappa a}\left[1-\frac{(\kappa a)^2}{12}\right]\int_{\infty}^{\kappa a}\frac{e^{-u}}{u}du$$

Figure 2.4 demonstrates the variation of Henry's function, *f*, with κa. At the two extremes, $\kappa a << 1$ and $\kappa a >> 1$, the electrophoretic velocity reduces to the Hückel and the Helmholtz-Smulochowski equations, respectively.

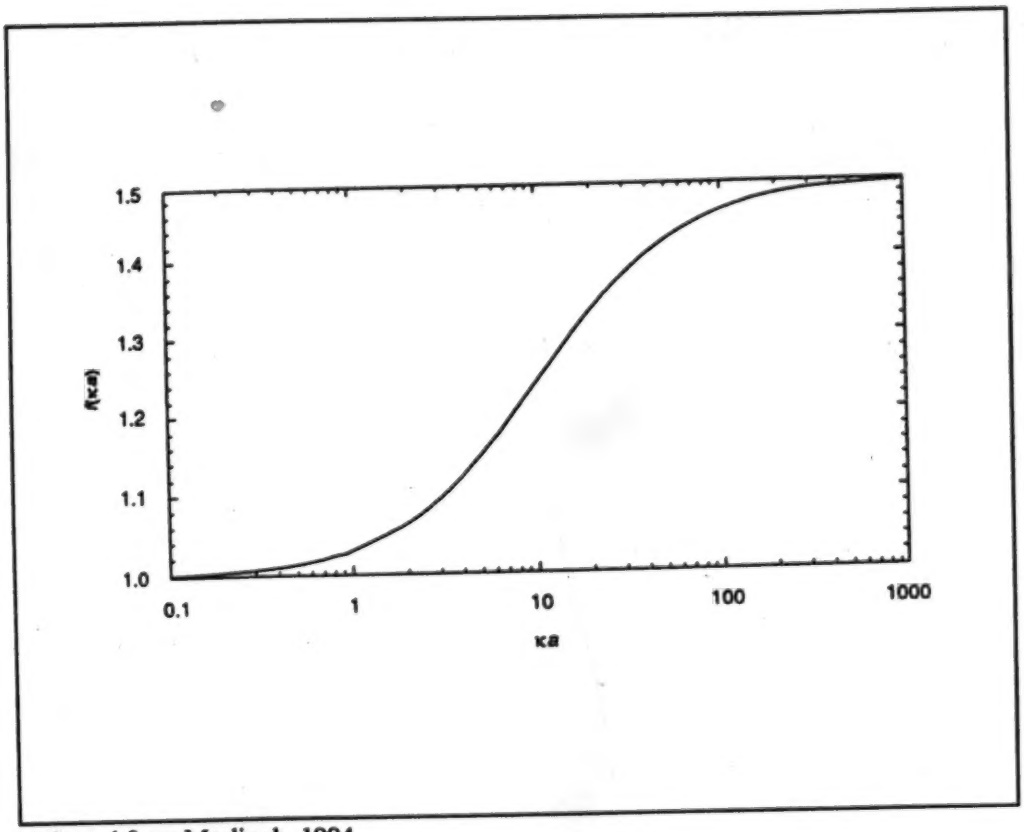

Adapted from Masliyah, 1994

Figure 2.4 Variation of Henry's Function with κa

2.2.2.2 O'Brien and White Model

Henry's analysis holds for small ζ such that the Debye approximation is valid. O'Brien and White (1978) devised a numerical solution for spheres with constant surface potential that encompasses a wide range of ζ, accounting for double layer relaxation, electrophoretic retardation, and surface potential effects. Using dimensionless parameters, ζ^*, β^*, and U^*_P, the Hückel, Helmholtz-Smulochowski, and Henry equations can be re-written respectively as Equations 2-5, 2-6, and 2-7.

(2-5) $$U^*_P = \frac{2}{3}\beta^*\zeta^*$$ Hückel

(2-6) $$U^*_P = \beta^*\zeta^*$$ Hemholtz-Smulochowski

(2-7) $$U^*_P = \frac{2}{3}\beta^*\zeta^* f(\kappa a)$$ Henry

where the dimensionless groups are defined by:

(2-8) $$\zeta^* = \frac{e\zeta}{kT}$$

(2-9) $$\beta^* = \frac{aeE_\infty}{kT}$$

(2-10) $$U^*_P = \frac{U_P}{\varepsilon\varepsilon_0\left(\frac{kT}{e}\right)^2\left(\frac{1}{\mu a}\right)}$$

Figure 2.5 shows O'Brien and White's solutions plotted as U^*_P/β^* against ζ^* for a spherical particle in aqueous KCl. For $\kappa a \to 0$, and $\zeta^* \leq 2$, the solution approaches the Hückel Equation. Conversely, for $\kappa a \to \infty$, and $\zeta^* \leq 2$, the solution approaches the Helmholtz-Smulochowski Equation. Deviations from the Henry Equation occur at $\zeta^* \geq 2$.

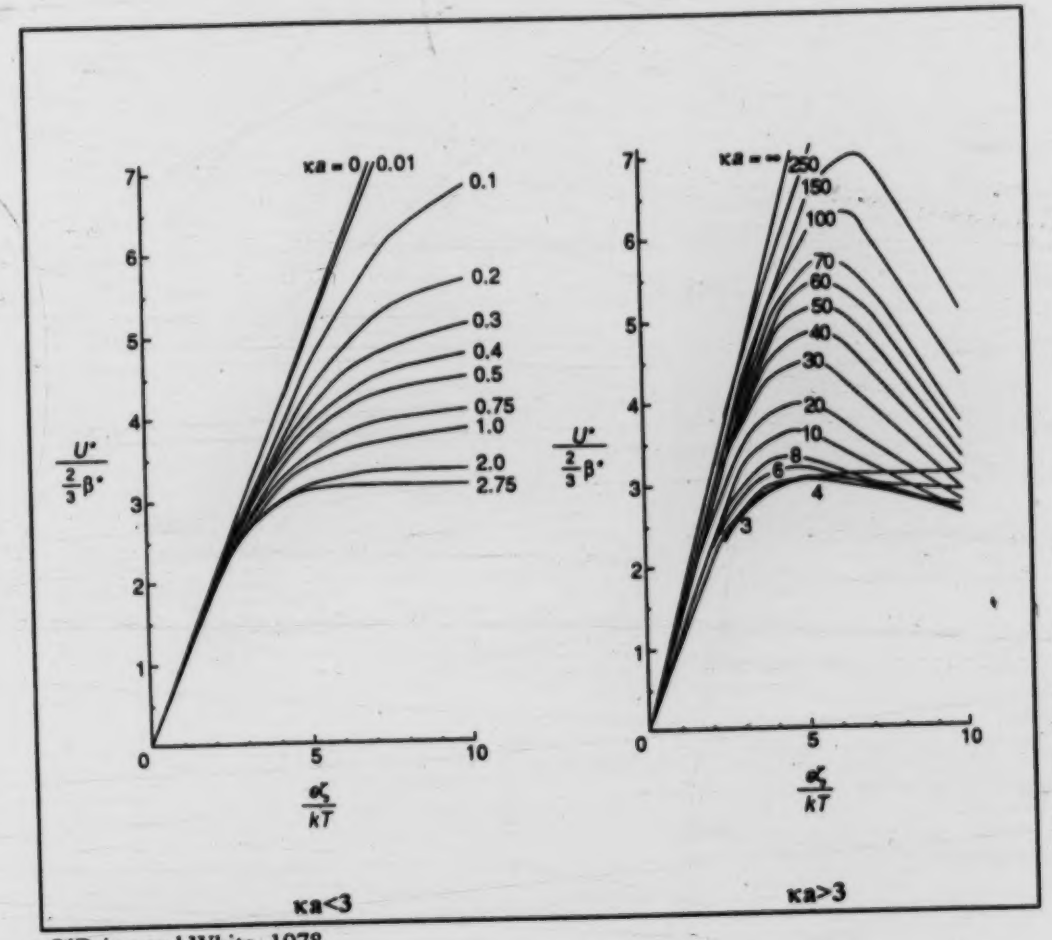

O'Brien and White, 1978

Figure 2.5 **O'Brien and White's Solutions for the Electromobility of a Solid Nonconducting Spherical Particle in KCl with κa<3 (left) and κa>3 (right)**

2.3 EFFECT OF ELECTROOSMOSIS ON ELECTROPHORESIS

Electroosmosis is defined as the motion of a fluid under the influence of an electric field, due its proximity to a stationary charged surface. Such a situation can occur in an electrophoresis cell. The geometry of such a cell can be closely approximated by a closed rectangular duct. The inner cell walls, in contact with the solution, develop an electrical potential. Thus, when an electric field is applied, the fluid next to the walls is dragged by the motion of ions adjacent to the walls. In consequence, any particle whose electromobility is being measured is actually affected by both electrophoretic and electroosmotic components.

(2-11) $$U_{obs} = (U_P + U_E) \times MF$$

where U_{obs} is the observed velocity of the particle (m/s),
U_E is the electroosmotic component of the velocity (m/s), and
MF is the magnification factor of the optical device (dimensionless).

It is possible to calculate the variation of electroosmotic velocity as a function of distance from the wall of the duct. Figure 2.6a illustrates the axial electroosmotic velocity profile in a closed rectangular duct for increasing values of κy. Figure 2.6b defines the coordinate system of this hypothetical duct. Here, W and Y are defined as half the width and depth of the duct, respectively. Effectively, Figure 2.6a is a view of an electrophoresis cell as seen from above. The assigned depth of the cell for this calculation is 2×10^{-3} m (or Y = 1×10^{-3} m). In addition, the zeta-potential of the wall is assumed to be positive. Equation 2-12 is derived from first principles in Appendix 2-2.

(2-12) $$\frac{U_E \mu}{\varepsilon \varepsilon_0 \zeta_S E_\infty} = \frac{3}{2}\left[1 - \frac{y^2}{Y^2}\right]\left[1 - \frac{\sinh(\kappa Y)}{\kappa Y \cosh(\kappa Y)}\right] - \left[1 - \frac{\cosh(\kappa y)}{\cosh(\kappa Y)}\right]$$

where ζ_S is the zeta potential of the zeta-potential of the walls (V),
y is the distance from the centre of the cell toward the cell wall, (m), and
Y is half the depth of the cell (m).

Due to the negative ions near the duct wall, the fluid adjacent to the duct wall is pulled in the direction opposite the electric field. Because the duct is closed at both ends, a counterflow is established around the central axis. As a result, a plane is established at which the net electroosmotic flow is zero. This is called the stationary level. As κy gets progressively larger, the location of this plane approaches a fixed position at 58% of Y, as measured from the central axis. Due to symmetry, two such stationary levels would actually be formed; at the front and at the back of the cell, respectively.

We can take advantage of this flow pattern by taking electrophoretic measurements of particles that are located at the stationary levels. The velocity of these particles would consist of only the electrophoretic component, while the electroosmotic component would be reduced to zero. Unfortunately, the electroosmotic velocity gradient becomes very steep in the vicinity of the stationary levels. In consequence, if the particle moves even a small distance away from a stationary level, its measured electromobility can be vastly changed. This can lead to a major source of experimental error.

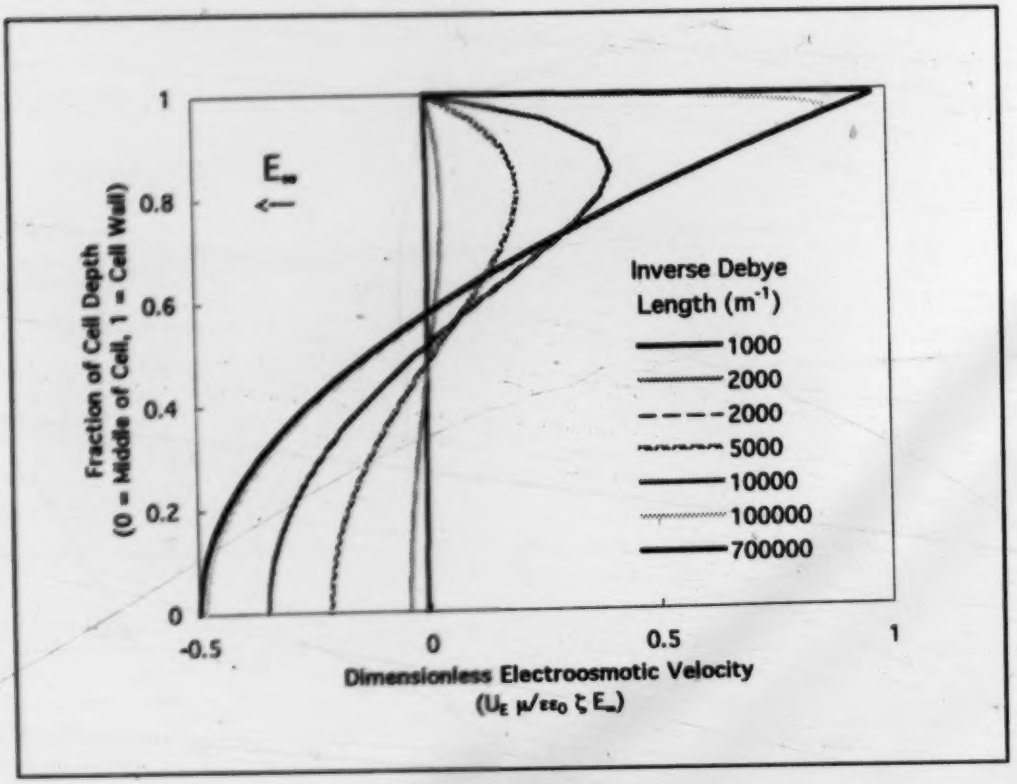

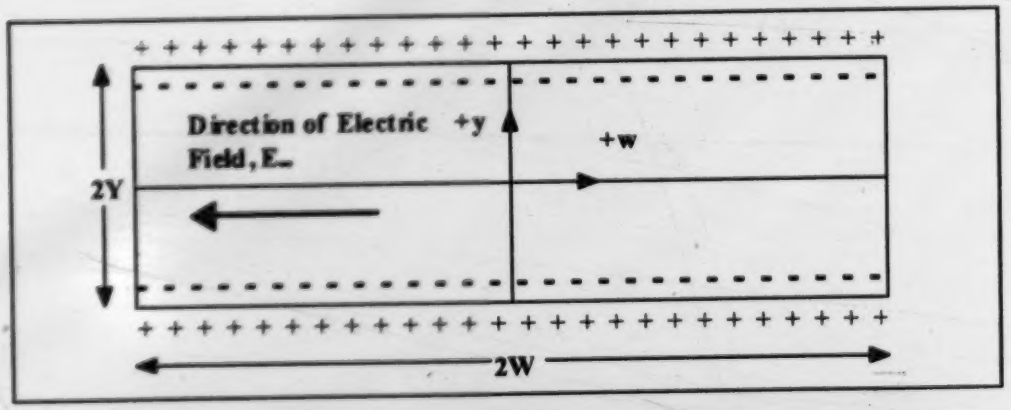

Figure 2.6a (above) **Calculated Electroosmotic Flow Profile in a Closed Rectangular Duct with Depth = 2×10^{-3} m, Assuming Positively Charged Walls (calculations shown in Appendix 2-2)**

Figure 2.6b (below) **Coordinate System for Closed Rectangular Duct**

An alternative to the "stationary levels" method is to take advantage of the fact that there is no net flow of liquid through a closed cell. Thus, assuming a uniform profile along the height of the cell, and that the end effects at the top and bottom of the cell are negligible:

$$2\int_0^Y U_E dy = 0 \qquad \textbf{(2-13)}$$

Integrating Equation 2-11 over the entire depth of the cell, we get:

$$\frac{2}{MF}\int_0^Y U_{obs} dy = 2\int_0^Y U_P dy + 2\int_0^Y U_E dy \qquad \textbf{(2-14)}$$

If we now substitute Equation 2-13 into 2-14, and taking into account that the electrophoretic component is independent of the cell depth, we arrive at an expression to describe the electrophoretic velocity that excludes the electroosmotic component:

$$U_P = \frac{1}{Y \times MF}\int_0^Y U_{obs} dy \qquad \textbf{(2-15)}$$

The main advantage of this method, commonly called the "depth-profile" method, is that it is less susceptible to errors caused by steep gradients in the electroosmotic velocity profile. The main drawback to this technique is that it requires a very large number of measurements, to ascertain that the profile is indeed uniform along the axial and vertical axes. Spitzer et al. (1981) describes a practical approach to applying this method.

2.4 SUMMARY

The zeta-potential serves as an estimate of a particle's surface potential. This parameter cannot be directly measured, but can be inferred from the particle's observed electrokinetic behaviour. In particular, electrophoresis is a common method of experimentally determining ζ. Electrophoretic measurement is complicated by the presence of electroosmotic flow. There is no direct way to distinguish between an particle's electrophoretic and electroosmotic velocity vectors. However, the "stationary level" and "depth-profile" methods offer indirect ways to circumvent this difficulty.

CHAPTER 3 THE BUBBLE-PRODUCING SYSTEM

3.1 BACKGROUND

Electrophoretic measurement of gas bubbles in aqueous solutions is difficult to perform because the bubbles are very buoyant, and hence rise quickly. The horizontal electrophoretic velocity of bubbles is usually very small relative to the vertical velocity. Consequently, electrophoretic motion must be observed through a microscope with a high magnification (100 to 300×). However, the larger the magnification, the faster the bubble will seem to race across the viewing area. Therein, the problem lies in capturing the bubble in the viewing field for long enough to make a reasonable measurement.

To demonstrate the problem, consider an air bubble in water at 25°C, with a zeta-potential of 0.025 V, subjected to a linear electric field of 1000 V/m. The rise velocity of the bubble can be estimated by Stokes Law, and the electrokinetic velocity estimated by the Helmholtz-Smulochowski Equation (see Chapter 2). Figure 3.1 shows both velocities as functions of the bubble diameter. The detailed calculations are shown in Appendix 3-1. Figure 3.1 clearly demonstrates that, to achieve a reasonable ratio between the vertical and horizontal velocity (within one order of magnitude), the bubble cannot be larger than 17 μm in diameter.

Making such small bubbles is not a trivial task. The Laplace pressure acting on bubbles increases rapidly as diameters shrink to less than 1 μm, hence making the bubbles unstable. To demonstrate, Figure 3.2 shows the relation between the calculated Laplace pressure and bubble diameter, for an air bubble in water at 298 K. The surface tension for the calculation is assumed to be 0.0720 N/m (Metcalf and Eddy, 1979), and the equation used is given by:

(3-1) $$P_{Laplace} = \frac{4\gamma_{G/W}}{d_B}$$

where $\gamma_{G/W}$ is the surface tension at the gas/liquid interface (N/m) and
d_B is the diameter of the gas bubble (m).

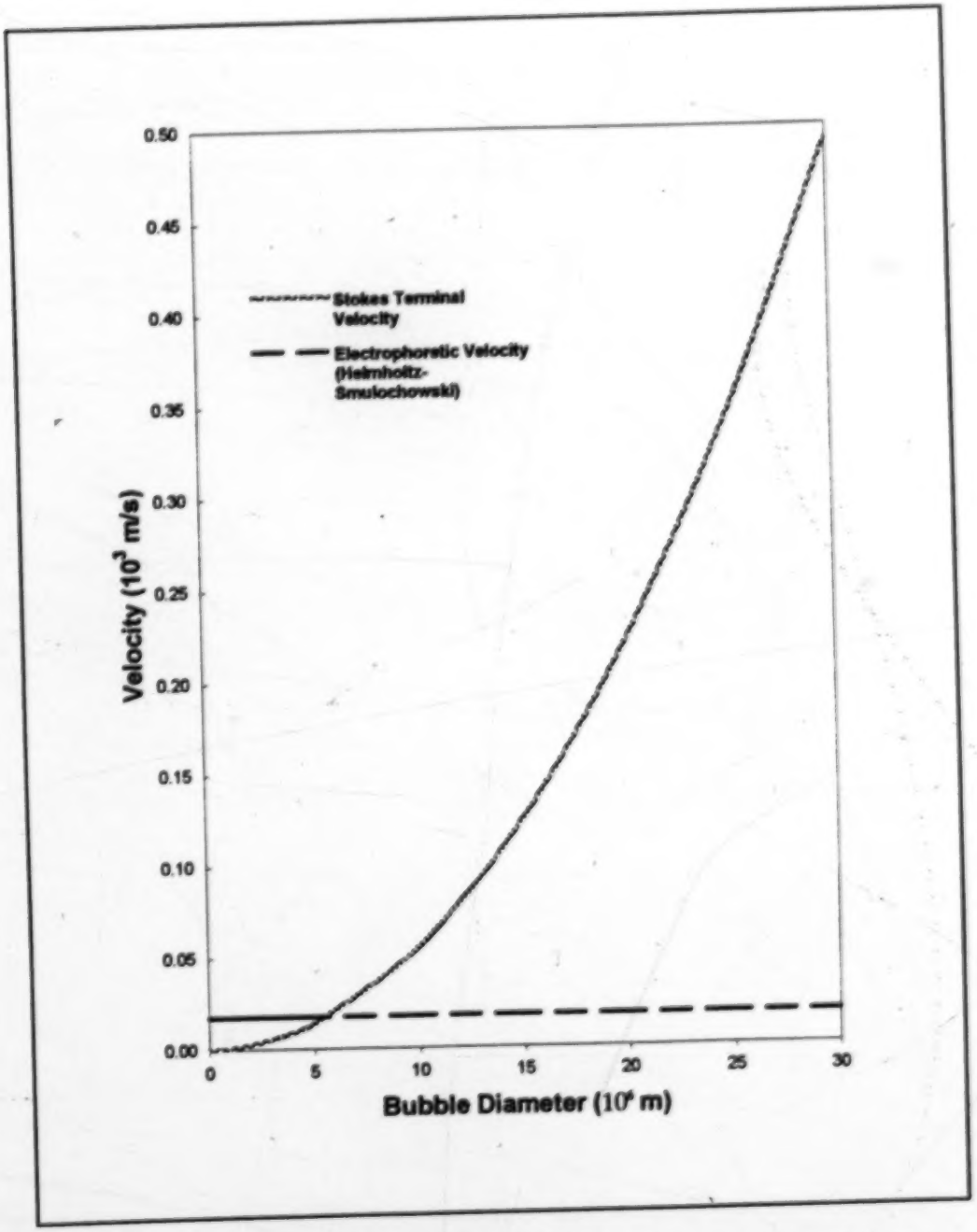

Figure 3.1 **Comparison of Calculated Terminal and Electrokinetic Velocities of an Air Bubble in Water at 298 K**

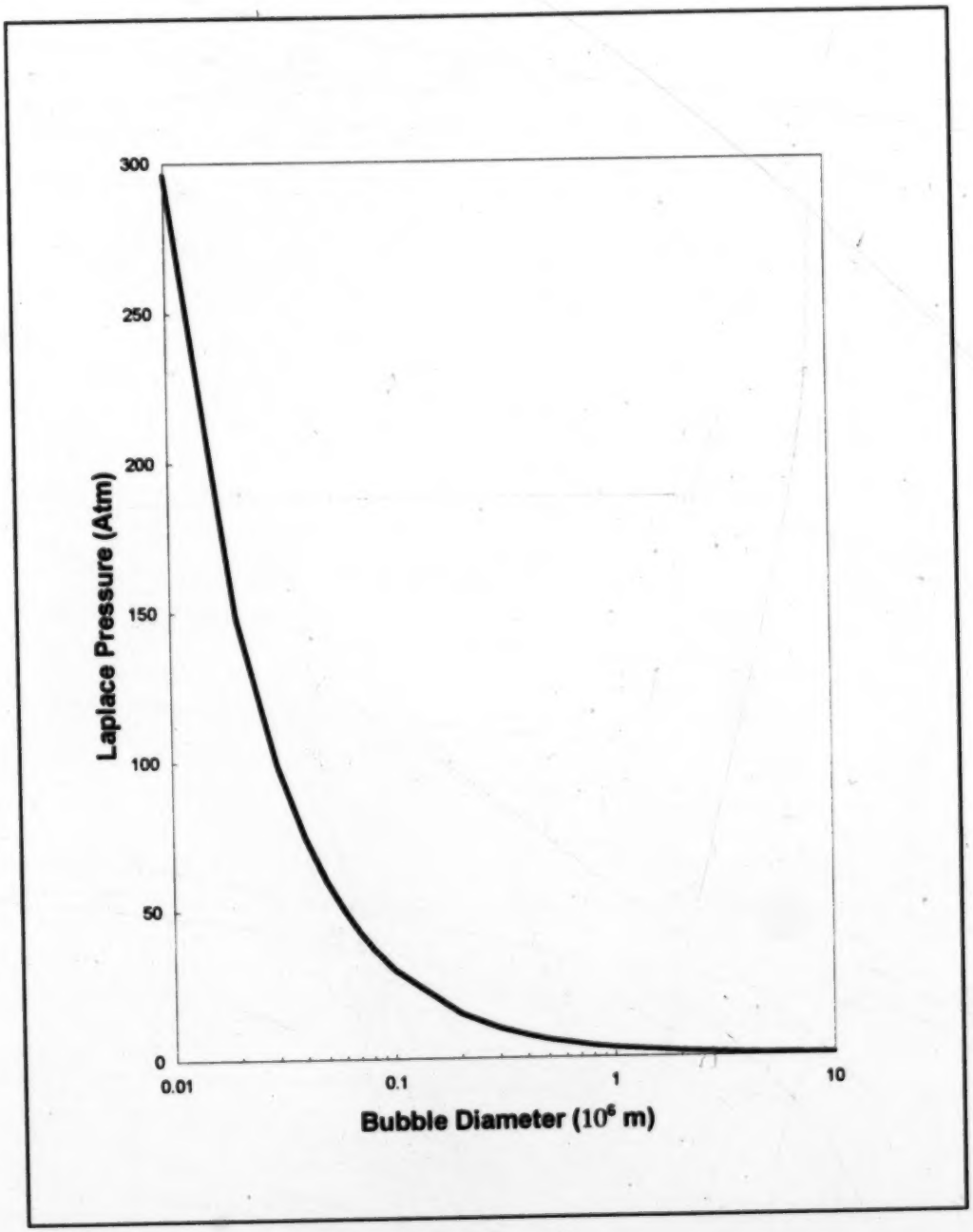

Figure 3.2 **Variation of Laplace Pressure with Bubble Diameter for an Oxygen Bubble in Water at 298 K**

3.2 LITERATURE REVIEW OF BUBBLE-PRODUCING METHODS

The problem of producing stable micron-size bubbles has prompted researchers to adopt several highly original methods. For example, Okada et al. (1987, 1988, 1990) created bubbles by forcing air into solution at high pressure, and then releasing the pressure slightly to release bubbles formed from the dissolved air. Okada's apparatus is shown in Figure 3.3. The equipment consisted of a pressure chamber and a manifold intake system. The manifold served to divert bubbles into a viewing chamber where they could be observed. In this way, the size distribution of the bubbles could be ascertained before allowing them into the electrophoresis cell. The upright nozzle was a special feature that further prevented large bubbles from entering the electrophoresis chamber.

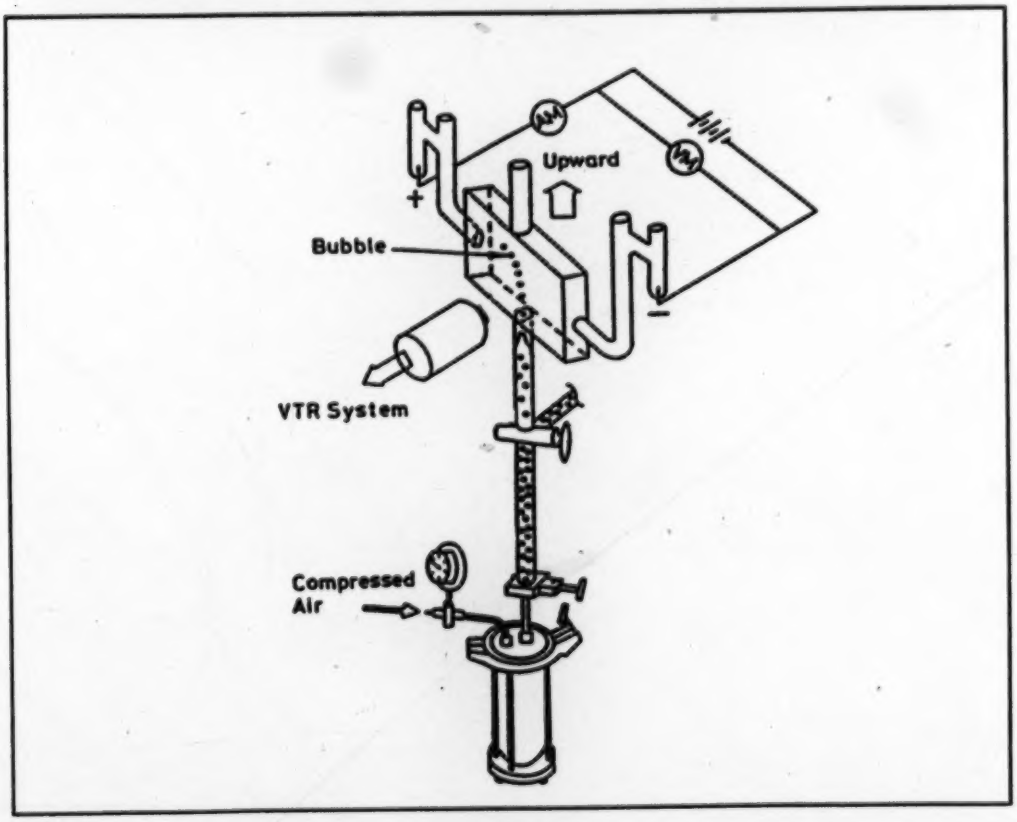

Figure 3.3 **Okada's Apparatus for Electrophoresis of Bubbles (Okada et al., 1987)**

Kubota and Jameson (1993) expanded upon Okada's idea. In their version, nitrogen gas was forced under pressure into an unfiltered aqueous solution. However, once the pressure was released, the resultant swarm of bubbles was allowed to dissipate. When the solution cleared, it was poured into a standard electrophoresis cell. A low intensity light beam was then focused on the cell, causing tiny bubbles to nucleate at random sites.

Electrolysis is a popular method of producing gas bubbles. It was adopted by many researchers, including Collins and Jameson (1977, 1878), Fukui and Yuu (1979, 1982), and Brandon and Kelsall (1985a and b). To explain the concept, Fukui and Yuu's apparatus is shown in Figure 3.4. Two fine platinum wires, sealed into the top and bottom of the cell, acted as a bubble-producing electrode and counter-electrode respectively. The electrodes were specially positioned at a stationary plane. Electrolyte solution was poured into the cell, and served to complete the electrical circuit. When a short burst of 2 to 5 V was applied, small bubbles would form on the bottom wire, and rise due to their inherent buoyancy.

Still others produced bubbles by forcing gas into solution through a porous frit (Li and Somasundaran, 1991, 1992) or an aspirator (Sebba, 1971; Yoon and Yordan, 1986), and circulating the solution through a conventional electrophoresis cell.

3.3 EXPERIMENTAL WORK

Rudimentary tests were conducted to choose a suitable means of making small bubbles. The first method tested was Okada's pressurization technique. A bomb was partially filled with reverse osmosis (RO) water, and connected to an air outlet, as shown in Figure 3.5. Air was forced in at 200 kPa for 30 minutes. At five minutes intervals, the bomb was sealed, disconnected from the gas flow, and shaken vigourously. This was done to enhance the transfer of gas into the water. Upon completion of the half hour, the airflow was ceased. The lower valve was opened very slightly, forcing bubble-laden liquid into the adjoining glass tube. The resulting bubbles were observed through an image analyzer to estimate their diameter.

This procedure was considered inadequate for several reasons. Firstly, the bubbles formed in an uncontrolled swarm, with a wide distribution of sizes. Secondly, flow disturbances caused bubbles to coalesce as they rose along the tube. It would have been impossible to distinguish electrokinetic motion from the erratic path of these rising bubbles.

Electrolysis proved to be a more promising method. Several electrodes were fabricated from fine 30 μm platinum wire (Brandon et al., 1985; Dai, 1994). One such

electrode is shown in Figure 3.6. The electrodes were made by stringing wire through the narrow sawed-off tip of a micropipette. The glass was flame sealed at each end to provide a protective case for the wire. The platinum wire protruding from the wide end of the casing was wrapped around a stronger contact wire and glued in place. The entire electrode was then inserted in a narrow glass tube that further protected the delicate contact. Finally, the fine wire protruding from the narrow end of the pipette was trimmed. It was important that this tip of wire was cut as short as possible to prevent bubbles from sticking to the metal and growing too large.

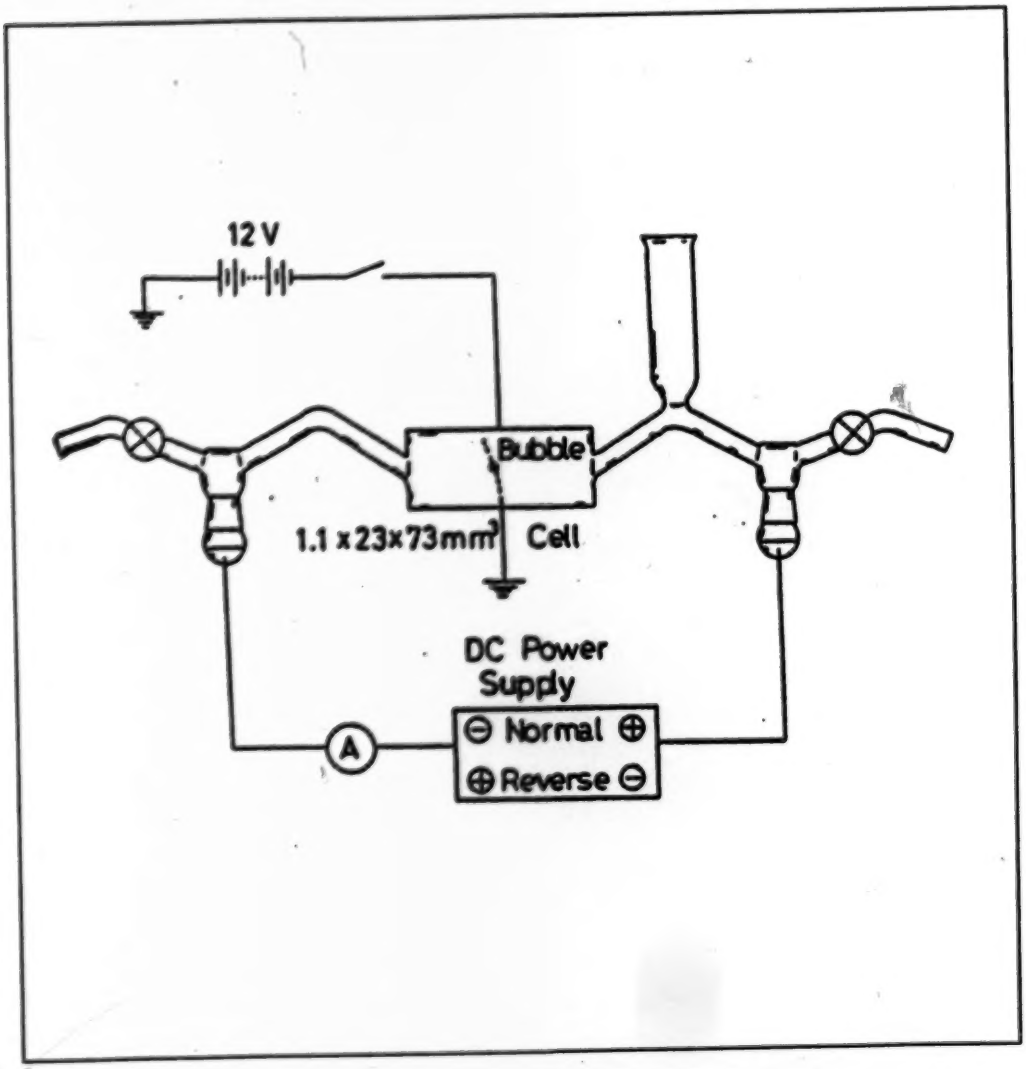

Figure 3.4 **Fukui and Yuu's Apparatus for Producing Micron-Size Bubbles by Electrolysis (Fukui and Yuu, 1982)**

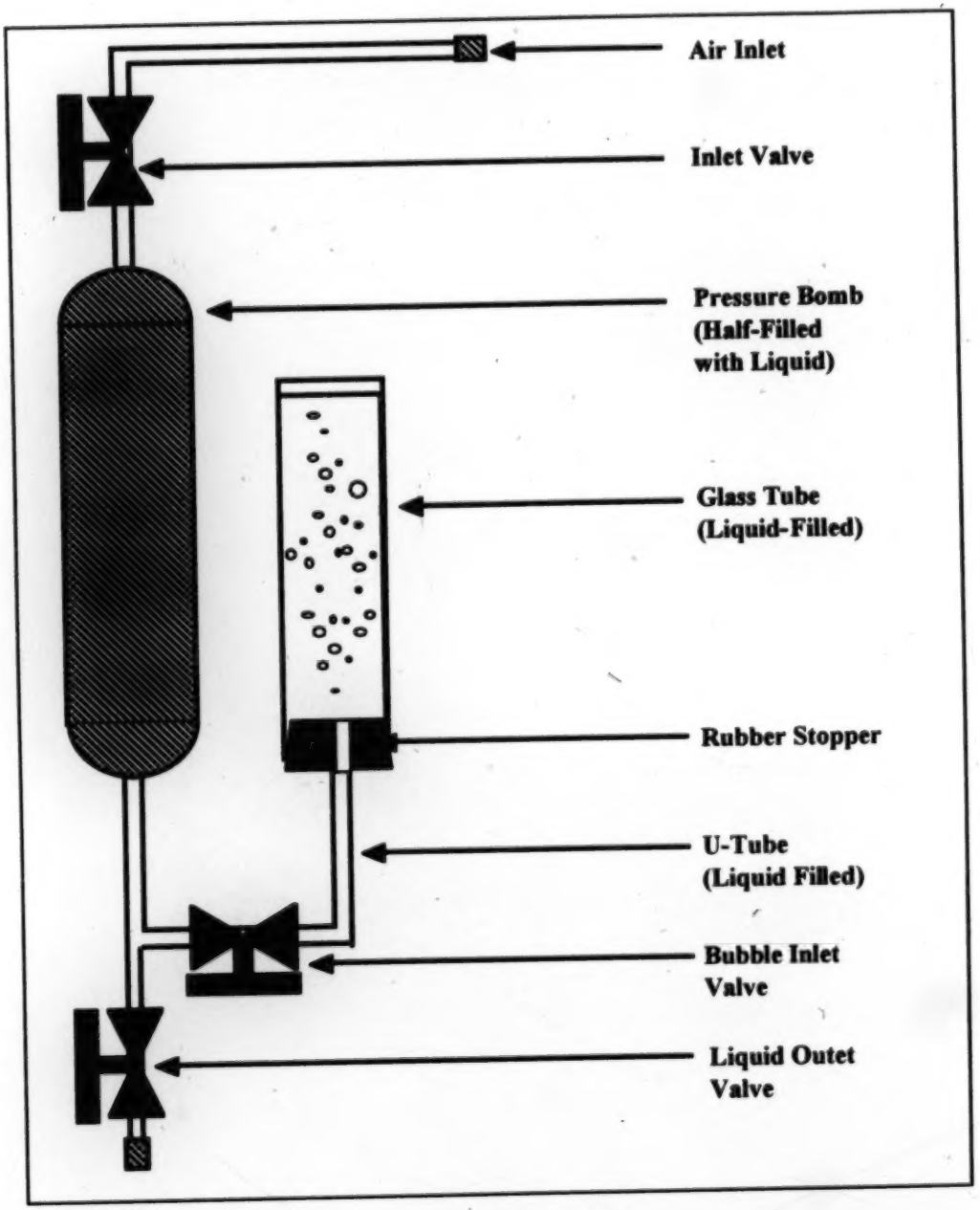

Figure 3.5 **Equipment Used to Form Bubbles by Pressurized Dissolution of Air in Water, Followed by Incremental Pressure Release**

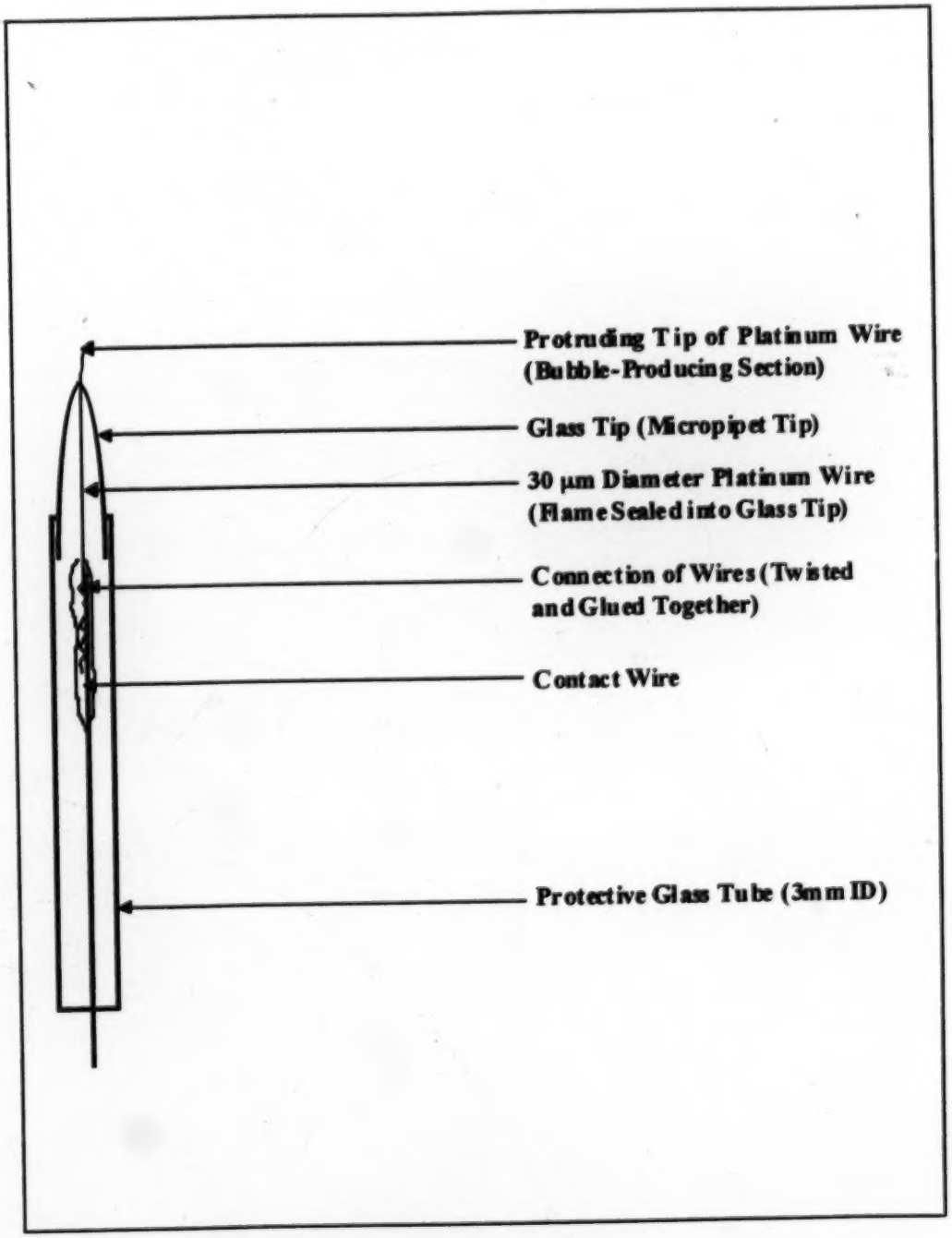

Figure 3.6 **Bubble-Producing Platinum Wire Electrode**

To test the electrodes, a rectangular Plexiglas column was constructed. The column was 30 cm in height and had two ports drilled into one side. These were located respectively at 3 cm and 6 cm above the base. Two platinum wire electrodes were fitted into these ports and connected in series to a direct current power supply. The column was filled with RO water and short 20 second bursts of 10 V were applied. Under these conditions, the electrodes produced a smooth stream of bubbles.

Observations through a microscope showed that bubbles as small as 7 μm in diameter were being formed. Unfortunately, an excess of large (50 to 200 μm) diameter bubbles were also being produced. The large bubbles tended to release sporadically from the platinum wire and disturbed the motion of the smaller, more suitable bubbles. In the presence of 0.01 M NaCl, the electrodes emitted bubbles more vigourously than in "pure" water. It also appeared that a greater proportion of oversized bubbles were being released. Evidently, while electrolysis was a promising method, some additional measures had to be implemented.

One option was to add a surfactant to the system. It should be noted, however, that the presence of a cationic or anionic surfactant can influence the sign and magnitude of the zeta-potential measurements (Okada et al., 1990; Kubota and Jameson, 1993). Nonionic surfactants can also influence the magnitude of the zeta-potential, but to a much lesser extent (Okada, 1990). For this reason, the choice of a surfactant had to be limited to a nonionic type. Triton-X 100 (Fisher Scientific), a common brand of nonionic surfactant, was found to be very effective at inhibiting large bubbles from appearing.

An alternative method was to pretreat the liquid by driving off dissolved gases. Mass transfer theory predicts that a bubble released into a partially degassed liquid should shrink more quickly than a bubble in a liquid saturated with gas. A simple shrinking sphere model was used to approximate the behaviour of oxygen and hydrogen bubbles in water. To begin the algorithm, the bubble diameter was set to 1×10^{-4} m, and the amount of the given gas in water was set to 25, 50, 75, or 100 percent of the saturation concentration. The saturation concentration was estimated by Henry's Law. The mass transfer of gas into the liquid phase was calculated by Equation 3-2, whereby the mass transfer coefficient, k_L, was estimated by correlations. Details are provided in Appendix 3-2. Figures 3.7, 3.8, and 3.9 show samples of the results.

(3-2) $$m' = k_L\left(C_{G,S} - C_{G,B}\right)\pi\, d_B^{\,2}$$

where m' is the rate of mole transfer from the bubble to the bulk liquid (kmol/s)
k_L is the mass transfer coefficient (m/s),
$C_{G,S}$ is the molar concentration of gas at the bubble surface (kmol/m^3), and
$C_{G,B}$ is the molar concentration of gas in the bulk solution (kmol/m^3).

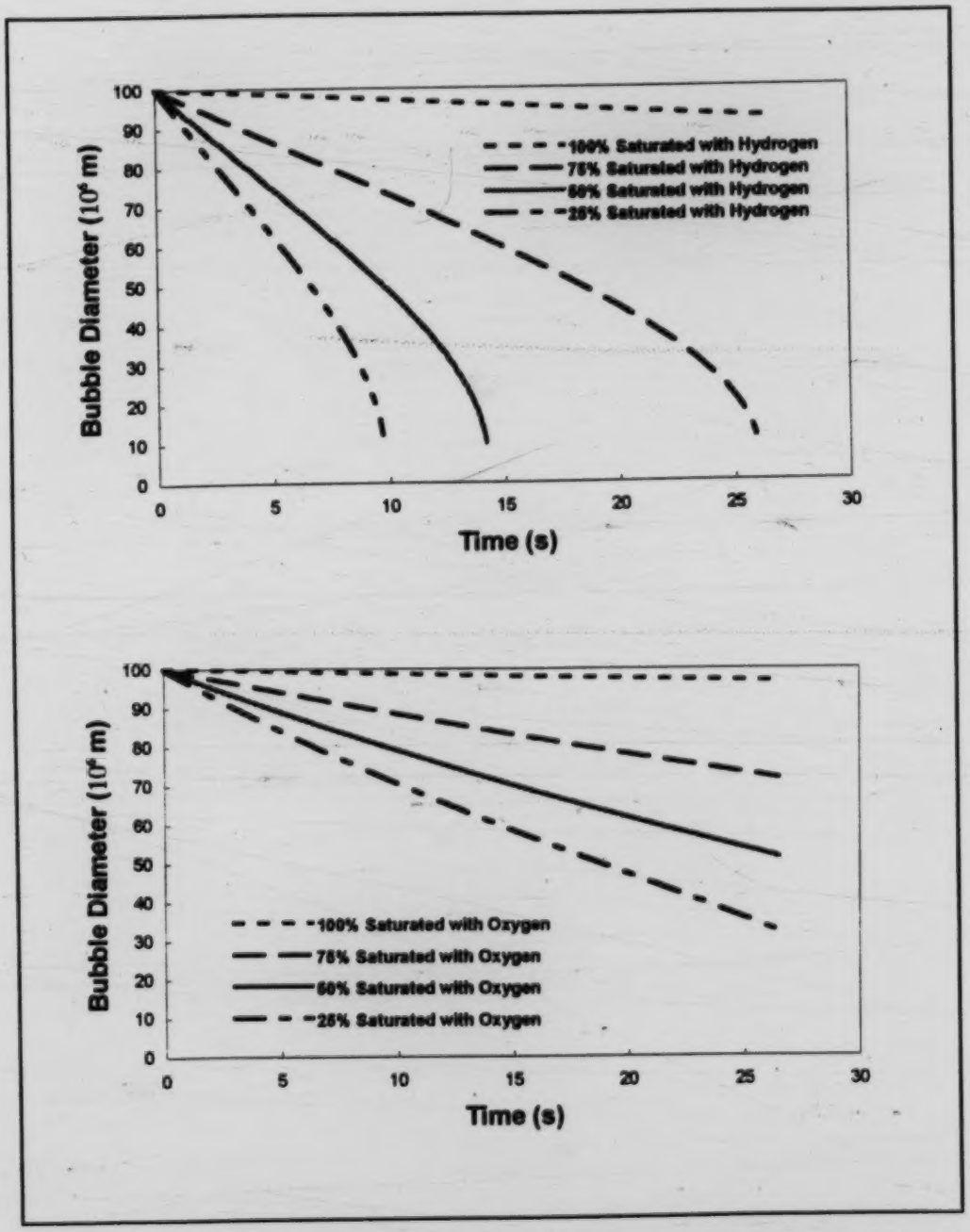

Figure 3.7 **Calculated Shrinkage of Oxygen and Hydrogen Bubbles in Partially Degassed Water**

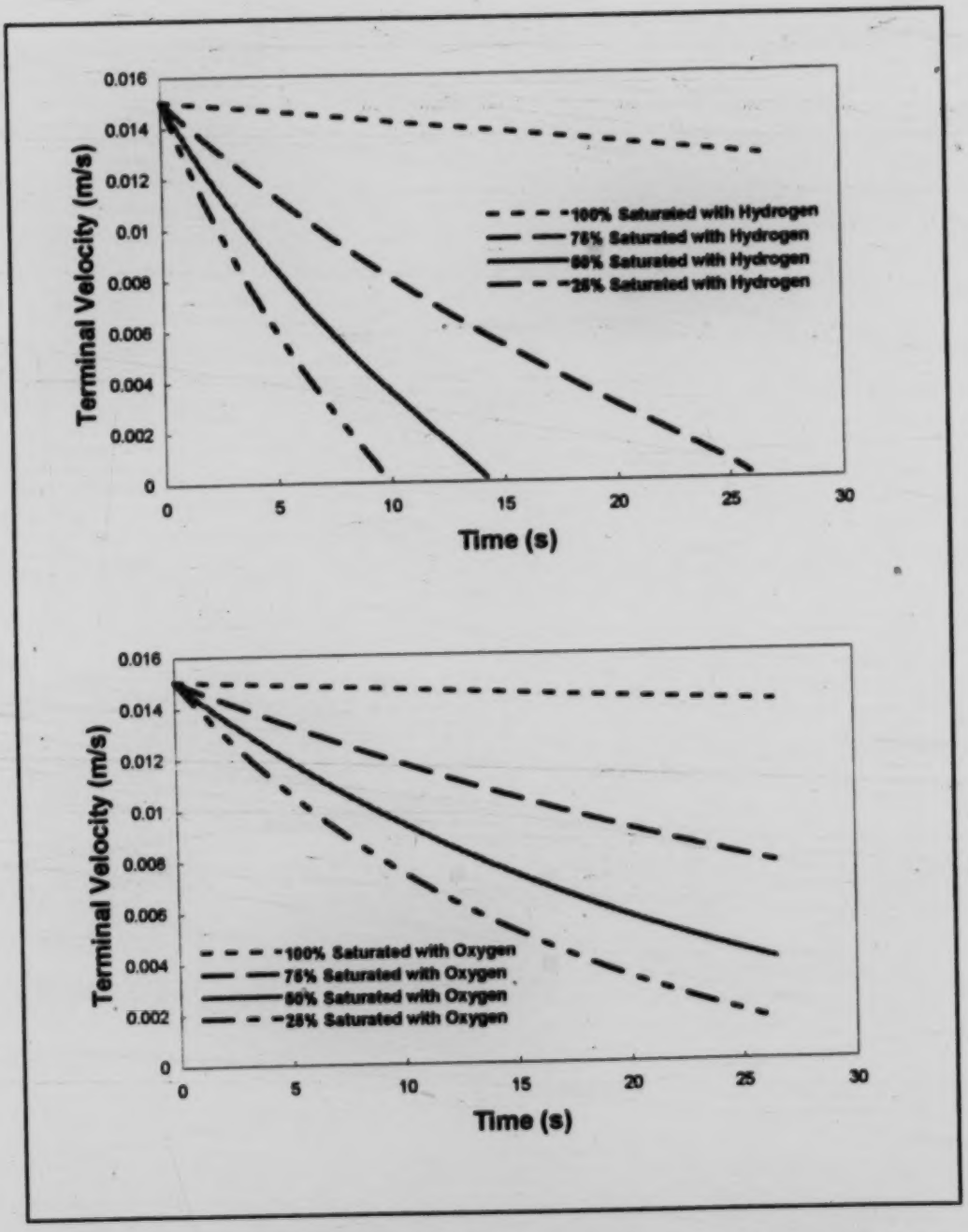

Figure 3.8 **Calculated Terminal Velocities of Hydrogen and Oxygen Bubbles in Partially Degassed Water**

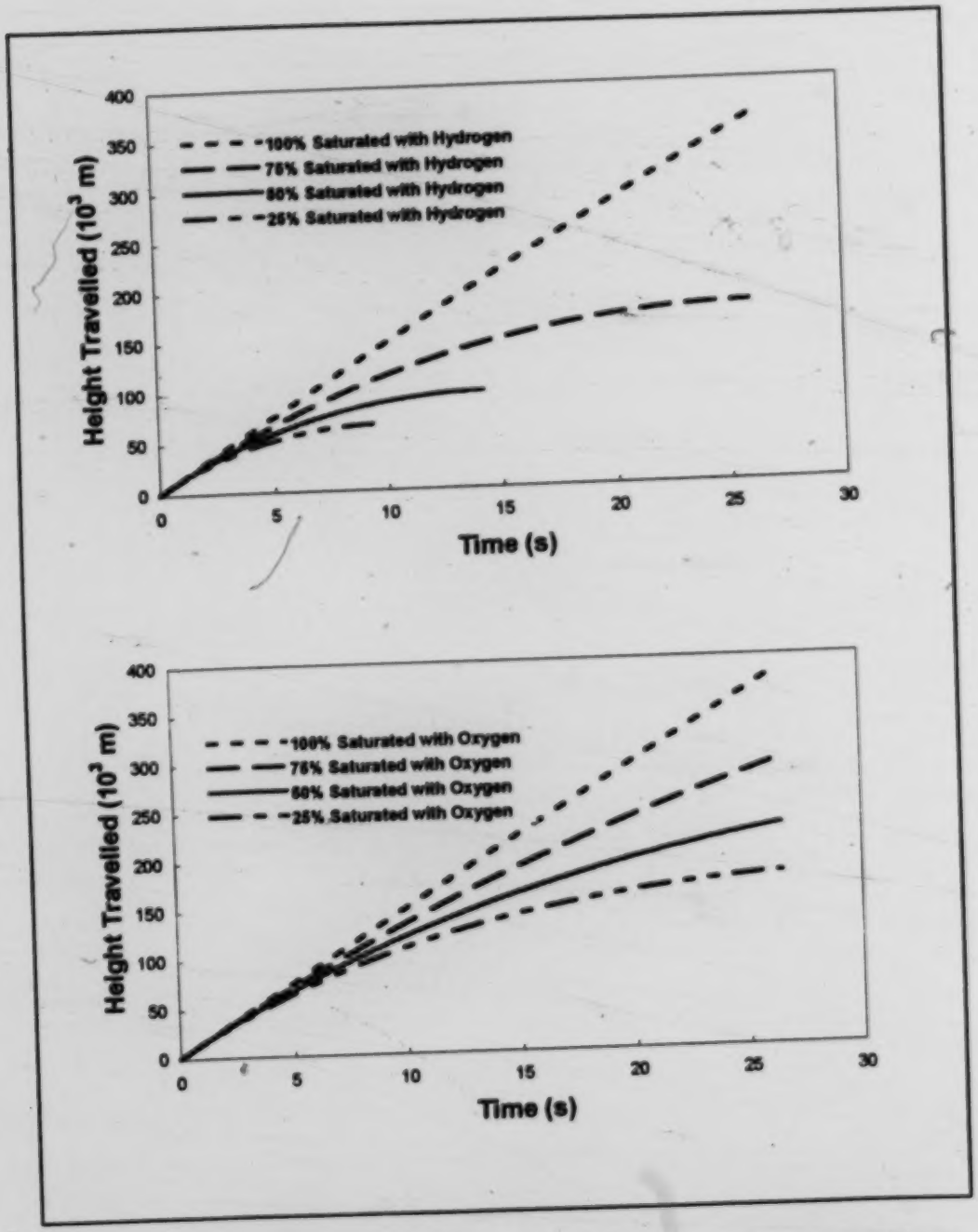

Figure 3.9 **Calculated Height Gain of Hydrogen and Oxygen Bubbles in Partially Degassed Water**

In practice, the simplest way to drive dissolved gases from RO water was to boil the water vigorously for several minutes. The water was then transferred to a volumetric flask, which was tightly sealed and cooled to room temperature. It was found that the water had to boil properly for at least five minutes for this method be effective. Upon opening the flask, the water would remain usable for about one day.

The effect of degassing was clearly visible when tested in the rectangular Plexiglas column. The RO water was vigorously boiled in a kettle for five minutes, and then cooled as described in the previous paragraph. Bubbles leaving the cathode (hydrogen) disappeared at 3 to 4 cm above the bubble-producing electrode. Bubbles leaving the anode (oxygen) disappeared within 8 to 10 cm. This difference in shrinkage rates was predicted by the stepwise integration model. Obviously, this rapid shrinkage rate was unacceptable for electrophoresis, as the bubbles would disappear long before reaching the electrophoresis cell. A simple resolution was found by mixing degassed water with untreated (presumably saturated) RO water. After several trials, it was determined that a mixture containing 50% degassed water and 50% RO water was suitable.

3.4 SUMMARY

Creating small bubbles for electrophoretic measurements is no trivial task. Stokes Law and the Helmholtz-Smulochowski Equation predict that a comparable ratio between vertical and horizontal (electrophoretic) velocities can only be achieved with a bubble that is no larger than 17 μm in diameter.

Two methods of generating small bubbles were tested. In the first method, gas was dissolved into water at an elevated pressure and then released when the pressure was reduced slightly. The technique was not very effective because the produced bubbles included many that were too large.

The second method, electrolysis, was found to be more effective, so long as either a surfactant was present, or the solution was partially degassed. It was elected to use a degassed liquid and omit the presence of surfactant. This decision was made to keep the solution as chemically "pure" as possible.

Observations showed that bubbles could be produced with diameters as small as 7 μm. However, when the image was magnified by the microscope (300×), even bubbles of this size tended to move swiftly across the field of view. Evidently, further measures had to be taken to slow the apparent rate of bubble ascent. At this point, the emphasis of the design shifted away from bubble generation, to making modifications to the electrophoresis cell itself.

CHAPTER 4 THE ELECTROPHORESIS CELL

4.1 SCOPE OF THE PROBLEM

In Chapter 3, a method for producing very small bubbles was developed. The platinum wire electrode, coupled with a partially degassed solution, was capable of making bubbles whose diameters ranged from 7 μm to 30 μm in diameter. However, even these bubbles moved too quickly across the view field to make an adequate electrophoresis measurement.

Many researchers had encountered the same difficulty. Most resorted to lowering the cell assembly downward at a rate comparable to the bubbles' upward motion (Fukui and Yuu, 1982; Collins et al., 1978; Okada et al., 1990). In this way, the bubbles' apparent motion relative to the viewer appeared to be either stopped or at least slowed significantly. McShea and Callaghan (1983) chose to keep their bubbles "immobile" with a spinning cylinder technique. Still others dispensed with electrophoresis altogether and opted to use streaming or Dorn potential methods (Usui et al., 1978; Dibbs et al., 1974).

4.2 PRELIMINARY CELL DESIGN

In the first attempt at bubble electrophoresis, it was decided to use the strategy of moving the cell downward. A rudimentary cell was created to fit with the bubble-making electrodes developed in Chapter 3. Two basic forms were considered for the cell; cylindrical and rectangular. Each shape has its advantages and disadvantages. With the cylindrical shape, the location of the stationary levels can be exactly determined, but the rounded shape produces optical distortions. Compensation for optical distortions have to be built into the design (for example, with an optical flat). Alternatively, only approximate solutions exist for stationary levels in a rectangular cell, but the construction is relatively simple and the optical distortions are less pronounced (Seaman, 1975). Ultimately, the rectangular form was chosen for its comparative simplicity. A diagram of the cell and holder is shown in Figure 4.1.

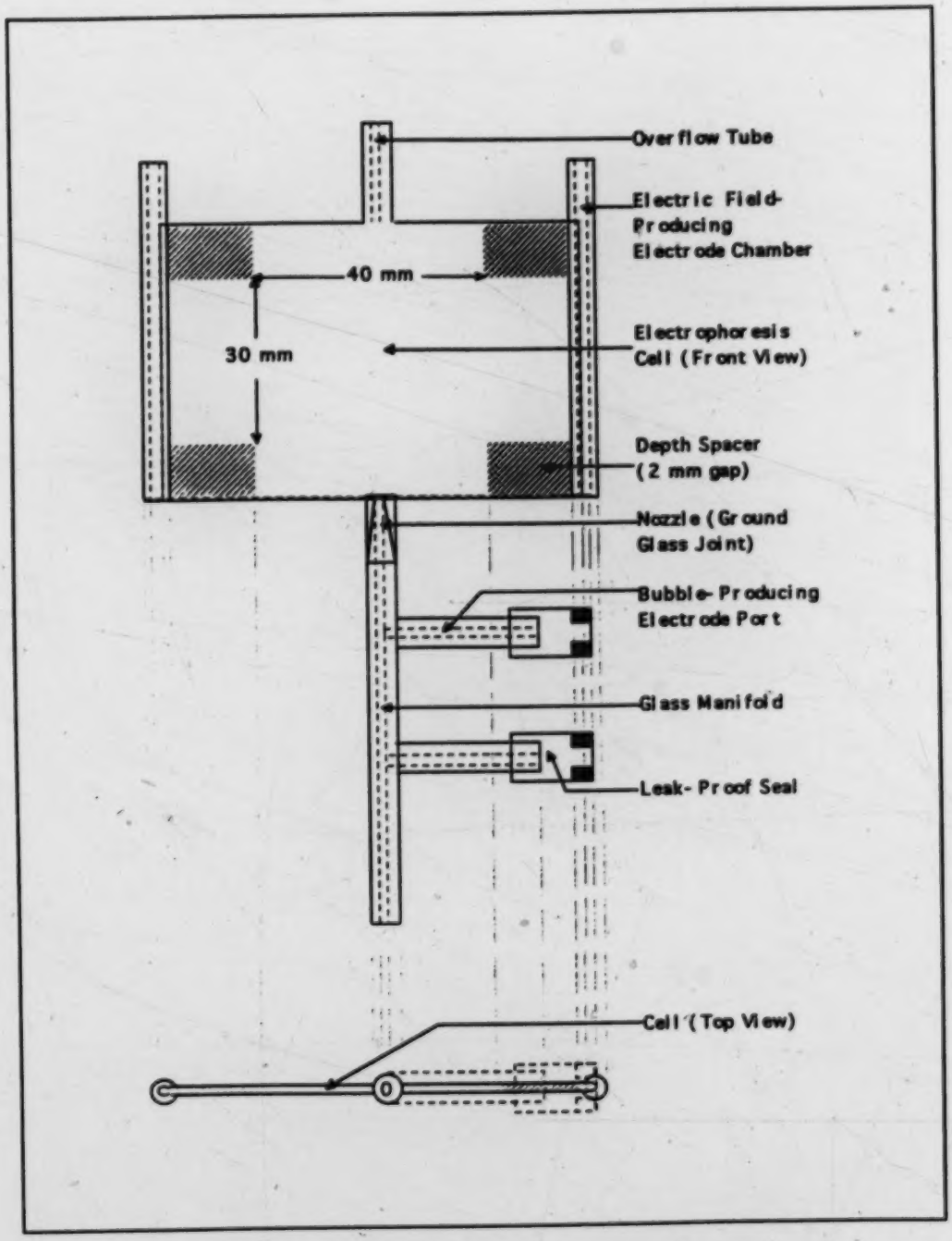

Figure 4.1 **Rudimentary Electrophoresis Cell and Bubble Manifold**

The cell was built by Peter Lea and Associates in the glass blowing shop at the University of Alberta. The walls were constructed from a single sheet of Pyrex glass, so as to keep their surface properties as similar as possible, and thus prevent the formation of a distorted electroosmotic flow profile (Seaman, 1975). The glass had a thickness of 1.2 mm. This was the thinnest glass that was readily available at the time. The entire assembly was held together with a waterproof epoxy resin.

A 2 mm gap was maintained between the sheets by thin Pyrex dividers, located near the corners of the cell. This gap was about twice the internal depth of most electrophoresis cells (Collins et al., 1978; Jameson and Kubota, 1990; Fukui and Yuu, 1978; Spitzer et al., 1981, Okada et al., 1978). Usually, the depth of the cells is made as small as possible to inhibit convection currents from forming. The separation used in our cell was the smallest possible gap that could be made without compromising the structural strength.

The chosen width of the cell was 80 mm. Literature studies recommend a width-to-depth ratio of at least twenty to one, so as to minimize the impact of the side walls (Seaman, 1975; Fukui and Yuu, 1978). In our case, this required the width between the spacers to be at least 40 mm.

The height of the cell was determined by estimating as follows. The terminal velocities of gas bubbles ranging from 10 to 200 μm in diameter were estimated by Stokes Law (see Chapter 3, Figure 3.1 and Appendix 3-1). It was then assumed that at least five seconds were needed to make a proper electrophoretic measurement. With these assumptions in place, it was determined that a bubble of 200 μm diameter would travel vertically at 6 mm/s over a distance of 30 mm. In consequence, the cell was designed to allow at least 30 mm of height between the spacers.

Cylindrical chambers, to house the electric-field-producing electrodes, were constructed from two glass capillaries. These electrodes are discussed in Chapter 5. The capillaries had internal diameters of 2 mm. Long vertical slits were cut into the tubes so that they fit like sleeves around the sides of the cell.

An opening was made at the top of the cell to prevent gas from accumulating above the liquid. A hole was also made at the cell bottom to allow the gas bubbles to enter from the glass manifold. This manifold, also depicted in Figure 4.1, was designed to house a bubble-producing electrode and a counter-electrode. The electrodes were inserted into the appropriate ports and held in place by water-tight sleeves. The manifold itself was attached to the cell by a ground glass male/female joint. Teflon tape was wound around the male joint to ensure a snug fit in the socket. Just as with Okada's apparatus (1988), the nozzle was an important feature which blocked large bubbles from entering the cell. As a further precaution, the connection as made water and air tight by smearing several layers of rubber cement on the outside.

The entire cell and manifold were mounted onto a motorized stand, donated by the Alberta Research Council. The cell was mounted onto the vertical metal plate, and held in place by elastic straps. This vertical portion contained an opening to allow light to pass through and illuminate the cell. The movable platform, shown in Figure 4.2, was propelled by a motor-mike and pulley system. However, this setup had barely enough power to move the cell fast enough to keep up with the bubbles. This made the operator's task of simultaneously controlling the motor control and the electric field, a cumbersome and difficult feat to accomplish.

In consequence, a new approach had to be undertaken. In the new approach, the cell was to remain fixed while the solution was to flow slowly downward. The liquid flowrate would be adjusted by a needle valve to "hold" the bubbles within the viewing field. This method could allow the operator to "trap" a bubble at one height before having to deal with the other aspects of electrophoretic measurement. The concept is illustrated by Figure 4.3.

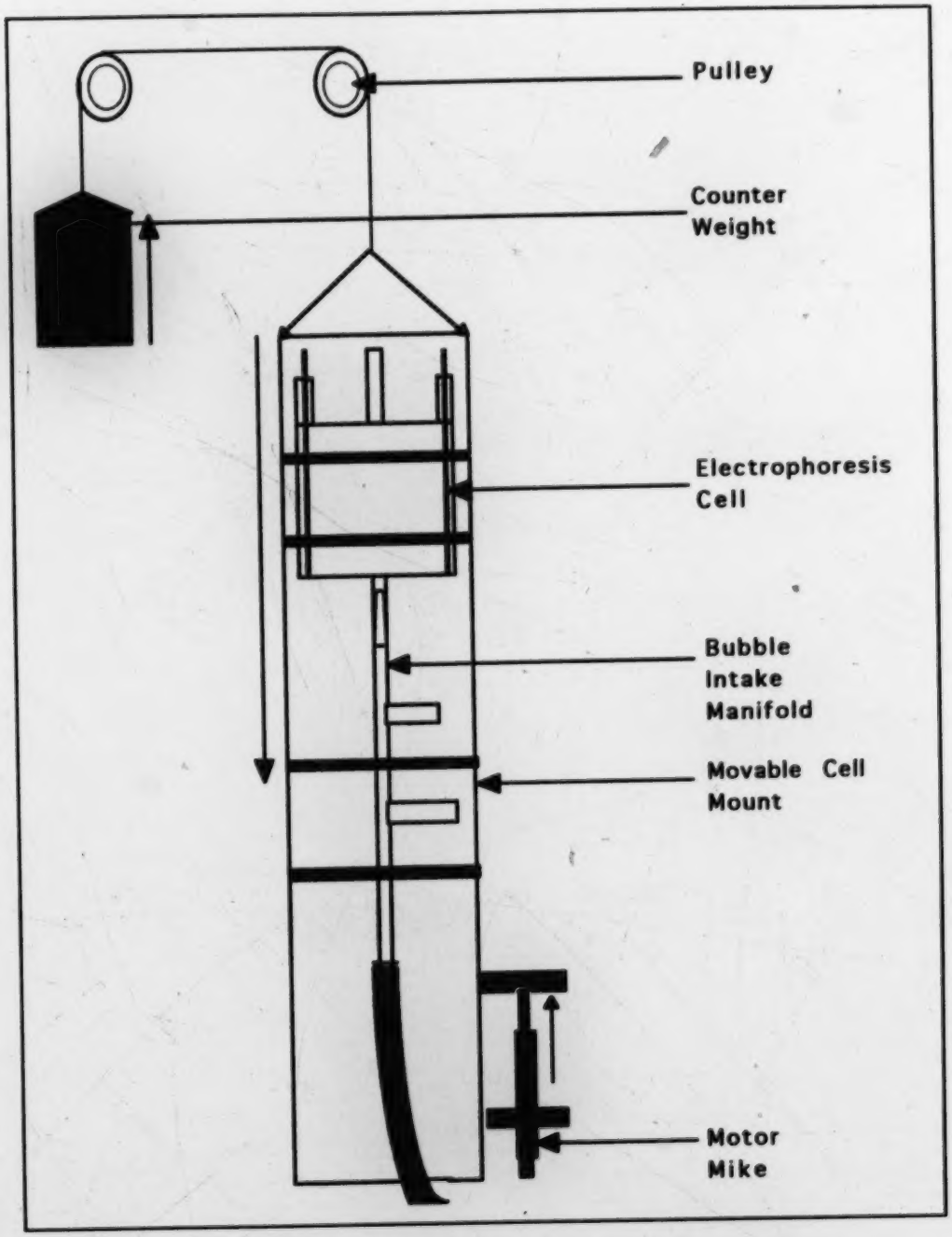

Figure 4.2 **Preliminary Cell Mounted onto Motorized Adjustable Stand**

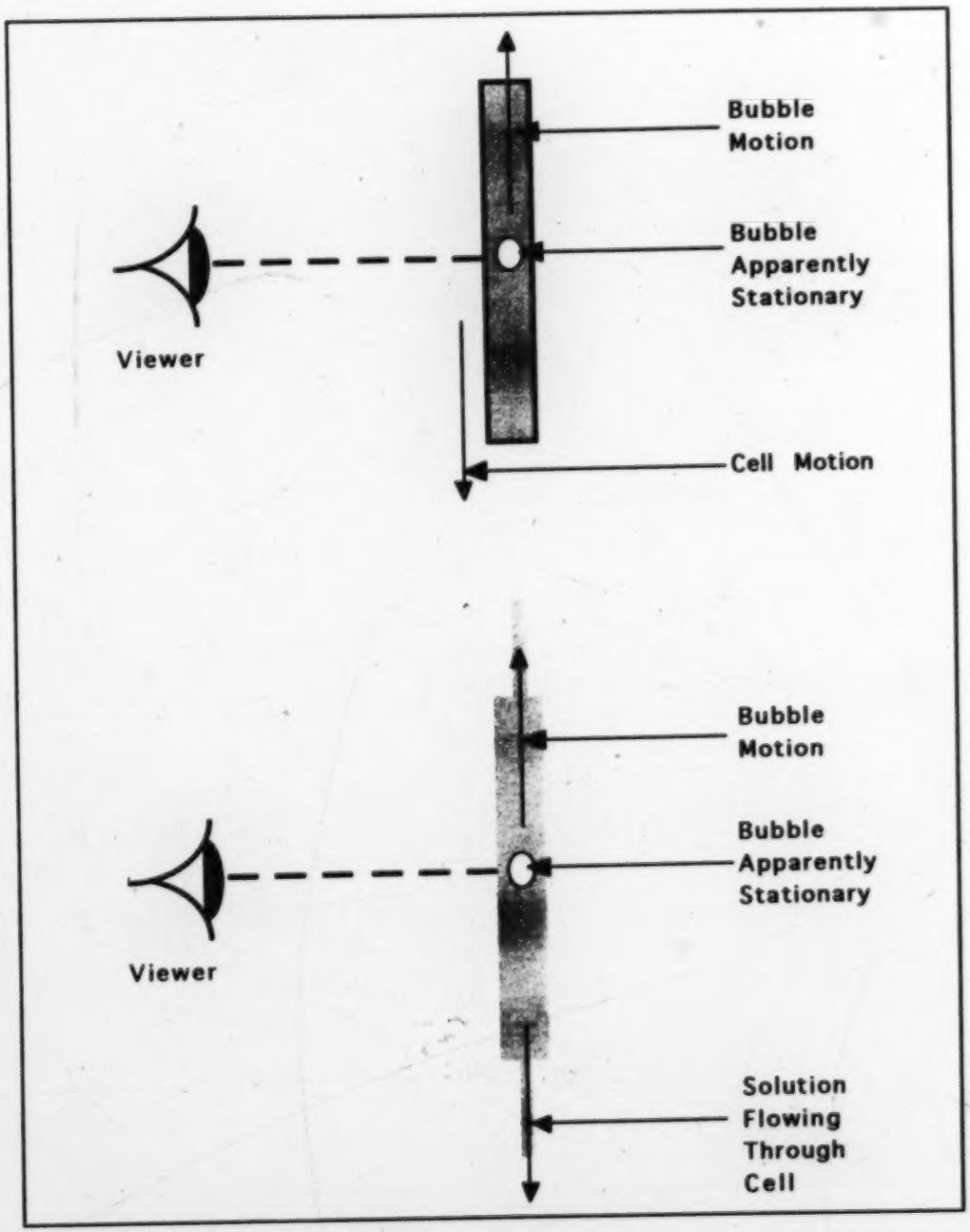

Figure 4.3 **Illustration of "Flow-Through" Concept**

4.3 THE "FLOW-THROUGH CELL"

4.3.1 Cell Design

The main challenge to this "Flow-through" concept was to prevent liquid flow disturbances from interfering with the electrophoretic effects. This issue was particularly critical in the expansion and contraction zones near the top and bottom of the cell. There were two possible solutions to this problem. The first approach was to lengthen the cell such that the inlet and outlet disturbances would not extend into the electrophoresis area. The second approach was to taper the inlet and outlet so as to create a gradual change of width. This latter idea was discarded because a tapered cell would have been impractical to construct.

The new cell's depth was maintained at 2 mm, but the width was reduced to 6 cm. The reduction in width was made to lessen the burden on the electric-field generating electrodes, while still maintaining the recommended twenty-to-one width to depth ratio.

The question that now remained was how long to make the new cell. Fortunately, computer flow simulations provided the means to resolve the issue. FLOW-3D proved to be an invaluable tool in the design of the new cell. The program gave solutions to mass and momentum balances for the chosen cell geometry. The cell was modeled as a rectangular duct with the inlet and outlet located at the center of the top and bottom respectively. The duct had dimensions of 60 mm by 180 mm by 2 mm. A right-handed coordinate grid was imposed onto the structure. The origin was located in the center of the duct, and the width, depth, and height of the cell were respectively defined by the w, x, and y axes. Movements from left to right were considered positive, as did motion from bottom to top, and from back to front. The coordinate system is depicted in Figure 4.4. The solution was modeled as an incompressible Newtonian fluid with the properties of water at 293 K. "No-slip" boundary conditions were imposed at the cell walls.

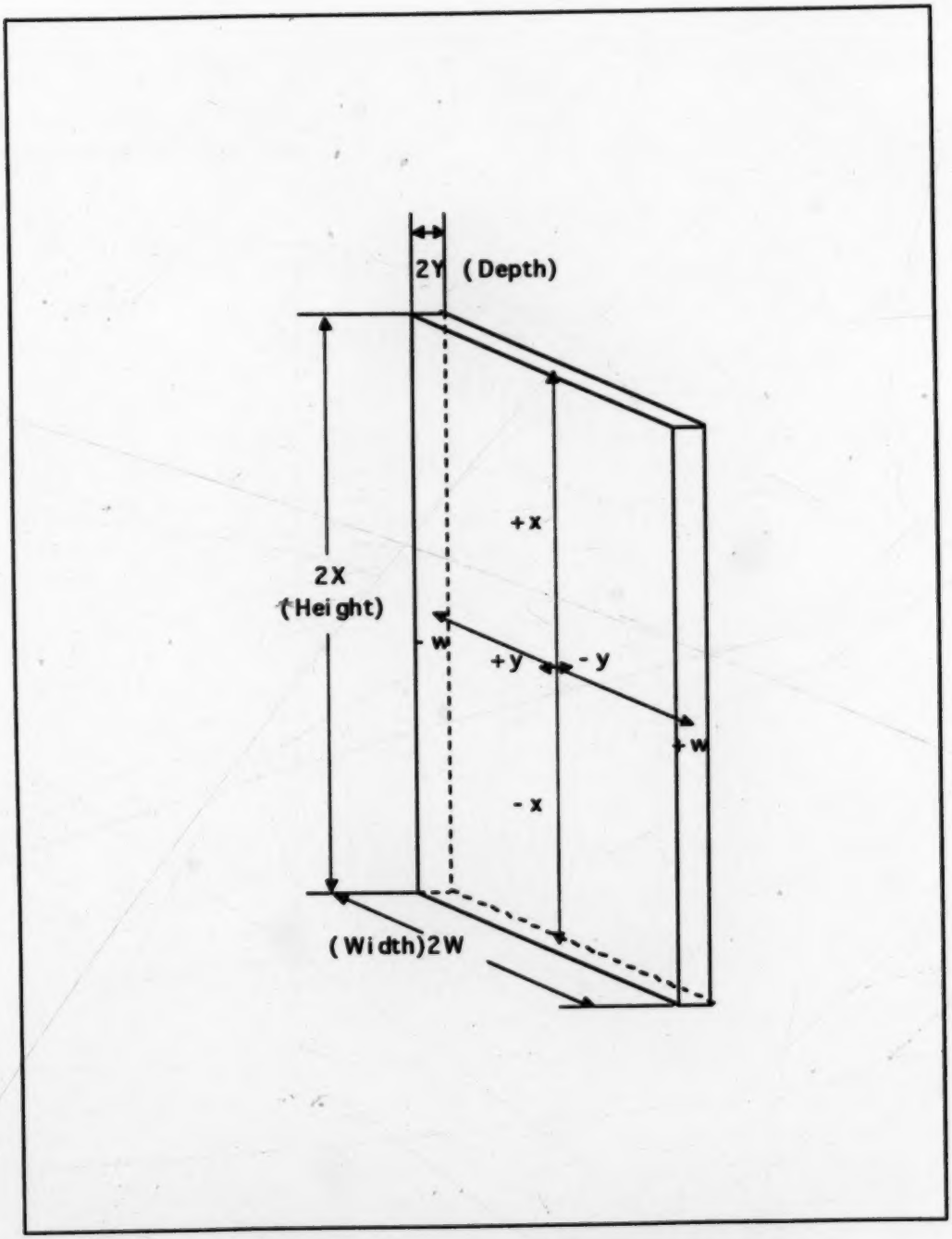

Figure 4.4 **Coordinate System Used for Computer Flow Simulations**

Before any simulations could be made, it was necessary to establish a reasonable range of inlet flowrates. To do so, the terminal velocities of bubbles of diameters 5 μm to 25 μm were calculated using Stokes law (see Appendix 3-1). The bubbles were assumed to be moving up the front stationary level, located at 21% of the cell's depth, as measured from the front wall (see chapter 2, Figure 2.7). In order to vertically "immobilize" bubbles in this size range, the down-coming liquid velocity at the stationary level had to equal that of the rising bubbles. It was further assumed that the liquid flow profile along the x-y plane was laminar (confirmed by calculating the Reynolds number of the fluid). Using this information, the average liquid velocities and the flowrates were estimated using the following equations:

(4-1) $$U_{T,bubble} = -U_{T,liquid}$$

(4-2) $$U_{T,Avg} = \frac{2U_{T,liquid}}{3\left(1-\frac{y^2}{Y^2}\right)}$$

(4-3) $$Q_{liquid} = U_{T,Avg} \times (2Y) \times (2W)$$

where $U_{T,bubble}$ is the terminal velocity of the bubble (m/s),
$U_{T,liquid}$ is the velocity of the liquid at the stationary plane (m/s),
$U_{T,avg}$ is the average liquid velocity (m/s),
Q_{liquid} is the liquid flowrate (m^3/s),
Y is half the depth of the cell (m), and
W is half the width of the cell (m).

The simulation program required inlet conditions to be specified in terms of liquid velocities. The inlet velocity inputs were determined by first calculating the working range of bubble terminal velocities. The down-coming average liquid velocities were then assigned the same values, but in the opposite direction. These values were multiplied by the cross sectional area of the cell to derive the flowrates. These, in turn, were divided by the cross sectional area of the inlet to arrive at the inlet velocities. The calculations are depicted in Table 4.1.

Table 4.1 Calculation of Inlet Velocity Range for Computer Simulations

Liquid Viscosity:	0.001 Pa s
Liquid Density:	1000 kg/m^3
Gas Density:	~0 kg/m^3
Gravitational Constant:	9.8 m/s^2
Cell Width	6×10^{-2} m
Cell Depth	2×10^{-3} m
Inlet Width	2×10^{-3} m
Inlet Depth	2×10^{-3} m

Bubble Diameter[1] (μm)	Bubble Terminal Velocity[2] (m/s)	Liquid Velocity[3] At Stationary Level (m/s)	Average (m/s)	Reynolds Number for Liquid[4]	at Inlet (m/s)	Liquid Flowrate (m^3/s)
0.5	1.4×10^{-7}	-1.4×10^{-7}	-1.4×10^{-7}	2.7×10^{-4}	-4.3×10^{-4}	1.7×10^{-11}
5[5]	1.4×10^{-5}	-1.4×10^{-5}	-1.4×10^{-5}	2.7×10^{-2}	-4.3×10^{-4}	1.7×10^{-9}
10	5.5×10^{-5}	-5.5×10^{-5}	-5.5×10^{-5}	1.1×10^{-1}	-1.6×10^{-3}	6.6×10^{-9}
20	2.2×10^{-4}	-2.2×10^{-4}	-2.2×10^{-4}	4.3×10^{-1}	-6.5×10^{-3}	2.6×10^{-8}
30	4.9×10^{-4}	-3.4×10^{-4}	-3.4×10^{-4}	9.8×10^{-1}	-1.0×10^{-2}	4.1×10^{-8}

(1) Bubble assumed to rise up stationary level (at $y = \pm 5.8\times10^{-4}$ m)

(2) Calculated using Stokes Law for $Re < 1$.

(3) Convention dictates that motion in downward direction be considered as negative.

(4) Calculated with average velocity of liquid.

(5) Expected "normal" range of usable bubbles is from 5 μm to 30 μm.

4.3.2 Computer Simulations of Flow Patterns

Sample computer outputs are shown in Figures 4.5 to 4.9. The figures present cutaway views of the cell at the vertical plane, $y = 0$ (crossing through the midpoint of the cell depth). The contours represent liquid velocity vectors in the horizontal (w) direction, in the absence of any electrical forces. The white segments at the top and bottom are areas where the horizontal velocity exceeds 0.5 μm/s (except in Figures 4.8 and 4.9, in which the top and bottom white segments are areas in which the horizontal velocity exceeds 5, and 10 μm/s, respectively). These represent the developing regions of flow. Within these areas, the magnitude of horizontal flow would have interfered with the electrophoretic motion of the bubbles. The "usable region" was defined to extend from the lowest point on the upper disturbances to the highest point on the lower disturbances.

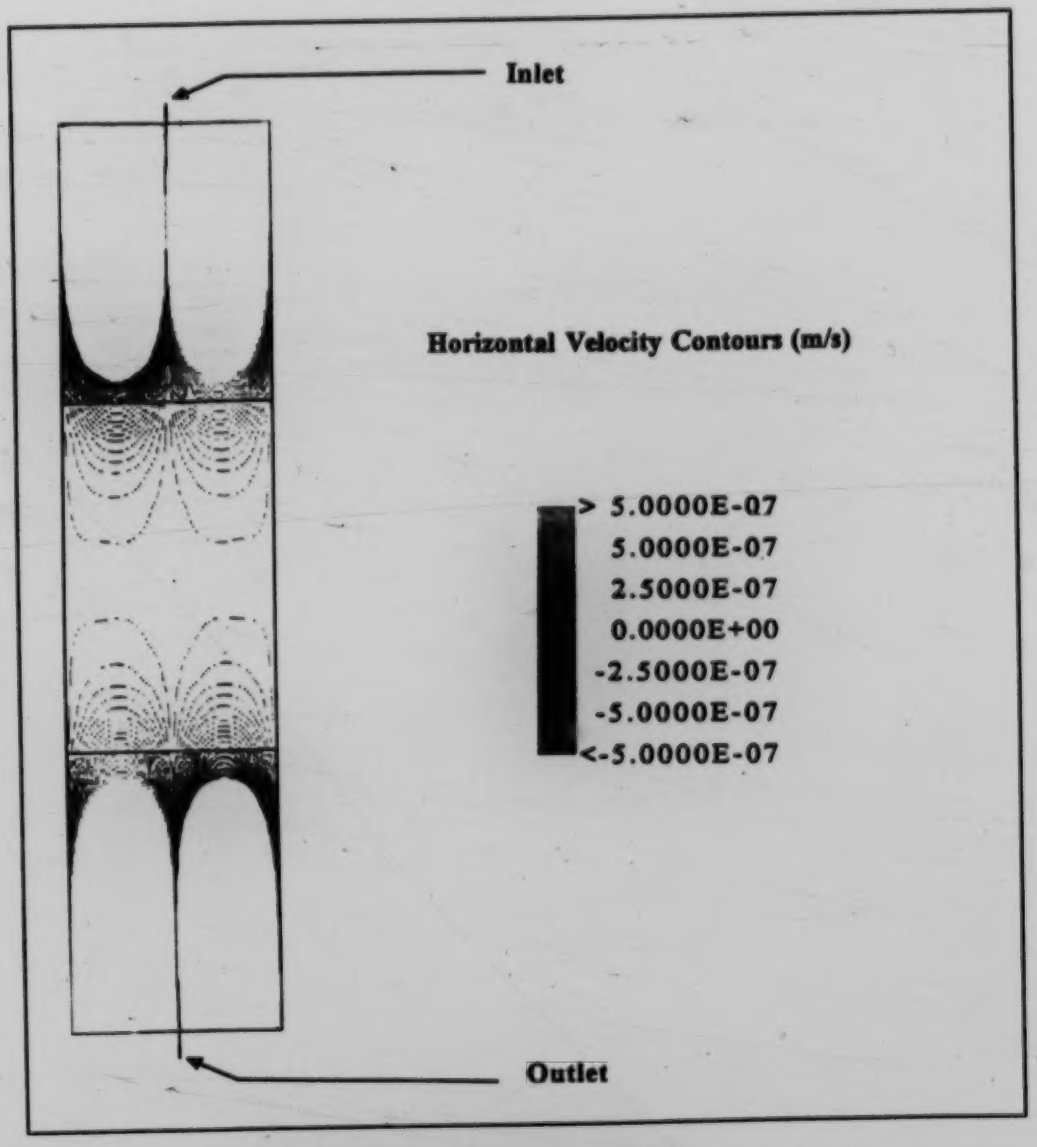

Figure 4.5 **Sample FLOW 3D Output File: m44.fc**
Cutaway View of the Central Plane (y=0)
(Contours represent liquid velocity in the horizontal (w) direction. White areas at the top and bottom show regions where the horizontal velocity exceeds 5×10^{-7} m/s.)
Inlet width = 2.07×10^{-3} m; liquid inlet velocity = 5×10^{-3} m/s.
Inlet and outlet located at centre line (w=0).

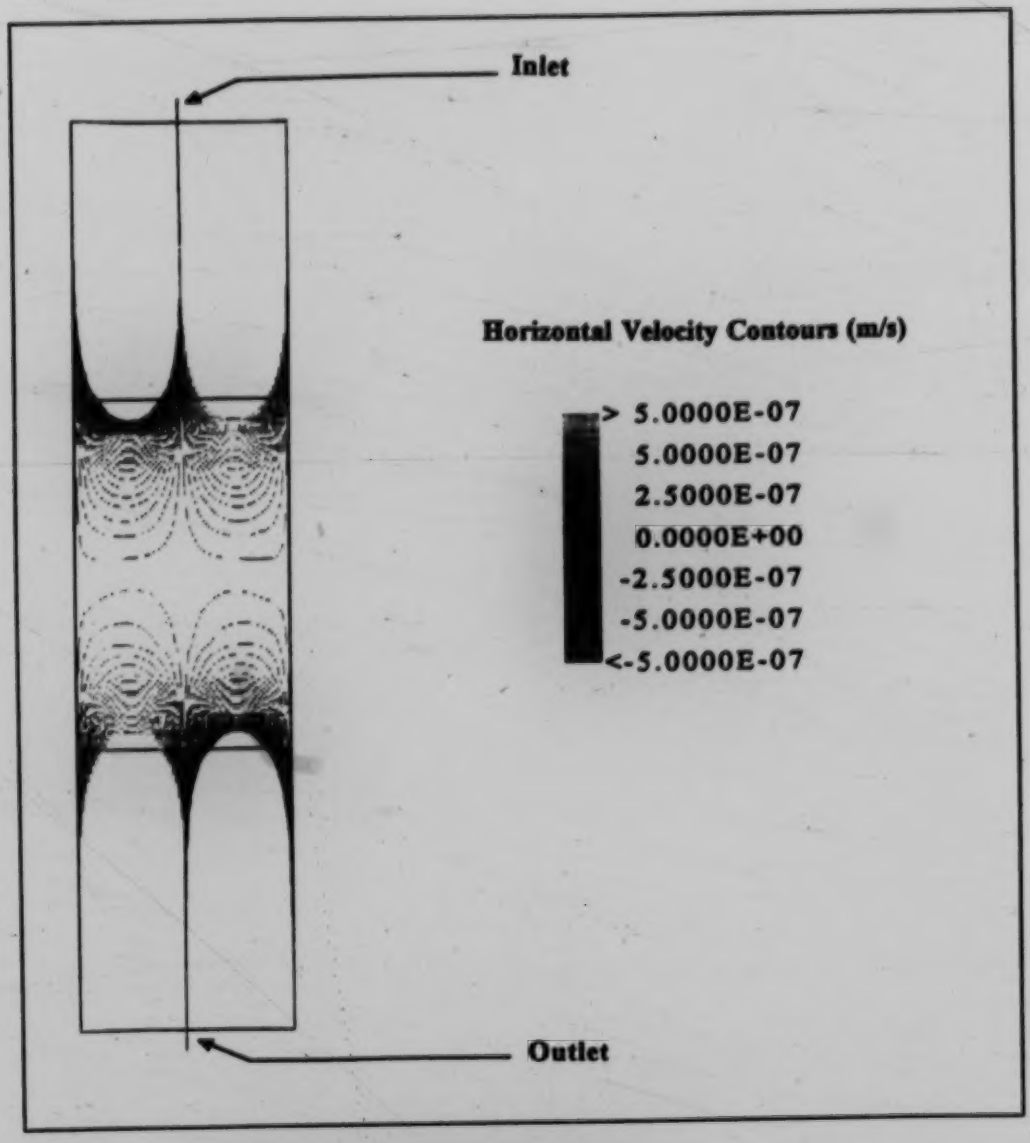

Figure 4.6 **Sample FLOW 3D Output File: m45.fc**
Cutaway View of the Central Plane (y=0)
(Contours represent liquid velocity in the horizontal (w) direction. White areas at the top and bottom show regions where the horizontal velocity exceeds 5×10^{-7} m/s.)
Inlet width = 6.21×10^{-3} m; liquid inlet velocity = 5×10^{-3} m/s.
Inlet and outlet located at centre line (w=0).

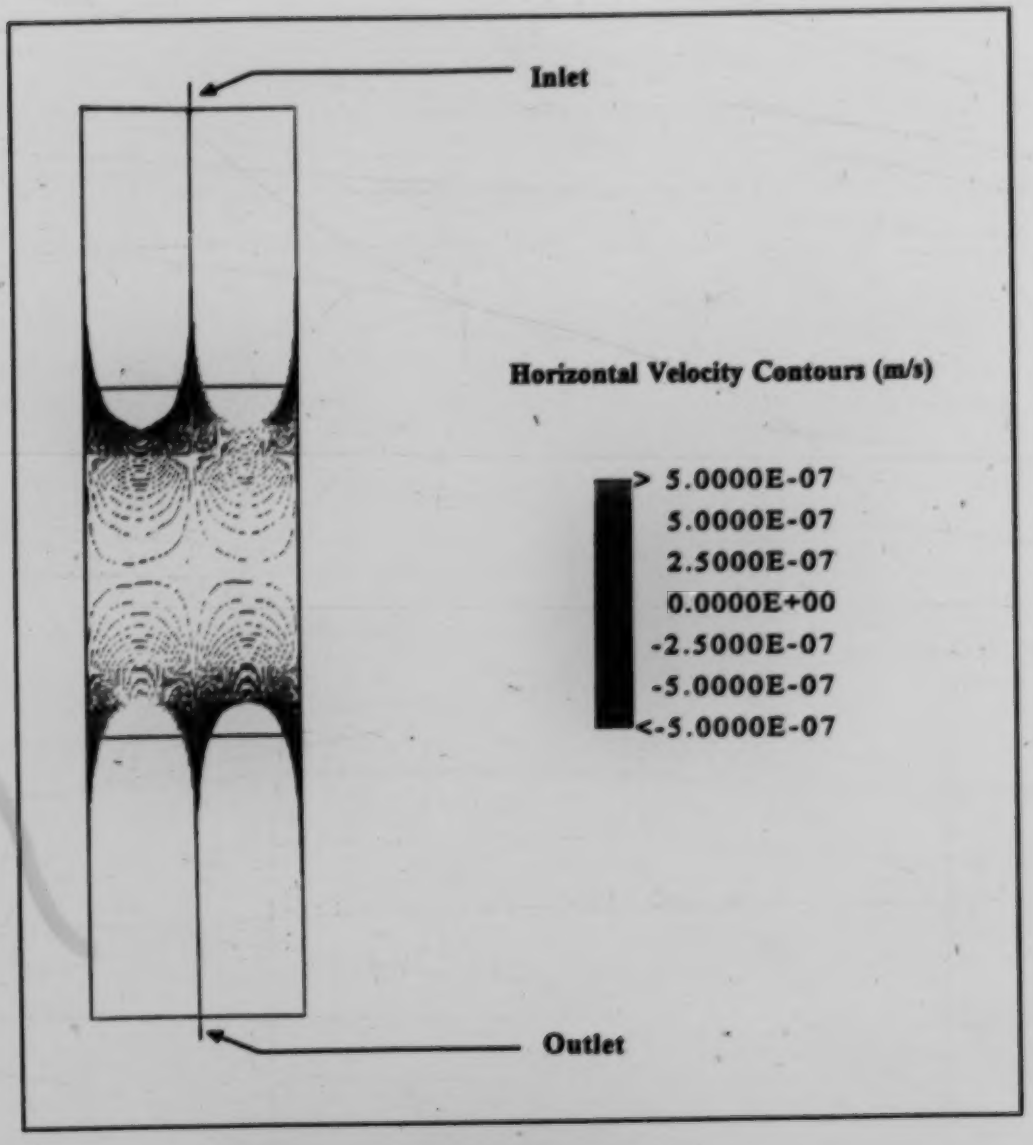

Figure 4.7 **Sample FLOW 3D Output File: m46.fc**
Cutaway View of the Central Plane (y=0)
(Contours represent liquid velocity in the horizontal (w) direction. White areas at the top and bottom show regions where the horizontal velocity exceeds 5×10^{-7} m/s.)
Inlet Width = 10.35×10^{-3} m; liquid inlet velocity = 5×10^{-3} m/s).
Inlet and outlet located at centre line (w=0).

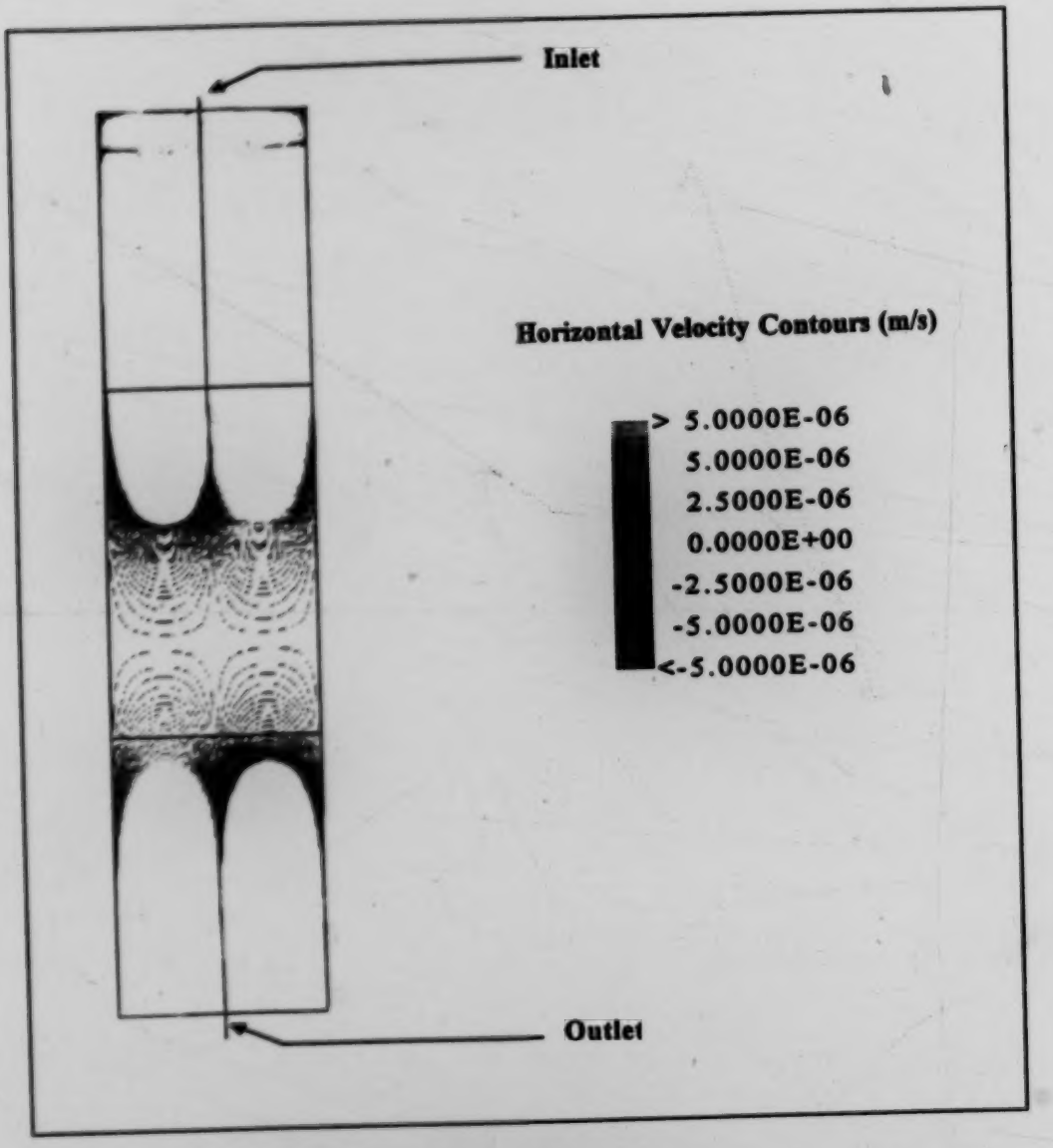

Figure 4.8 **Sample FLOW 3D Output File: m60.fc**
Cutaway View of the Central Plane (y=0)
(Contours represent liquid velocity in the horizontal (w) direction. White areas at the top and bottom show regions where the horizontal velocity exceeds 5×10^{-6} m/s.)
Inlet width = 2.07×10^{-3} m; liquid inlet velocity = 5×10^{-2} m/s.
Inlet and outlet Located at centre line (w=0).

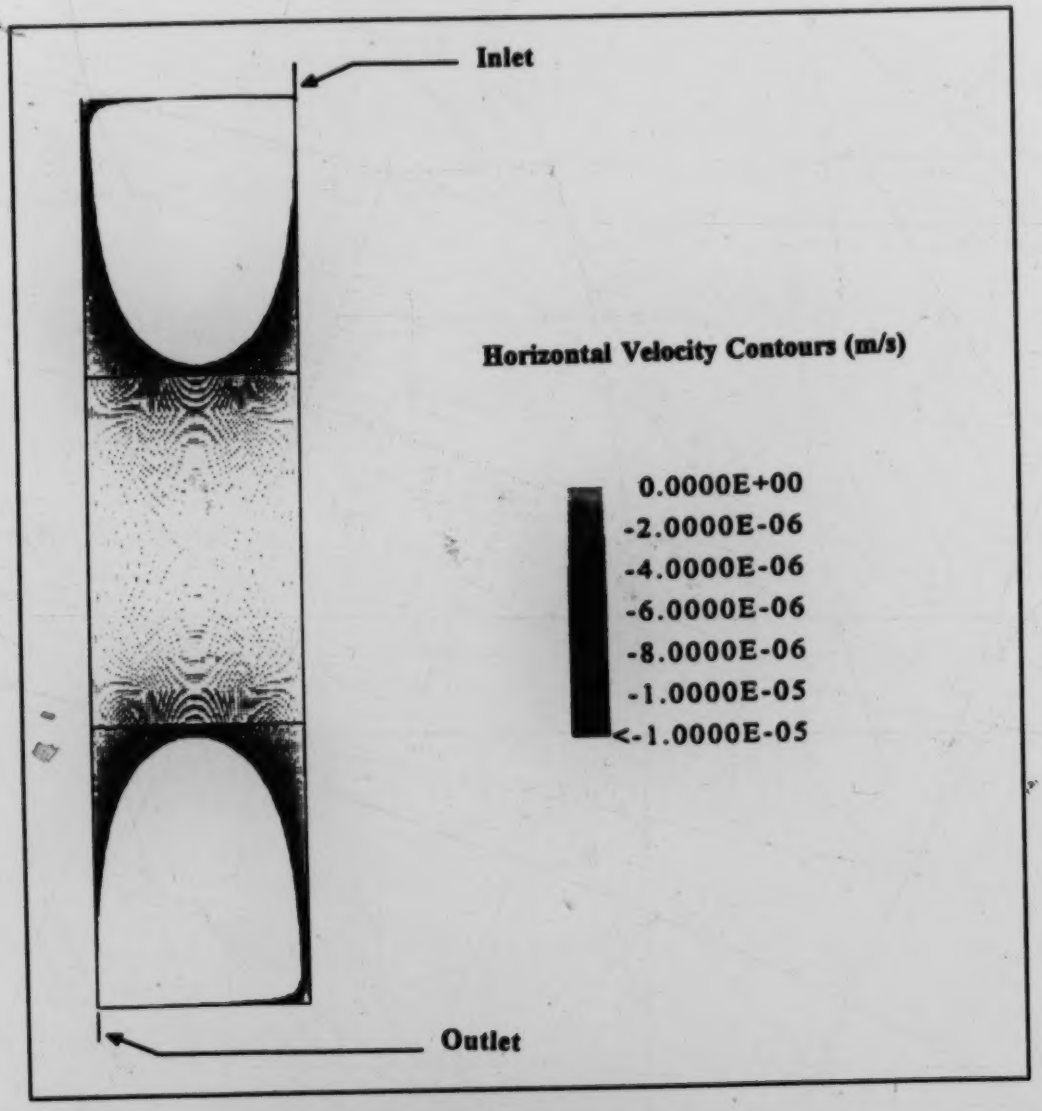

Figure 4.9 **Sample FLOW 3D Output File: m48.fc**
Cutaway View of the Central Plane (y=0)
(Contours represent liquid velocity in the horizontal (w) direction. White areas at the top and bottom show regions where the horizontal velocity exceeds 10×10^{-6} m/s.)
Inlet width = 2.07×10^{-3} m; liquid inlet velocity = 5×10^{-3} m/s.
Inlet and outlet located at opposite corners ($w=+3\times10^{-2}$ m and -3×10^{-2} m, respectively).

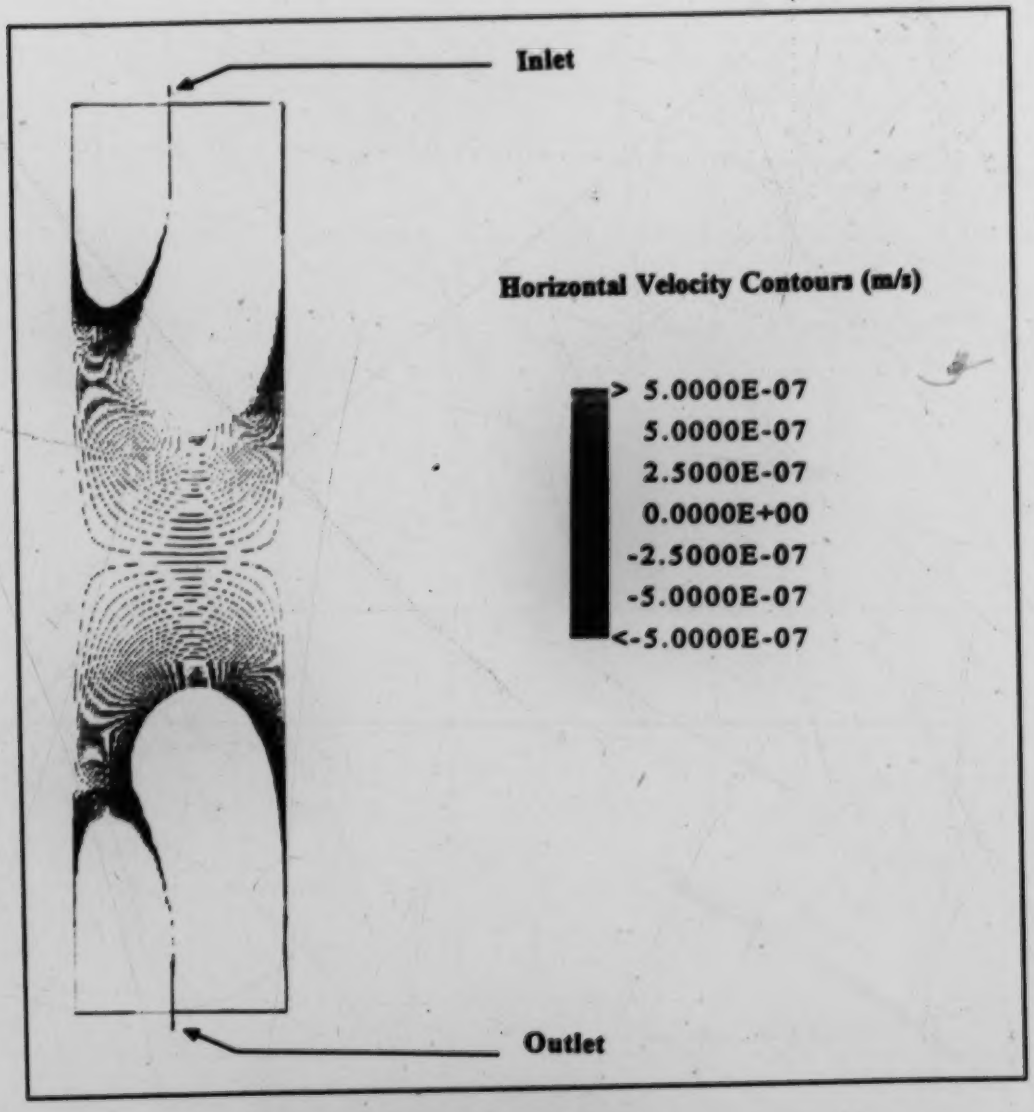

Figure 4.10 **Sample FLOW 3D Output File: m47.fc**
Cutaway View of the Central Plane (y=0)
(Contours represent liquid velocity in the horizontal (w) direction. White areas at the top and bottom show regions where the horizontal velocity exceeds 5×10^{-7} m/s.)
Inlet width = 2.07×10^{-3} m; liquid inlet velocity = 5×10^{-3} m/s.
Inlet and outlet located off centre (both at w=-2.07×10^{-3} m).

The first set of simulations was performed to study the effect of the liquid inlet velocity on cell flow patterns. Figures 4.5 to 4.7 show the effect of increasing the flowrate by widening the inlet (and outlet). The inlet velocity was fixed at 5 mm/s. This corresponded to the flowrate required to stop bubbles ranging from 18 μm to 30 μm in diameter.

The widening of the inlet from 6.2 cm to 10.4 cm had only a minimal effect on the extent of the disturbances. The upper disturbances only increased from 8.6 cm to 9.2 cm, while the lower disturbances only increased from 8.6 cm to 9.0 cm in length.

An extreme case is shown in Figure 4.8. Here, the assigned input velocity and inlet width were 5 cm/s and 2.07, mm respectively. This condition corresponded to the flow needed to stop a bubble of 56 μm in diameter. The usable portion of the cell was considerably reduced in size.

A second group of simulations studied the effect of offset inlets and outlets. Figure 4.9 shows an extreme case of openings at opposite corners. Here, a horizontal flow was formed that spanned across the length of the cell. The strength of flow in the center was 1.3 μm/s. This would be strong enough to affect electrophoretic measurements. Figure 4.10 shows the effect of both openings placed just a little off center, but still directly opposite to each other. This might occur due to a flaw in the cell construction. Here, the disturbances lost their symmetry, but the usable region was still a respectable size. Table 4.2 summarizes the results from the simulations depicted in Figures 4.5 through 4.10

Table 4.2 Summary of Simulations Depicted in Figures 4.5 to 4.10

Figure	Inlet		Outlet		Inlet Liquid Velocity[2]	Length of Flow Development Region[3]	
(Number)	Width (10^{-3} m)	Position[1] (10^{-3} m)	Width (10^{-3} m)	Position[1] (10^{-3} m)	(10^{-3} m/s)	Upper (10^{-3} m)	Lower (10^{-3} m)
4.5	2.07	0	2.07	0	-5	8.1	7.2
4.6	6.21	0	6.21	0	-5	8.5	8.5
4.7	10.35	0	10.35	0	-5	9.2	9.0
4.8	2.07	0	2.07	0	-50	11.9	6.6
4.9	2.07	+30.0	2.07	-30.0	-5	7.8	7.7
4.10	2.07	+2.07	2.07	-2.07	-5	9.4	9.4

1) Horizontal position measured from midpoint of the cell width (x = 0); positive sign denotes positions to the right of the centre line (and vise versa).

2) Convention dictates that downward motion be designated by a negative sign.

3) Development regions defined to include regions in which the liquid velocity magnitudes are greater than 5×10^{-7} m/s (except Figures 4.8 and 4.9, in which the region's liquid velocity is greater than 5×10^{-4} and 10×10^{-4} m/s).

4.3.3 CELL CONSTRUCTION

The new cell was also constructed by Peter Lea and associates at the University of Alberta. The width and depth of this cell were 60 mm and 2 mm, respectively. Based on the computer flow simulations, it was determined that a height of 30 cm could provide a usable area with minimal flow disturbances. The cell was made from two sheets of Pyrex glass, separated by 2 mm thick glass wedges positioned on the corners of the cell. Two glass tubes were fitted along the side edges to house the electric field-generating electrodes. A neck was fitted to the top and bottom to allow the entrance and exit of fluid and bubbles. The entire structure was sealed together with glue. The final equipment arrangement is illustrated in Figure 4.11.

This cell was mounted on to the same motor-driven stand. In this case, the motor-mike and pulley system was redundant. A valve and piping network was attached to the base of the stand. This network was connected with tygon tubing to the base of the bubble-producing glass manifold. The system consisted of two valves. The needle valve provided fine flow control and was to be used during electrophoresis. The ball valve provided coarse control, and was designed to flush out the cell. A solution reservoir was placed overhead, and connected with tygon tubing to the neck at the top of the cell. Figure 4.12 provides a flow diagram of this system.

In practice, two problems were encountered with the flow control system. The first, was that air bubbles tended to get stuck in the liquid-inlet tubing. These were difficult to dislodge and disrupted the steady flow. The second problem was that the hydrostatic pressure of the reservoir was too high for the cell to withstand. Numerous trial runs had to be aborted when leaks were spotted along the seams of the cell. Consequently, the reservoir tank was disconnected altogether, and the cell was operated in an "outflow only" mode. Before each trial, the cell was filled to the top. The liquid was allowed to drain slowly during the experiments. When the meniscus dropped below the field of view, the run was stopped, and the cell was refilled. While this procedure was tedious, it did work.

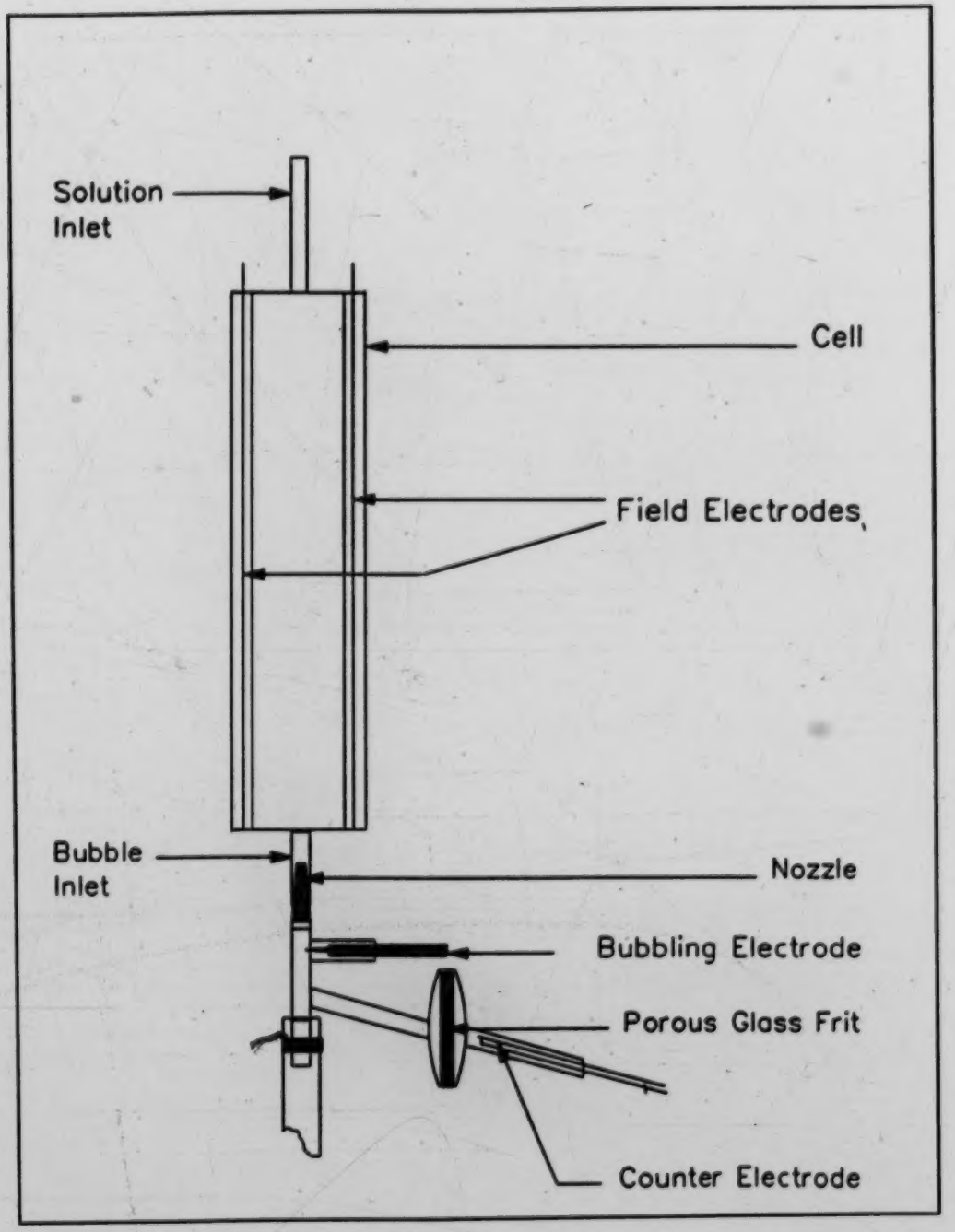

Figure 4.11 The "Flow-Through" Cell

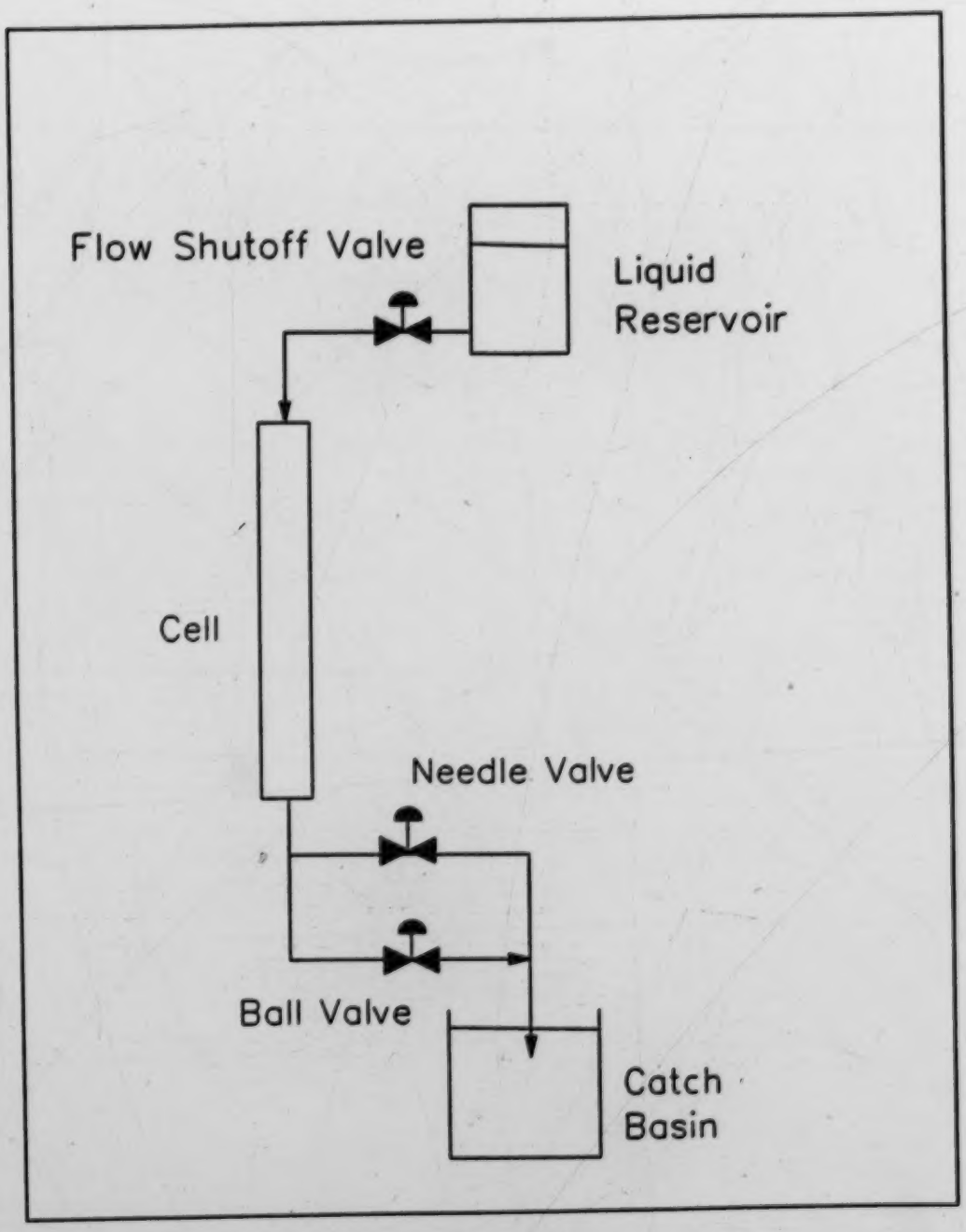

Figure 4.12 The Liquid Flow Control Network

4.5 SUMMARY

Despite efforts described in Chapter 3, it was found that bubbles still travelled upward too quickly to be used for electrophoresis. The first attempt to deal with this problem was to mount the cell on a movable platform. The platform was expected to lower the cell at a rate comparable to the rise velocity of the bubbles, and thus "trap" them within the field of view. However, this method was not satisfactory, and the platform could not move the cell down fast enough.

In consequence, a new approach was taken. An electrophoresis cell was designed in which down-flowing liquid curtailed the rising bubbles. The shape and form of this new cell were determined, in part, by computer flow simulations using FLOW-3D software. The cell was originally designed for a continuous flow operation, but it was found to work better in an "outflow only" mode. In this configuration, the device worked very well at "trapping" bubbles for electrophoresis experiments.

CHAPTER 5 THE ELECTRIC FIELD-PRODUCING SYSTEM

5.1 PURPOSE AND OPERATING CRITERIA

The electric field-producing system forms the heart of an electrophoretic apparatus. A suitable system must be able to provide an electric field that is:

1. of sufficient magnitude to induce electrokinetic motion,
2. stable over the time period needed to make an electrophoretic velocity measurement,
3. uniform within the volume in which electrophoresis takes place.

5.2 DESCRIPTION OF SYSTEM COMPONENTS

In its simplest form, the electric field-producing system consists of a high voltage power supply connected in series to a pair of electrodes. The electrodes are immersed in the electrolyte solution. When an electrical potential is applied across the electrodes, the electric field is formed across the gap. A circuit diagram of a simple system is shown in Figure 5.1. The individual components used in this work are described in the next sections.

5.2.1 Power Supply

The power supply consisted of a Zeta-Meter (ZM-80) direct current (DC) power unit, adapted for use with the "Flow-through" electrophoresis cell. The device supplies a constant potential, and can deliver up to 300 V. The direction of the current and magnitude of the potential are controlled respectively by the directional switch and adjustment knob. Details are provided in the Zeta-Meter (ZM-80) Manual (1980).

5.2.2 Ammeter

The current through the circuit was measured by a Fluke 77 Multimeter, connected between the power supply and the cell assembly.

5.2.3 Switch Box

The switch box connected the power supply to the field generating electrodes. The electrode connectors were colour coded, red and black, to ensure consistent placement of the electrodes. The switch box also provided terminals to connect a voltmeter across the electrode gap.

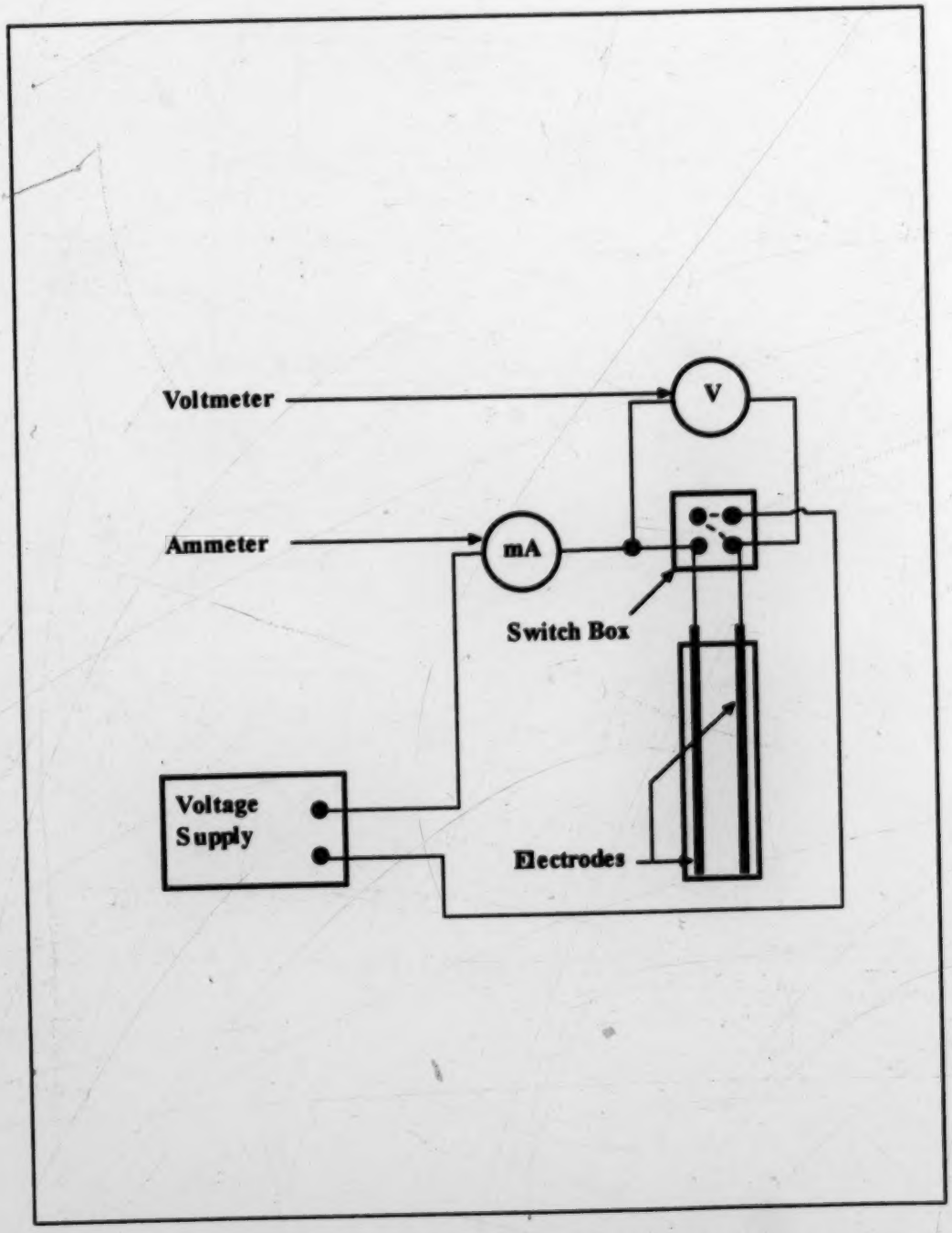

Figure 5.1 **Schematic Layout of the Electric Field-Producing System**

5.2.4 Voltmeter

The voltmeter consisted of another Fluke 77 Multimeter. The device was connected across the field generating electrodes, and served to verify that the selected electrical voltage drop was actually being supplied.

5.2.5 Electrodes

The purpose of the electrodes is to provide the electric field that actually drives the electrophoretic motion. In addition to providing a stable electric field, the electrodes must also be able to sustain a high current density without:

1. polarization,
2. degassing,
3. ohmic heating, or
4. releasing byproducts into the system.

Much effort was spent on ensuring that a suitable pair of electrodes was selected. Finding electrodes to fulfill all these criteria was not a trivial matter. Several types were available to choose from. In general, electrode types can be classified into two categories: reversible and irreversible.

Reversible electrodes are commercially available devices, usually used in conjunction with analytical chemistry applications. Common examples of these are Ag/AgCl, $Zn/ZnSO_4$, and $Cu/CuSO_4$. Such electrodes can carry high current density without polarization or degassing, but they tend to dissolve ions into the surrounding solution. Researchers have tried to overcome this problem by imposing semipermeable barriers, such as filter paper, agar gel, plaster of Paris, and sintered glass (Seaman, 1975).

Irreversible electrodes consist of noble metal foils or wires that are placed in direct contact with the system solution. They are inert, simple to implement, and can be available in very pure form. Unfortunately, these electrodes cannot withstand high current density without polarization and degassing.

The unusually tall "Flow-through" electrophoresis cell created some additional restrictions. By virtue of their shape, irreversible electrodes were preferable, as they were easy to adapt to the cell. However, the problem of polarization still had to be surmounted.

A literature search unearthed a useful document, prepared by Neihof (1969). Neihof claimed that by charging palladium wire with hydrogen, he was able to increase the metal's ability to withstand high current density without polarization or degassing. On the surface, this seemed like an ideal solution to the polarization problem. Notably, Sirois and Millar (1973) used a pair of platinum/palladium-hydrogen to generate the electric field in their cell. In consequence, research efforts focused on developing palladium-hydrogen electrodes to fit with the "Flow-through" electrophoresis cell.

5.3 PALLADIUM-HYDROGEN ELECTRODES

5.3.1 Background

The ability of palladium to absorb large quantities of hydrogen has been well documented (Lewis, 1967). Hydrogen may be introduced into metals either by gas absorption, or by cathodic electrolysis. The latter method is simpler to achieve.

Electrolytic charging usually takes place in dilute hydrochloric or sulphuric acid. Two palladium foil or wire electrodes are immersed in the acid. The first palladium electrode, connected to the negative terminal of a power supply, acts as the cathode to be charged with hydrogen. The second electrode is connected to the positive terminal, and functions as a counter-electrode. Figure 5.2 presents a simple diagram of this circuit

According to Neihof (1969), the palladium-hydrogen electrodes inhibit polarization through the following mechanism:

(5-1) $$xH_3O^+ + Pd_{x-1} + xe^- \Leftrightarrow PdH_x + xH_2O$$ (in acidic media)

(5-2) $$xH_2O + Pd_{x-1} + xe^- \Leftrightarrow PdH_x + xOH^-$$ (in basic media)

At the cathode (negative terminal), the palladium provides a sink for hydrogen, as described in Equation 5.1. Hydrogen is actually pushed into the metal lattice, thus preventing a positive charge build up at the at the metal-liquid interface. At the anode (positive terminal), surface hydrides combine with hydroxide ions to form water molecules, in the manner shown in reaction 5.2 (in reverse).

It is evident that the electrodes can inhibit polarization so long the palladium is neither depleted of its hydrogen, nor filled to capacity. In addition, the mechanism can only function properly if the metal surface is easily accessed by the ions. Thus, the palladium surface must be very clean and free of oxide films.

5.3.2 Development of Preparatory and Testing Procedures

Initial tests were conducted to ascertain whether Neihof's method warranted further attention. Palladium wire, 0.5 mm in diameter, was cut into two 6 cm segments. One of the segments was cathodically charged in 0.1 M HCl solution, another functioned as the counter electrode during the electrolysis sessions, and the third was left untreated. Charging took place for two minutes, with an applied potential drop of 10 V.

The first test took place in a glass beaker filled with 500 mL RO water. The hydrogen-charged palladium wire was immersed in the water and connected to the positive terminal of a power supply. A platinum wire of the same diameter and length was similarly attached to the negative terminal. The wires were positioned about 5 cm apart. An electrical potential of 10 V was applied across the wires for a burst of 30 seconds. The platinum wire began bubbling almost immediately, but the palladium wire did not bubble at all within this period. The same observations were noted with the terminals reversed. The hydrogen-charged wire was then replaced with the untreated palladium wire, and the procedure was repeated. The untreated palladium wire bubbled, just like the platinum wire. Finally, the hydrogen-charged palladium wire was returned to the negative terminal, and 10 V was applied across the circuit. After two minutes this wire began to produce bubbles.

The second experiment was identical to the first, except that the wires were tested in aqueous 1 M NaCl. In this test, all the wires produced bubbles vigorously as soon as the electrical potential was applied.

These observations indicated that there was indeed some benefit to be gained by charging the palladium with hydrogen, but that the effect was perhaps limited to electrolyte solutions of low concentrations. Furthermore, the bubble-suppressing effect was of limited duration, alluding that an electrode pair could not be used indefinitely.

At this point, testing graduated to full length electrodes that could be tested directly in the electrophoresis cell. Three segments, 30 cm in length, were cut from the same 0.5 mm diameter palladium wire. To save time, two of the wires were attached in parallel, and then charged simultaneously. The third wire was used as a counter electrode. Charging took place in 0.1 M HCl, as usual. After charging for 10 minutes, the cathode wires began bubbling. After charging for 30 minutes at 10 V, the acid solution turned yellow, and subsequently darkened to orange. The colour appeared to be streaming from the tip of the anode. By this time, the cathode wires were forming bubbles rapidly, and were bending at the ends. The bubbling continued for 20 minutes, even after the potential was shut off. Upon close inspection, the surface of these wires appeared dull and darkened.

Presumably, the observed colour in the acid was a result of ions being leached from the anode. Probably, chloropalladous acid was being formed, which is described in the literature as having a red-brown in colour (Pourbaix, 1974).

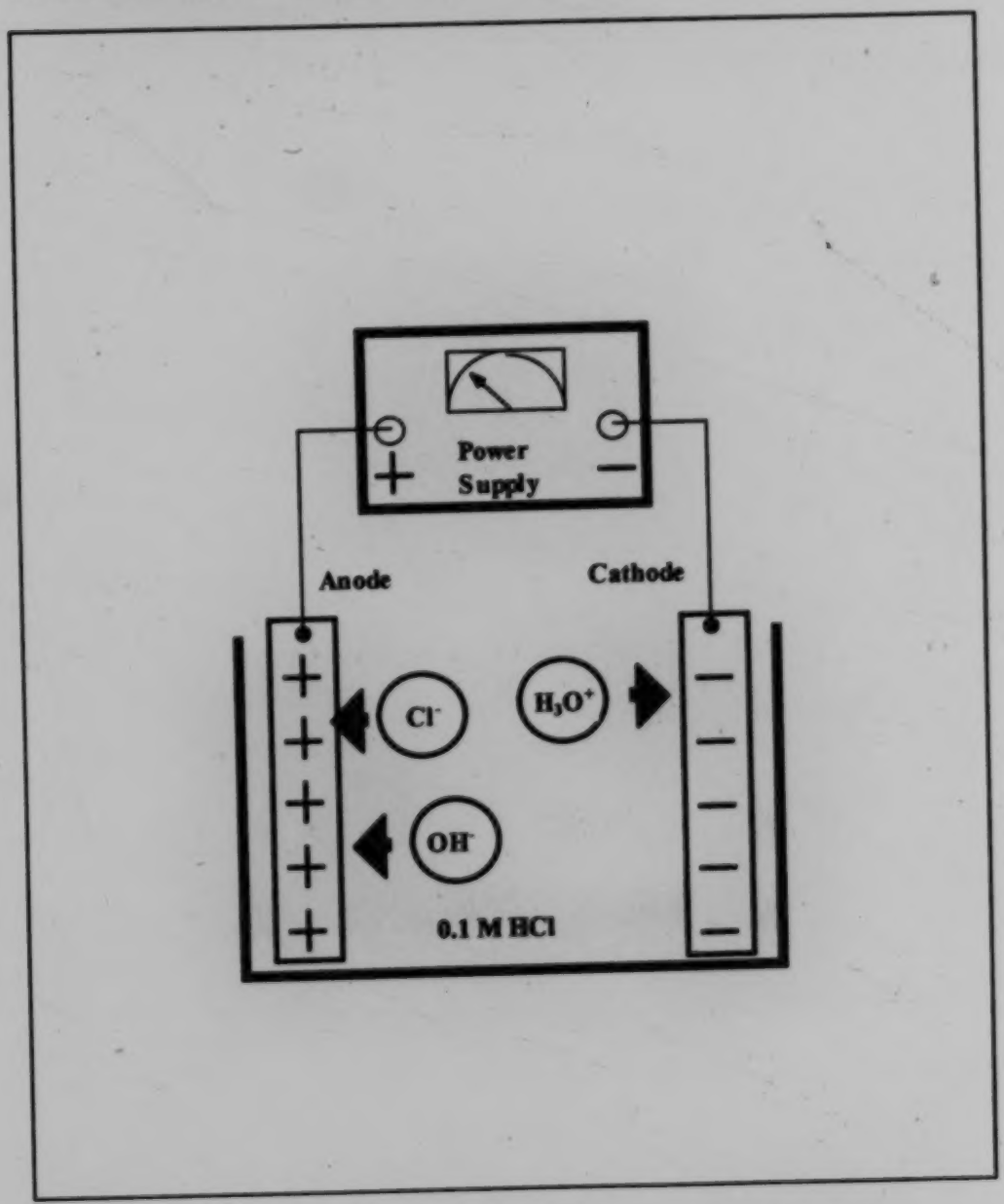

Figure 5.2 **Circuit Diagram for Electrolytic Charging of Palladium Wires**

The spontaneous bubbling was believed to indicate oversaturation of the metal with hydrogen. Several attempts were made to find an optimum charging period. These were not successful, primarily because the time period before bubbling was not reproducible. It was much simpler to oversaturate the palladium with hydrogen for a fixed period and then to allow the excess to dissipate. It became routine to cathodically charge the electrodes overnight and then to let them "rest" in the dilute HCl with the current switched off for three hours. (This was a convenient arrangement, as the electrophoretic cell preparation and calibrations were normally accomplished within those three hours).

As a final modification, the 0.5 mm diameter wires were replaced by 1 mm diameter palladium wires. The thicker wires could provide more surface area for charge transfer, and also retained their shape better during the electrolysis process.

5.3.3 Electrode Performance Tests

Three groups of experiments were conducted on the electrodes within the cell itself. Test Group 1 gave a preliminary overview of the electrodes' behaviour in terms of electric field strength and stability. This first group revealed several issues that had to be resolved before more rigorous testing could commence. Test Group 2 rigorously examined the effect of voltage drop and liquid volume on the electrode performance for a specified electrolyte solution within a defined two minute time period. Test Group 3 examined the effects of various electrolytes on the electrodes, for specified voltage drops and liquid volumes.

Each group of tests consisted of several sets. Within the context of this chapter, the word "set" refers specifically to a series of tests that were made per a single charging of the electrodes. In other words; a new set was defined each time the electrodes were cleaned and recharged with hydrogen. However, before any tests were commenced, it was first necessary to define the criteria with which the "performance" could be evaluated.

5.3.3.1 Estimation of Required Electric Field Magnitude

First, and most importantly, it was required that the electrodes could produce a strong enough field to induce the electrophoresis of bubbles. However, the optical system was not ready at the time of these tests, so there was no way to visually verify whether the electrodes were actually able to do this. Instead, the literature was consulted to determine a range of field strengths that would be most likely to produce the desired effect.

To calculate the required range of electric field strengths, a set of "typical" electrophoretic mobilities was selected from the literature. Table 5.1 lists bubble mobilities, as determined experimentally by two independent groups of researchers. The

data were obtained from systems of various electrolyte concentrations without surfactants present. From Table 5.1, it seemed that U_M could reasonably range from 10^{-9} to 10^{-7} $m^2/V\,s$. Next, the following relationship was assumed to be valid:

(5-3) $$E_\infty = \frac{U_{obs}}{U_M} \times \frac{1}{MF}$$

where E_∞ is the strength of the electric field (V/m).
U_M is the bubble electrophoretic mobility ($m^2/V\,s$)
U_{obs} is the observed electrophoretic velocity on a video screen (m/s), and
MF is the magnification factor between the true velocity and U_{obs}.

By definition,

(5-4) $$U_M = \frac{U_P}{E_\infty}$$

A set of desired U_{obs} was then chosen. This set corresponded to bubbles travelling 5, 10, and 20 cm across the video screen in a period of two minutes. Two minutes was believed to be a reasonable period to make an electrophoretic measurement. With an assumed magnification factor of 300, and designated sets of U_M, and U_{obs}, Equation 5-4 was applied to generate plots of E_∞ vs. U_M. The graphs are shown in Figure 5.3, and the detailed calculations are provided in Appendix 5-1. As determined from Figure 5.3, an electric field magnitude ranging from 1 to 10 V was needed to produce the desired range of U_M.

Experimentally, the electric field cannot be measured directly, but may be estimated using the following relationship:

(5-5) $$E_\infty = \frac{I}{A_{xy}\sigma} = \frac{I}{(H \times 2Y)\sigma}$$

where E_∞ is the electric field (V/m),
I is the current through the circuit (A),
A_{xy} is the effective cross sectional area defined by the x and y unit vectors (m^2),
σ is the conductivity of the solution ($1/\Omega\,m$),
V is the voltage drop across the cell (V),
2Y is the effective depth of the cell (m), and
H is the height of solution in the cell (m).

The coordinate system describing the cell dimensions is shown in Chapter 4. Equation 5-5 provided the means to checking not only the magnitude of the electric field, but also its stability. A fluctuating current, naturally, indicated an unsteady field.

Table 5.1 Typical Experimentally Determined Electrophoretic Mobilities Found by Various Researchers

Reference	Electrophoretic Mobility ($m^2/V\ s$) [1]	Electrolyte Type and Concentration [2]	pH
Kubota and Jameson (1993) [3]	-0.7×10^{-8}	NaCl, 10^{-2} M	5.6
"	-1×10^{-8}	NaCl, 10^{-3} M	"
"	-1.3×10^{-8}	NaCl, 10^{-4} M	"
"	-2.2×10^{-8}	NaCl, 10^{-5} M	"
"	-0.3×10^{-8}	$MgSO_4$, 10^{-2} M	"
"	-2.1×10^{-8}	$MgSO_4$, 10^{-5} M	"
"	$+0.4 \times 10^{-8}$	$AlCl_3$, 10^{-3} M	"
"	$+1.4 \times 10^{-8}$	$AlCl_3$, 10^{-4} M	"
"	-0.8×10^{-8}	$AlCl_3$, 10^{-5} M	"
"	$+1.4 \times 10^{-8}$	$AlCl_3$, 10^{-6} M	"
Brandon et al. (1985) [4]	-6×10^{-8}	Na_2SO_4, 1 M	6.9
"	-8×10^{-8}	Na_2SO_4, 10^{-2} M	"
"	-6×10^{-8}	$NaClO_4$, 1 M	"
"	-9×10^{-8}	$NaClO_4$, 10^{-2} M	"
"	-6.7×10^{-8}	$NaNO_3$, 1 M	"
"	-9.7×10^{-8}	$NaNO_3$, 10^{-2} M	"

(1) Negative sign denotes direction of motion relative to the electric field.

(2) No surfactant specified to be present

(3) Inert nitrogen bubbles

(4) Hydrogen bubbles

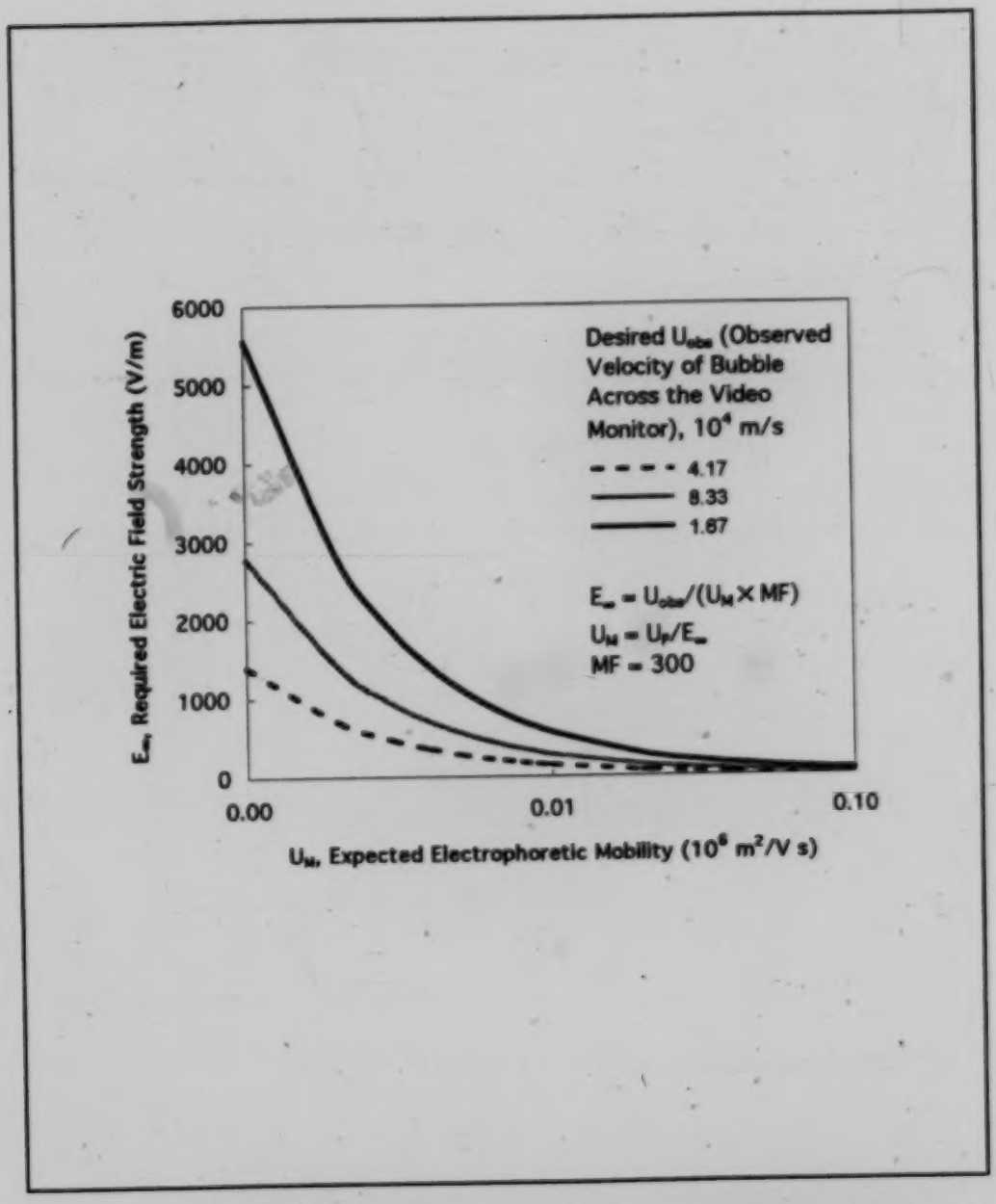

Figure 5.3 **Electric Field Strengths Required to Produce the Electrophoretic Mobilities in Listed in Table 5.1 (Calculations Shown in Appendix 5-1)**

5.3.3.2 Experimental Set-up and Method

The hydrogen-charged palladium electrodes were tested directly in the electrophoresis cell. Figure 5.4 shows the circuit layout. The cell was filled with electrolyte solution, and the liquid height was adjusted to the desired level. Electrodes were positioned down the sides of the cell, and connected to a modified Zeta-Meter (ZM-80) high voltage power supply. The connecting wires were colour coded so that the current direction could be easily identified. The red connecting wire was always attached to the left electrode, and the black wire was always attached to the right electrode. In this set up, the current was considered positive with the voltage directional switch set to the right, (and vise versa).

Before switching on the power supply, the circuit was manually inspected to make sure that connections were secure. For safety reasons, the cell assembly and electrodes were never touched once the power unit was turned on. The voltage selection was set to zero, and the direction selector placed on "standby" mode. This step was important to prevent an initial power surge from damaging the circuit. Once completed, it was safe to switch on the power and let the system warm up (five minutes was sufficient). The system was then ready for testing.

The test procedure simply consisted of turning the voltage selector to a desired value, placing the directional switch to the desired direction, and monitoring the resultant current over a given period. In between tests, the directional switch was placed on "standby" mode. If adjustments were to be made to the cell, then the power supply had to be turned off and unplugged.

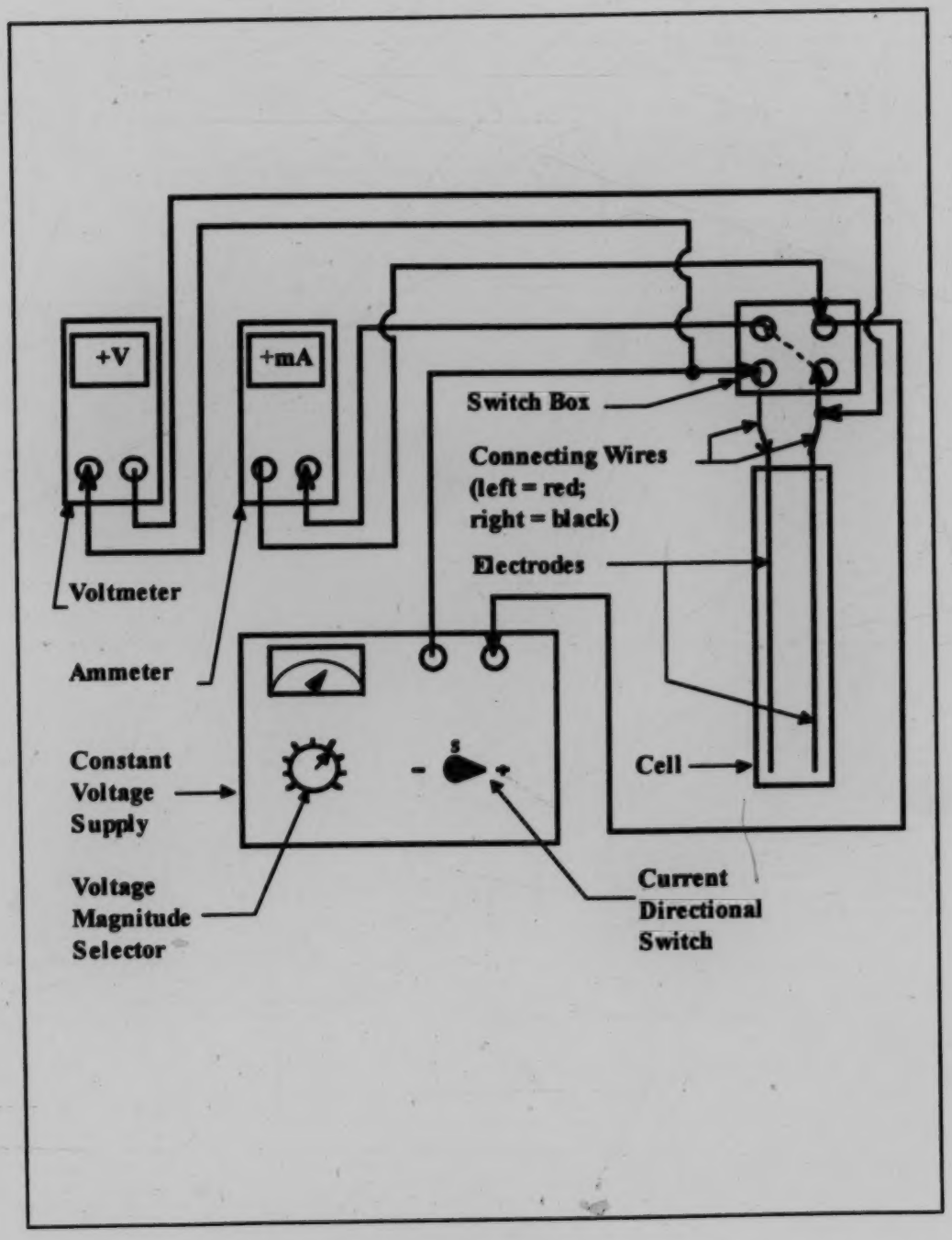

Figure 5.4 Configuration of Test Apparatus

5.3.3.3 Preliminary Electrode Tests (Test Group 1)

The electrolyte used in the first such test was an aqueous 0.1 M NaCl solution. The conductivity of this solution proved to be too high, causing a circuit breaker in the power supply to fail. The electrolyte was consequently replaced by a standard 67.3 ppm (0.0009 M) KCl solution (Fisher Scientific) with a very low conductivity of $1.01\times10^{-2}\ \Omega^{-1}m^{-1}$.

There was another motive for choosing to lower the concentration. It was noted from the literature that, in the absence of surfactants, the zeta-potential of bubbles often decreases in magnitude with increasing concentration of electrolyte. One explanation for this phenomenon is that the electrical double layer around the bubble is collapsed by the presence of extra ions, and therefore decreases the bubbles' response to the electric field (Brandon et al., 1985). One such example is shown in Figure 5.5 (Brandon et al., 1985). In this case, ζ rapidly approached zero when the concentration of electrolyte, Na_2SO_4, was raised above 10^{-2} M. Based on this observation and other researchers' work, (Okada et al., 1990; Brandon et al, 1985; Kubota and Jameson, 1993), it appeared that lowering the electrolyte concentration would improve our chance of producing electrophoretic effects.

Initial tests performed in this medium were disappointing, as the electrodes did not produce any current (and thus no electric field) at all. An investigation revealed that this problem was not related to the solution, but to the cleanliness of the electrodes. Apparently, prolonged use and repeated hydrogen charging cycles had produced a dark film on the surface of the metal. This film was responsible for inhibiting the current flow.

In response to this problem, a new cleaning procedure was devised. The old procedure consisted only of rinsing with 0.1 M HCl and RO water. The new routine involved several more steps. First, the electrodes were briskly rubbed with fine sandpaper. Next, a solution consisting of 10 mL 30 % hydrogen peroxide and 90 mL concentrated sulphuric acid was applied. These ingredients were mixed in advance, and allowed to cool before use. The wires were then rinsed with RO water, and finally with 0.1 M HCl.

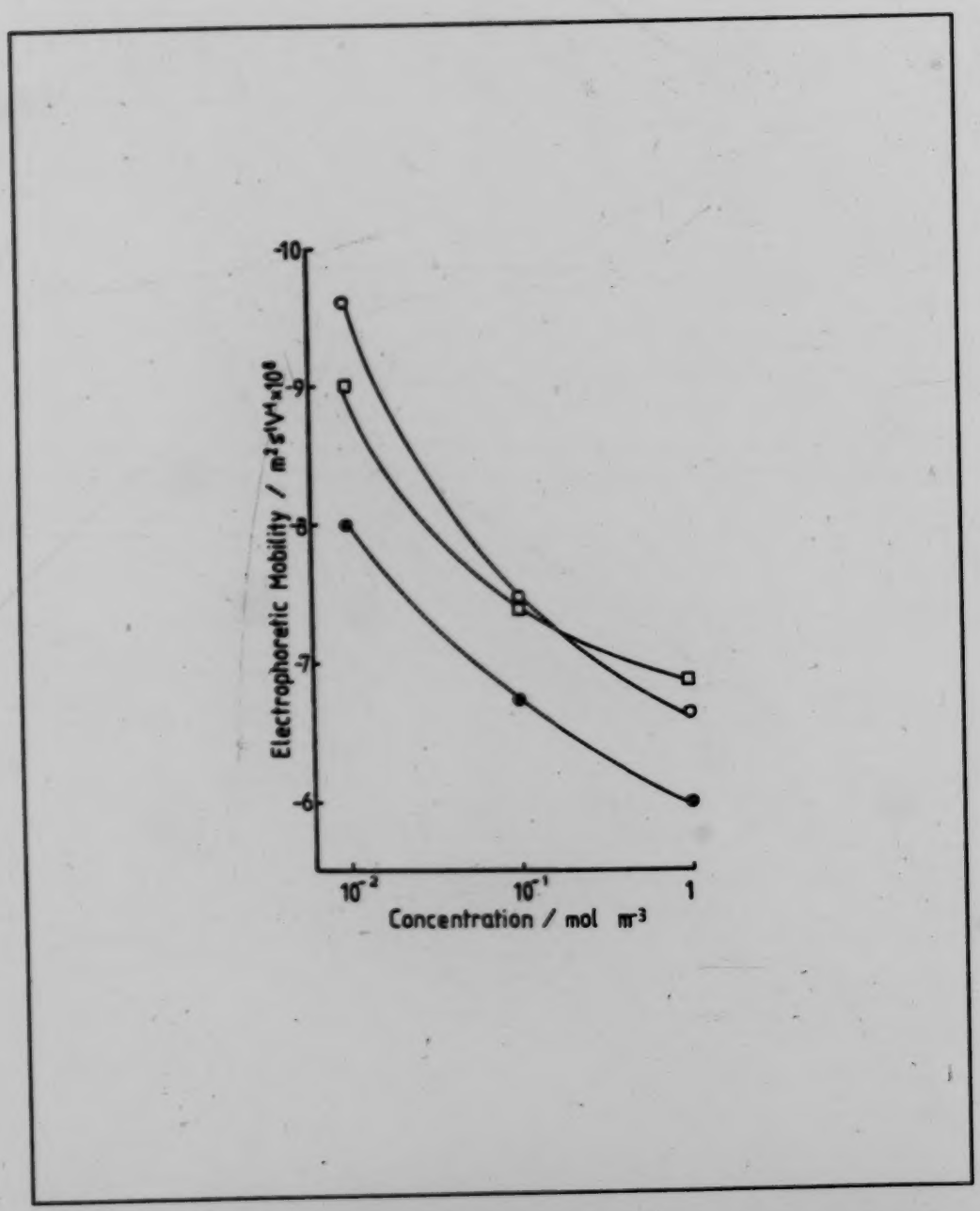

Figure 5.5 **Effect of Electrolyte Concentration on the Zeta Potential for Aqueous Surfactant-free Solutions of Na_2SO_4, $NaClO_4$, and $NaNO_3$ (Brandon et al., 1985)**

To prevent cross contamination of the electrodes during electrolytic charging, a special container was designed and built. The contraption, shown in Figure 5.6, consisted of two upright glass cylinders, connected by a horizontal tube to form an "H". Diffusion of large ions between the chambers was inhibited by two porous glass plugs. Thus cleaned and prepared, the electrode performance was improved considerably.

The results from a preliminary round of tests (Test Group 1) are shown in Figure 5.7. In preparation, the electrodes were cleaned in the manner outlined. The electrodes were charged with hydrogen overnight for 20 hours and 15 minutes, and then left to "rest" for another three hours. The electrophoresis cell was filled with standard KCl solution to a height of 15 cm. The electrodes were then assembled according to standard procedure. A series of electrical potentials were applied across the electrodes. The magnitude of the applied potentials was fixed at 50 V, but the direction and the duration of field application were picked at random.

As shown in Figure 5.7, the current tended to fluctuate between 2 and 6 mA. The current changed very rapidly within the first ten seconds of current application, and as such, no meaningful readings could be taken during this period. In the long term, the current tended to increase, but no other clear trends could really be established from this data. It was, however, possible to establish the magnitude of the electric fields that were being generated. Table 5.2 shows the field strengths, as calculated by applying Equation 5.4 and the following assumptions. The solution conductivity was known to be $1.01\times10^{-2}\ \Omega^{-1}m^{-1}$, the effective liquid height was 15 cm, and the cell depth was assumed to be 2 mm. It was thus determined that the electric field magnitudes were well above the estimated requirements (determined in section 5.3.3.1).

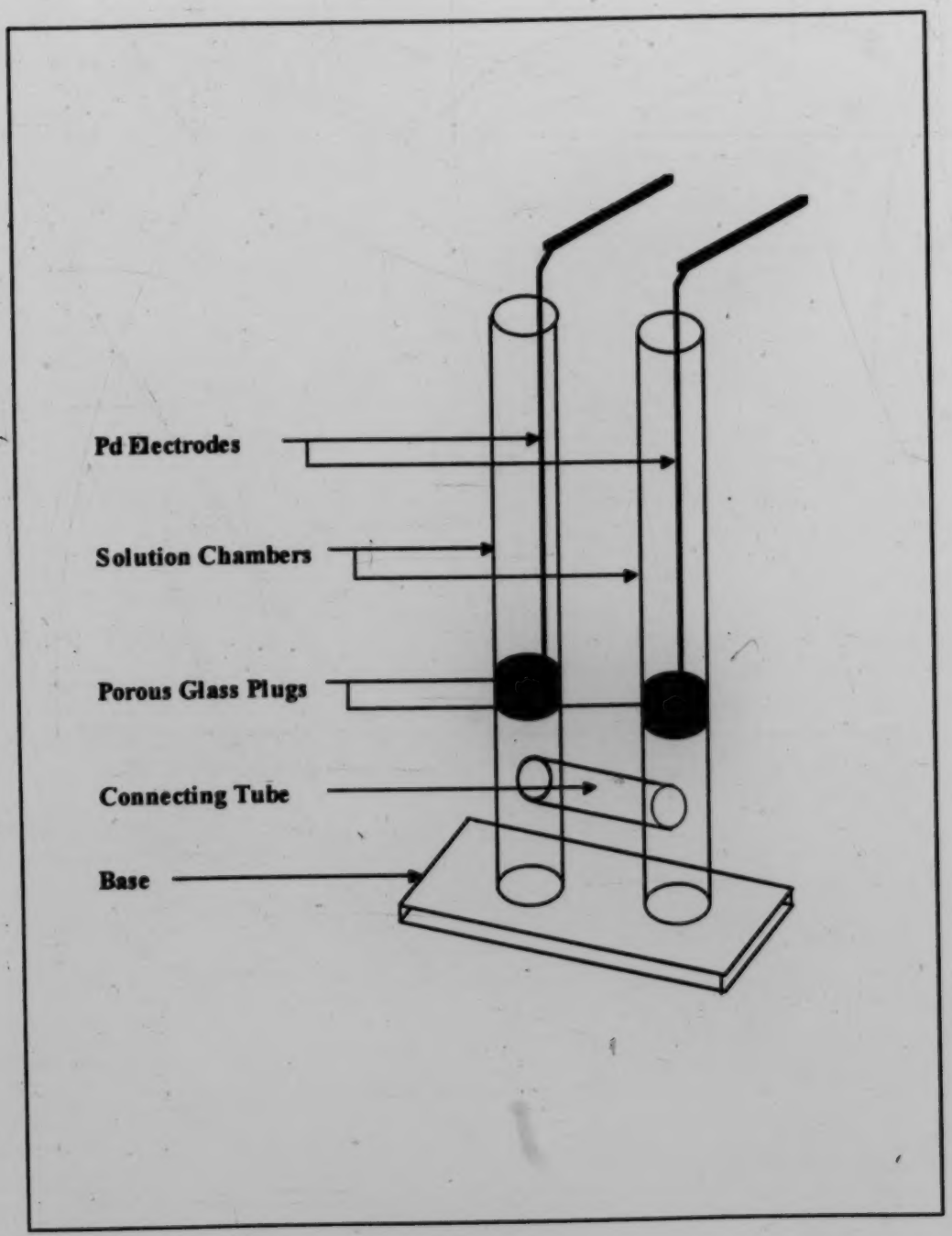

Figure 5.6 Re-Designed Electrolysis Chamber

Table 5.2 Electrode Tests, Group 1: Summary of Results

Test Number	Electric Field Strength (10^{-2} V/m)			
	Maximum	Minimum	Median [1]	Range [2]
1	10.8	8.2	9.8	2.6
2	15.9	13.0	14.7	2.9
3	-19.9 [3]	-13.1	-13.4	6.9
4	18.6	12.5	15.3	6.2
5	-18.1	-16.4	-16.7	1.7

(1) Median of the data points obtained per given test.

(2) Range defined as the maximum data point minus the minimum (it is desirable that the range be as small as possible).

(3) Negative/positive sign denotes direction of electric field.

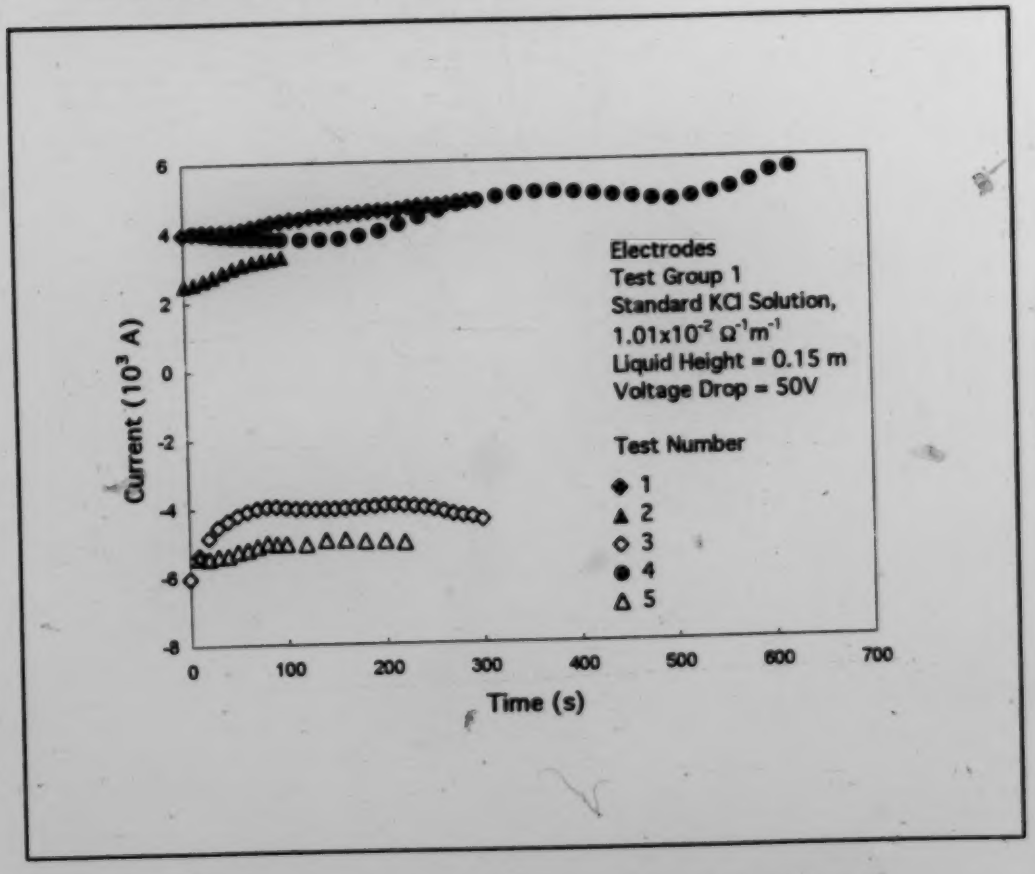

Figure 5.7 Results from Preliminary Electrode Tests (Test Group 1)

The observed fluctuations could have been caused by any combination of several factors, such as changes in palladium surface area (thereby changing the effective cross sectional area), localized heating producing convective currents, or changes in the solution conductivity with extended use. Additionally, extended use in any application may have either depleted or oversaturated either electrode with hydrogen. This postulation was supported by the observation that one of the electrodes began forming bubbles after current was applied for 270 consecutive seconds.

The design of the system made it impossible to isolate any of these factors. However, the electrode bubbling did emphasize that the system should not be used in any one current direction over an extended period. The question raised was, how long a period would be enough to record electrophoretic motion, but not so long as to erode the electric field performance? Again, the answer had to be based on an estimated electrophoretic performance. Given the range of electric field strengths shown in Table 5.2, and the electromobilities listed in Table 5.1, it was shown that two minutes should be a sufficient period.

5.3.3.4 Tests of Electric Field Stability Within a Specified Time Period (Test Group 2)

A second group of tests was designed and carried out (Test Group 2). The purpose of this second group was to determine whether the electric field behaviour over a two minute period could be characterized. The procedure closely resembled the preliminary tests in terms of hydrogen charge up and assembly, however, the conditions were more closely controlled. This set of tests was designed to follow a two-level, two-factorial model. The experimental design scheme is presented in Table 5.3. The two factors being investigated, potential drop and liquid height, were checked at 25 V and 50 V, and 15 cm and 25 cm, respectively. For every test, a potential was applied in one direction for 120 seconds, then in the opposite direction for 120 seconds. A rest period of 30 seconds was imposed between directional switching. Three replicates were made of each combination of voltage drop and height, resulting in twelve runs for every set of tests. A total of three such sets was conducted. Prior to each set, the electrodes were freshly washed and charged with hydrogen.

Table 5.3 Electrode Tests, Group 2: Experimental Design

Test Set	Test Number	Liquid Height (10^2 m)	Voltage Drop (V)
1[1]	1	25	50
"	2	25	50
"	3	25	50
"	4	25	25
"	5	25	25
"	6	25	25
"	7	15	25
"	8	15	25
"	9	15	25
"	10	15	50
"	11	15	50
"	12	15	50
2[1]	1	25	25
"	2	25	50
"	3	15	25
"	4	25	50
"	5	15	50
"	6	15	50
"	7	25	25
"	8	15	50
"	9	15	25
"	10	25	25
"	11	25	50
"	12	15	25
3[2]	1	15	50
"	2	25	25
"	3	25	50
"	4	15	50
"	5	25	25
"	6	25	50
"	7	15	25
"	8	15	25
"	9	15	25
"	10	25	25
"	11	15	50
"	12	25	50

(1) Standard KCl solution (Fisher Scientific), 9.04×10^{-3} M, 1.01×10^{-2} $\Omega^{-1}m^{-1}$.

(2) Solution prepared in laboratory, conductivity determined by meter, 9.0×10^{-3} M, 9.4×10^{-3} $\Omega^{-1}m^{-1}$.

Table 5.4 describes the conditions imposed during the three electrode charging sessions. Sets 1 and 2 were conducted with standard KCl solution having a conductivity of $1.01\times10^{-2}\ \Omega^{-1}m^{-1}$. The third set of tests utilized a KCl solution of the same concentration, prepared in the laboratory on the morning of the test. The solution was degassed according to the procedure described in Chapter 3. The conductivity of this solution was measured using a conductivity meter (Fisher Scientific).

Table 5.4 Electrode Tests, Group 2: Electrode Preparation

Test Set	Voltage Drop (V)	Initial Current (10^3 A)	Final Current (10^3 A)	Charging Time (hr:min)	Rest Time (hr:min)
1	1.8	10.05	9.47	15:00	3:00
2	1.8	10.07	9.38	16:00	3:00
3	1.6	10.56	9.70	13:56	3:17

The results from all the tests in this group were plotted in terms of current against the elapsed time. Figures 5.8 and 5.9 show two representative current-time plots. The distinct pattern was observed in all the 36 tests. The magnitude of fluctuation tended to be larger for the tests with 50 V than those with 25 V. The amount of fluctuation was quantified by calculating the median and the range for each two-minute time span. For example, in Figure 5.9, the current fluctuations in both negative and positive directions are minimal, and the corresponding ranges are, respectively, 0.08 and 0.10 mA. In comparison, Figure 5.8 shows more aggravated fluctuations of current. In Figure 5.8, the ranges in the negative and positive directions are 1.13 and 0.57 mA, respectively. Obviously, it is desirable to minimize the range. Table 5.5 shows the maximum, minimum, median, and range calculated for every test. Positive and negative current directions were assessed separately.

To evaluate trends, the resulting values from Table 5.5 were plotted against liquid height and voltage drop. Figure 5.10 presents the current ranges plotted against the liquid height for voltage drops of 25 V and 50 V. It was observed that the range of the current increased significantly as the voltage setting was increased. Moreover, the spread of the ranges tended to also increase with the voltage drop. In other words, increasing the voltage drop not only aggravated the degree of fluctuation, but also adversely affected the repeatability between individual tests.

Figure 5.11 shows the range of current plotted against the voltage drop, for liquid heights of 15 cm and 25 cm. The range of current increased proportionately with the liquid height, but the direction of the current did not seem to affect the range. It appeared that the current range was consistently small at the low values of voltage drop and liquid height. At the high values of voltage drop and liquid height, the current range varied considerably between tests.

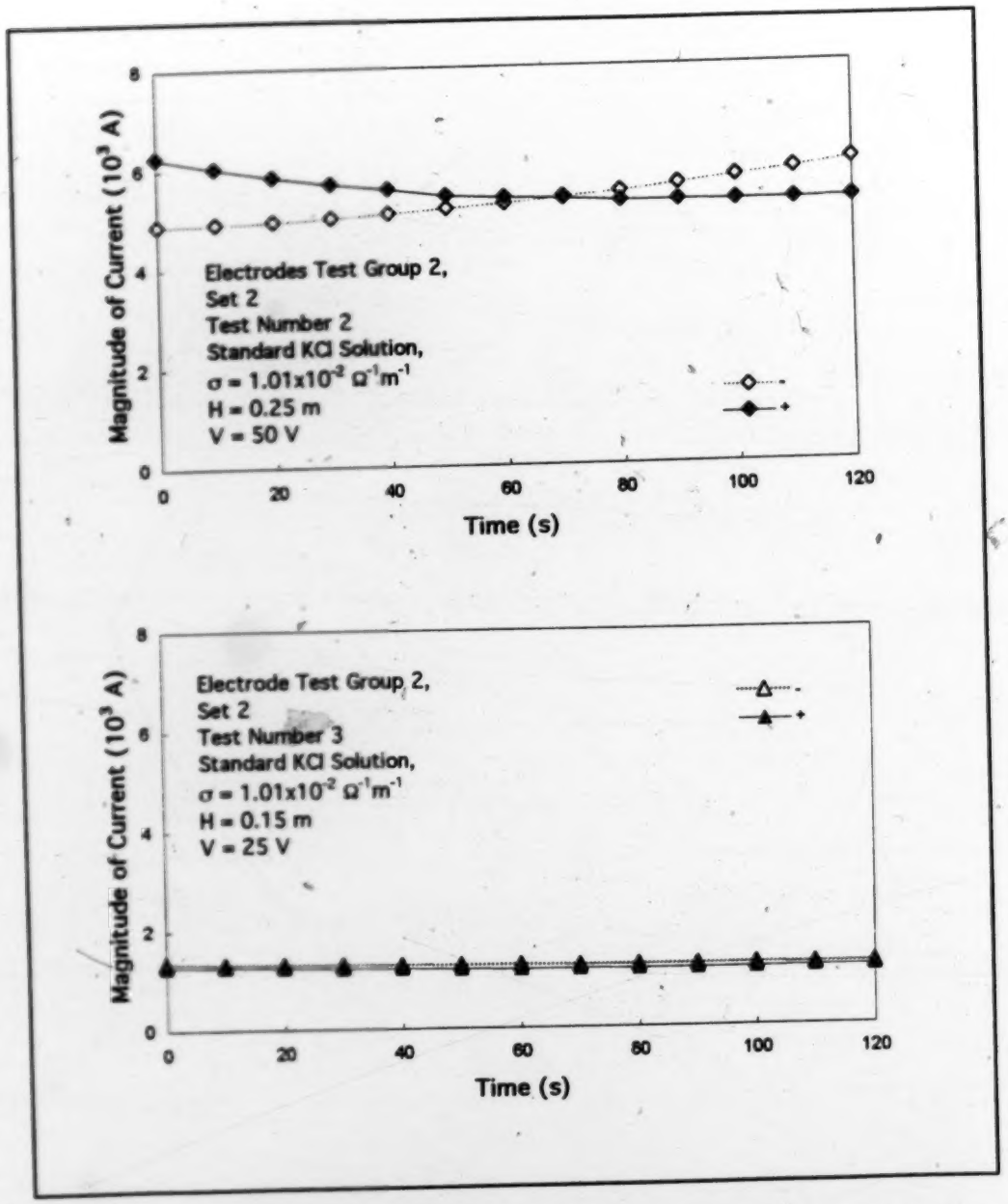

Figure 5.8 (above) **Sample Current-Time Plot Derived from Group 2, Set 2 (Test Number 2)**

Figure 5.9 (below) **Sample Current-Time Plot Derived from Group 2, Set 2 (Test Number 3)**

Table 5.5 Electrode Tests, Group 2: Summary of Results [1]

Test Set	Test Number	Liquid Height (10^2 m)	Voltage Drop (V)	Current (10^3A)							
				Maximum		Minimum		Median[2]		Range[3]	
				-[4]	+	-	+	-	+	-	+
1	1	25	50	4.80	4.75	3.83	4.06	4.21	4.24	0.97	0.69
"	2	25	50	4.73	4.64	3.94	4.05	4.22	4.14	0.79	0.59
"	3	25	50	4.53	4.44	3.89	3.99	4.03	4.03	0.64	0.45
"	4	25	25	1.99	1.99	1.91	1.91	1.93	1.94	0.08	0.08
"	5	25	25	2.07	2.29	1.96	2.06	1.99	2.10	0.11	0.23
"	6	25	25	2.31	2.27	2.07	2.05	2.20	2.10	0.24	0.22
"	7	15	25	1.17	1.20	1.10	1.10	1.14	1.11	0.07	0.10
"	8	15	50	3.04	2.96	2.40	2.41	2.64	2.51	0.64	0.55
"	9	15	25	1.16	1.17	1.10	1.09	1.12	1.11	0.06	0.08
"	10	15	50	2.94	2.92	2.34	2.36	2.53	2.46	0.60	0.56
"	11	15	25	1.16	1.17	1.09	1.09	1.12	1.11	0.07	0.08
"	12	15	50	2.76	2.72	2.30	2.30	2.42	2.37	0.46	0.42
2	1	25	25	2.11	2.14	2.07	1.97	2.09	2.02	0.04	0.17
"	2	25	50	6.03	5.83	4.90	5.26	5.30	5.31	1.13	0.57
"	3	15	25	1.31	1.27	1.23	1.17	1.26	1.18	0.08	0.10
"	4	25	50	6.15	6.55	4.96	5.00	5.39	5.48	1.19	1.55
"	5	15	50	3.28	3.57	3.01	3.04	3.10	3.14	0.27	0.53
"	6	15	50	3.35	3.35	2.97	2.95	3.04	3.02	0.38	0.40
"	7	25	25	2.86	2.84	2.81	2.57	2.83	2.61	0.05	0.27
"	8	15	50	4.03	3.96	3.34	3.33	3.53	3.42	0.69	0.63
"	9	15	25	1.65	1.54	1.51	1.47	1.54	1.49	0.14	0.07
"	10	25	25	2.44	2.57	2.37	2.29	2.41	2.37	0.07	0.28
"	11	25	50	5.64	5.57	4.81	4.69	5.06	4.83	0.83	0.88
"	12	15	25	1.38	1.37	1.32	1.20	1.33	1.33	0.06	0.17

(1) Standard KCl solution with conductivity, $1.01\times10^{-2}\ \Omega^{-1}m^{-1}$.

(2) The median for each test is defined as the midpoint current value, and is derived from a current-time plot such as those shown in Figures 5.8 and 5.9.

(3) The range is defined and the current maximum minus the current minimum. A range of zero represents no current fluctuation over time.

(4) Negative/positive signs above columns denote direction of current. Tests with negative current were assessed separately from tests with positive current, as indicated by separate columns.

Table 5.5 (Continued) **Electrode Tests, Group 2: Summary of Results** [1]

Test Set	Test Number	Liquid Height (10^2 m)	Voltage Drop (V)	Current (10^3 A)							
				Maximum		Minimum		Median[2]		Range[3]	
				-[4]	+	-	+	-	+	-	+
3	1	15	50	2.53	2.62	1.96	2.14	2.19	2.19	0.57	0.48
"	2	25	25	1.60	1.63	1.54	1.44	1.55	1.46	0.06	0.19
"	3	25	50	4.75	4.33	3.49	3.56	3.72	3.68	1.26	0.77
"	4	15	50	2.35	2.31	2.21	2.01	2.25	2.06	0.14	0.30
"	5	25	25	1.70	1.85	1.64	1.65	1.65	1.74	0.06	0.20
"	6	25	50	6.40	6.72	4.53	4.16	5.46	5.44	1.87	2.56
"	7	15	25	1.08	1.03	0.99	0.91	1.04	0.94	0.09	0.12
"	8	15	25	1.08	1.15	1.03	1.03	1.05	1.05	0.05	0.12
"	9	15	25	1.08	1.13	1.02	1.03	1.04	1.04	0.06	0.10
"	10	25	25	1.76	1.89	1.69	1.63	1.72	1.67	0.07	0.26
"	11	15	50	2.40	2.56	2.09	2.10	2.13	2.18	0.31	0.46
"	12	25	50	4.16	4.24	3.43	3.39	3.69	3.53	0.73	0.85

(1) Prepared KCl solution with conductivity, $9.4\times10^{-3}\ \Omega^{-1}m^{-1}$.

(2) The median for each test is defined as the midpoint current value, and is derived from a current-time plot such as those shown in Figures 5.8 and 5.9.

(3) The range is defined and the current maximum minus the current minimum. A range of zero represents no current fluctuation over time.

(4) Negative/positive signs above columns denote direction of current. Tests with negative current were assessed separately from tests with positive current, as indicated by separate columns.

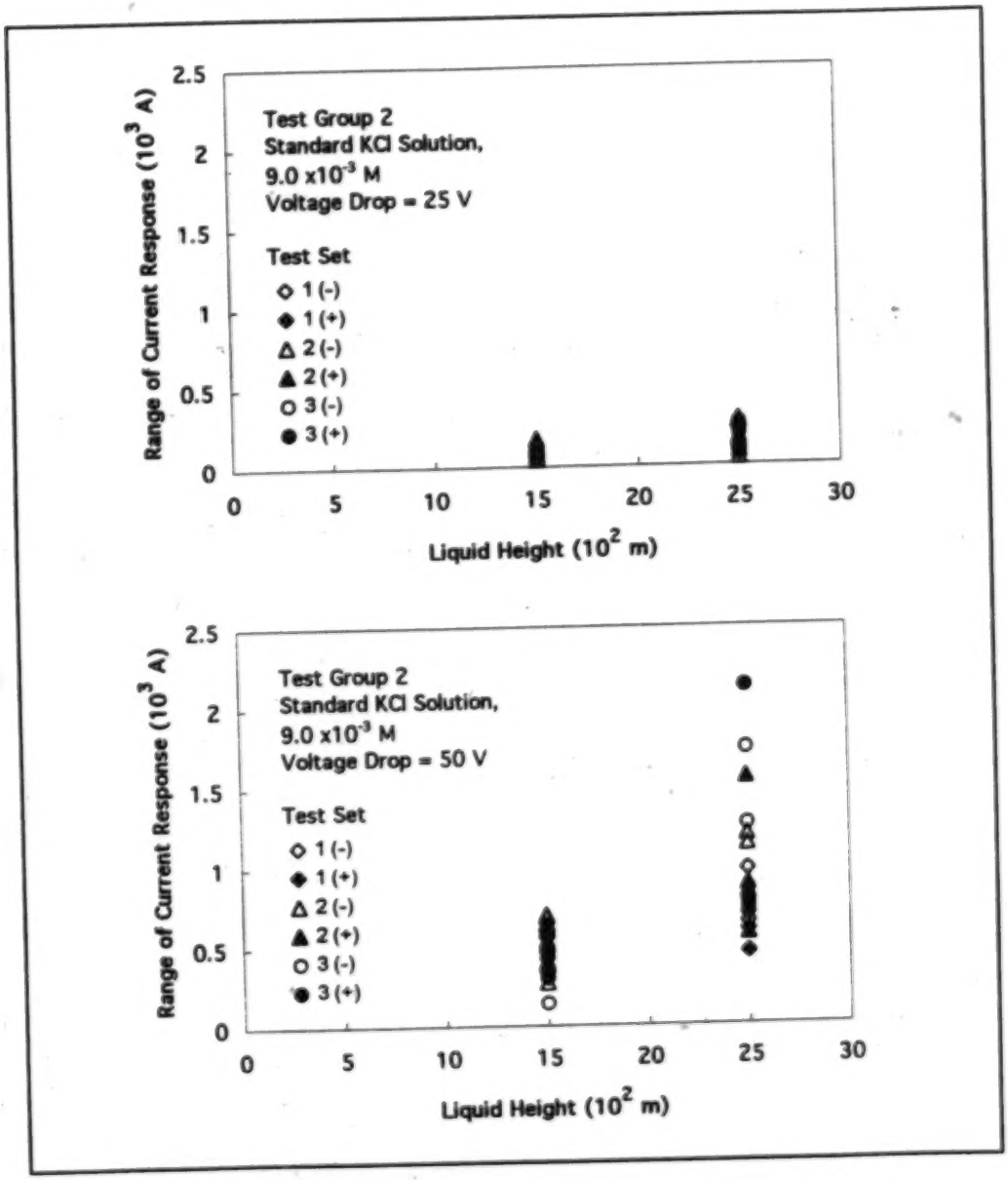

Figure 5.10 **Test Group 2: Variation of Current Range with Liquid Height for Voltage Drops of 25 V (above) and 50 V (below). Plots Derived From Data in Table 5.5.**

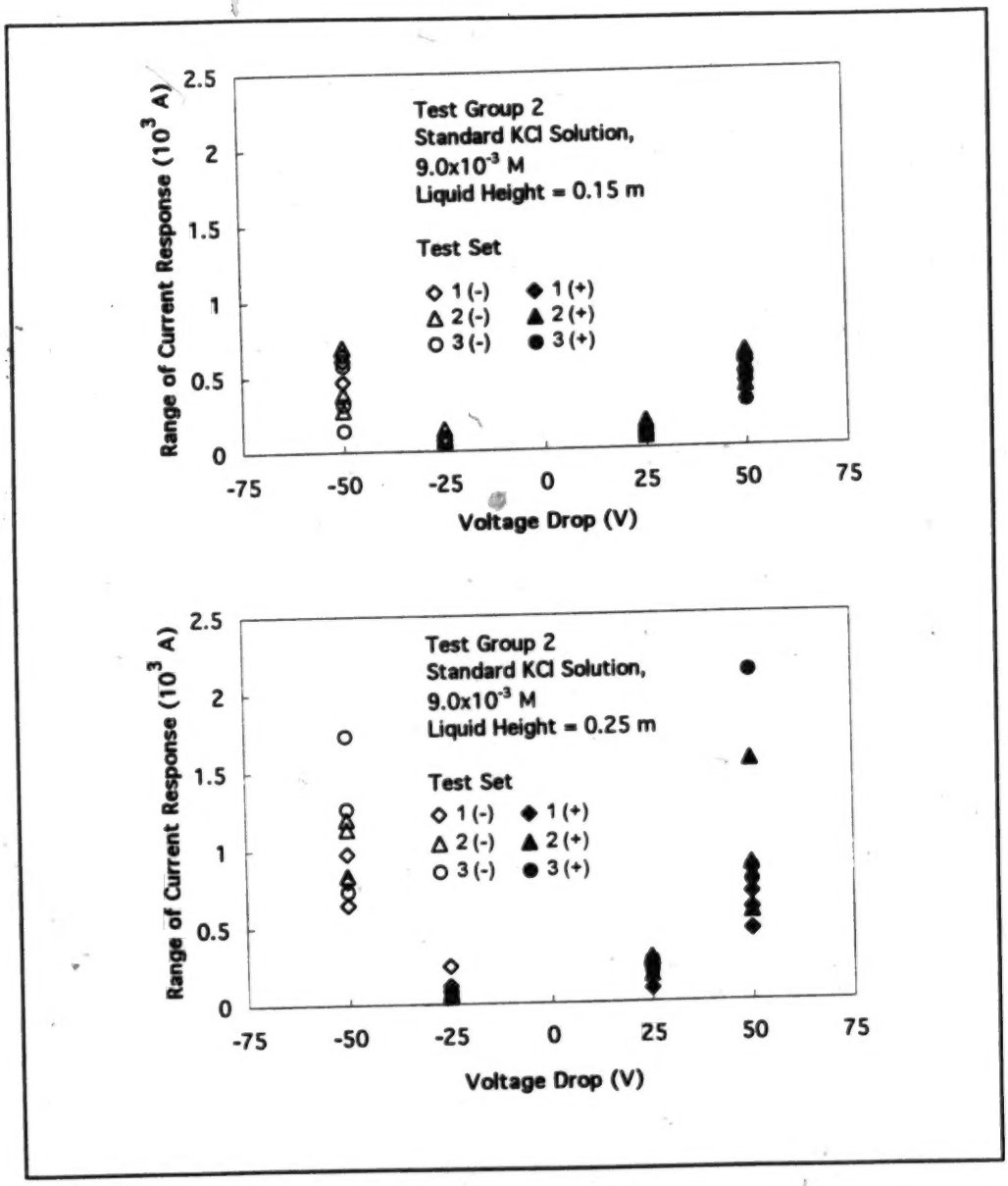

Figure 5.11 **Test Group 2: Variation of Current Range with Voltage Drop for Liquid Heights of 15 cm (above) and 25 cm (below). Plots Derived From Data in Table 5.5.**

Figure 5.12 gives a plot of the median of current as a function of the product of liquid height and voltage drop. Considering Equation 5-6, the results are not surprising.

$$I = \left[\frac{Y}{W} \times \sigma\right] \times V \times H \qquad \textbf{(5-6)}$$

where W is half the width of the cell (m), and
V is the voltage drop across the cell (V).

This relationship was upheld within the range of conditions tested. The quantity within the brackets can be considered as the cell constant of a given system. The cell constant was determined for each set by linear regression, and produced the values shown in Table 5.6. The lines displayed good linearity, but they did not cross through the origin as predicted by Equation 5-6. Within each set of tests, the cell constant was quite consistent, but the cell constant did vary considerably between sets. Consequently, a new cell constant had to be determined every time the electrodes were prepared.

Table 5.6 Electrode Tests, Group 2: Calculated Cell Constants

Test Set	Slope of Regressed Line [1] (Cell Constant) 10^4 A/V m	Intercept of Regressed Line [1] 10^4 A	Linearity (R^2)	Ratio of Effective Cell Width to Cell Depth [2]
1 (-)	3.4	-1.2	0.9924	29.7
1 (+)	3.4	-1.4	0.9959	29.7
2 (-)	4.4	-2.6	0.9751	23.0
2 (+)	4.5	-3.3	0.9728	22.4
3 (-)	3.1	-1.7	0.9713	30.5
3 (+)	3.0	-1.5	0.9866	31.5

(1) Regressed lines are shown in Figure 5.12, and refer to the variation of the median of current response with the product of the voltage drop and liquid height.

(2) The effective width to depth ratio was calculated by taking the inverse of the slope and multiplying by the solution conductivity. The conductivity was 1.01×10^{-2} $\Omega^{-1}m^{-1}$ for Test Sets 1 and 2, and 9.4×10^{-3} $\Omega^{-1}m^{-1}$ for Test Set 3.

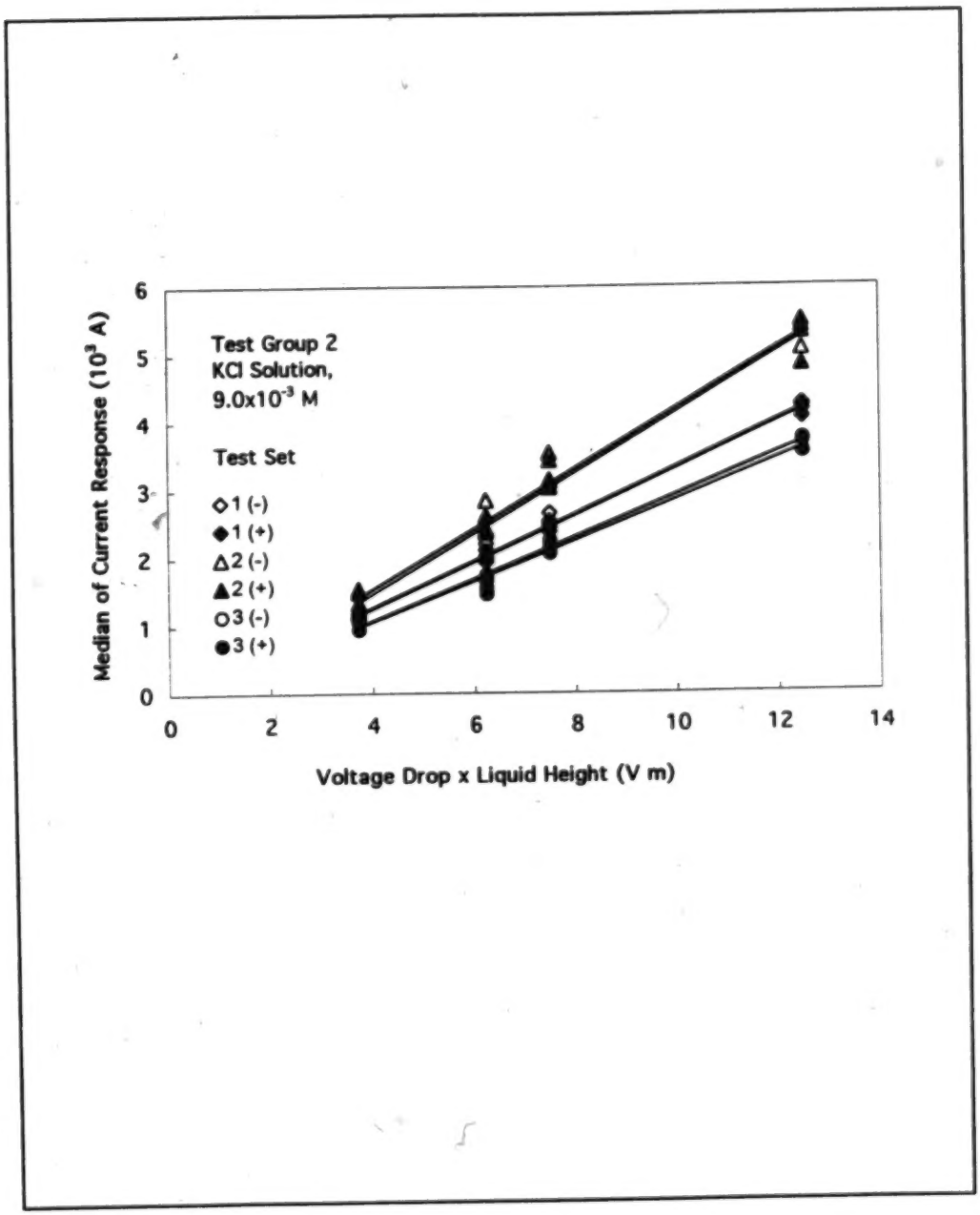

Figure 5.12 **Test Group 2: Variation of Current Median with Voltage Drop and Liquid Height**

5.3.3.5 Variation of Electrode Performance with Different Solutions (Test Group 3)

A third group of tests (Test Group 3) was conducted to characterize the effect of solution concentration on electrode performance. The electrodes were prepared according to standard electrolysis procedure, except that the hydrogen-charge and rest periods were reduced to one half hour each. The change was primarily made as a time saving measure. To compensate for the shorter period, the voltage drop was raised from 1.8 V to 3 V. At this potential, the cathodic wires generally began bubbling within 10 to 15 minutes. This was interpreted to mean that both these wires were being quickly saturated. Similarly, a thirty minute rest period was found to be sufficient to allow the excess bubbling to dissipate. Table 5.7 lists the conditions imposed during the electrode preparations.

Table 5.7 Electrode Tests, Group 3: Electrode Preparation

Test Set	Voltage Drop (V)	Initial Current (10^3 A)	Final Current (10^3 A)	Charging Time (hr:min)	Rest Time (hr:min)
1	3.1	25.3	24.1	0:35	0:30
2	3.0	25.0	23.2	0:27	0:30
3	3.0	25.7	25.0	0:30	0:30
4	3.2	25.7	25.5	0:30	0:30
5	3.1	25.6	25.5	0:30	0:30
6	3.1	24.9	24.7	0:27	0:30
7	3.2	26.5	26.2	0:30	0:30
8	2.8	25.0	24.2	0:30	0:30
9	3.1	24.9	24.7	0:30	0:30

The electrodes were mounted in the cell according to standard procedure. The cell was filled with electrolyte to 25 cm, and the standard two minute test was applied. For these tests, the electrical potential drop was 50 V. Two electrolytes were investigated; KCl and Na_2SO_4. Solutions of varying concentrations were mixed in the laboratory, degassed, and used within 24 hours of preparation. Table 5.8 summarizes the scheme of experiments.

The current-time plots for Test Group 3 had the same distinct pattern as Test Group 2, so again, it was logical to analyze each test in terms of current maximum, minimum, median, and range. Table 5.9 lists these values for all 27 tests in this group. Again, the negative and positive current directions were analyzed separately.

In Figures 5.13 and 5.14, respectively, the ranges and medians (from Table 5.9) are plotted against the conductivity of the solutions. The error bars denote the 95 percent confidence limits. The conductivity of the solution was measured with a conductivity meter from Fisher Scientific before the liquid was poured into the electrophoresis cell. Changes in conductivity that may have occurred within the cell could not be measured. (This was a limitation imposed by the design of the cell, and needs to be rectified in subsequent models).

Figure 5.13 shows that the current range increased proportionately with the solution conductivity. The confidence intervals were quite small for conductivities below $1.5\times10^{-2}\ \Omega^{-1}m^{-1}$. Above this threshold, the confidence intervals broadened. It is not understood why the confidence intervals should have been so large for the data at 2.37 and $1.83\times10^{-2}\ \Omega^{-1}m^{-1}$. Evidently, there were other factors, besides the conductivity, that were in play.

Figure 5.14 shows that the magnitude of the current median increased monotonically with the conductivity, while the precision of the data tended to decrease accordingly. In particular, the final two tests run with Na_2SO_4 (at 2.37 and $1.83\times10^{-2}\ \Omega^{-1}m^{-1}$), produced very erratic data. A suitable explanation for the deviance was not determined.

Equation 5.3 predicts that the magnitude of the current should be linearly dependent on the conductivity, but the data from Figure 5.14 did not display a good linear fit. This observation indicated that the cell constant was altered during every hydrogen-charging session. This should not be unexpected, as the metal surface was being altered each time the wires were sanded and cleaned.

Table 5.8 Electrode Tests, Group 3: Experimental Design [1]

Test Set	Test Number	Electrolyte	Concentration (M)	Conductivity ($10^2\Omega^{-1}m^{-1}$) [2]
1	1	KCl	0.0009	1.35
"	2	"	"	"
"	3	"	"	"
2	1	KCl	0.001	1.53
"	2	"	"	"
"	3	"	"	"
3	1	KCl	0.001	1.39
"	2	"	"	"
"	3	"	"	"
4	1	KCl	0.002	2.54
"	2	"	"	"
"	3	"	"	"
5	1	KCl	0.002	2.82
"	2	"	"	"
"	3	"	"	"
6	1	KCl	0.0005	0.848
"	2	"	"	"
"	3	"	"	"
7	1	Na_2SO_4	0.0005	1.17
"	2	"	"	"
"	3	"	"	"
8	1	Na_2SO_4	0.001	2.37
"	2	"	"	"
"	3	"	"	"
9	1	Na_2SO_4	0.0008	1.83
"	2	"	"	"
"	3	"	"	"

(1) Investigation of the effect of electrolyte solution type and concentration (liquid height = 0.25 m, voltage drop =50 V)

(2) Measured by conductivity meter (Fisher Scientific).

Table 5.9 Electrode Tests, Group 3: Summary of Test Results

Test Set	Test Number	Electrolyte Type & Concentration (M)	Conductivity ($10^2\ \Omega^{-1}m^{-1}$)	Current (10^3A) [1]							
				Maximum		Minimum		Median		Range	
				- [2]	+	-	+	-	+	-	+
1	1	KCl, 0.0009 M	1.35	6.38	6.36	5.44	5.37	5.87	5.52	0.94	0.99
"	2	"	"	6.05	6.02	5.27	5.27	5.56	5.38	0.78	0.75
"	3	"	"	5.65	5.64	5.08	5.08	5.31	5.18	0.57	0.56
2	1	KCl, 0.001M	1.53	7.72	7.96	5.75	6.55	6.47	6.75	1.97	1.41
"	2	"	"	8.64	7.55	6.64	6.73	7.42	6.96	2.00	0.82
"	3	"	"	7.80	8.64	6.87	7.55	7.06	7.80	0.93	1.09
3	1	KCl, 0.001 M	1.39	8.67	8.57	6.02	6.73	6.95	6.98	2.65	1.84
"	2	"	"	10.38	10.07	7.51	7.77	8.71	8.10	2.87	2.30
"	3	"	"	9.26	10.50	7.23	8.40	7.72	8.85	2.03	2.10
4	1	KCl, 0.002 M	2.54	14.40	16.30	10.50	13.10	12.00	13.70	3.90	3.20
"	2	"	"	14.60	14.30	11.90	12.40	12.65	12.50	2.70	1.90
"	3	"	"	14.20	13.90	12.00	12.00	12.50	12.25	2.20	1.90
5	1	KCl, 0.002 M	2.82	15.98	15.50	11.02	11.89	13.04	12.51	4.96	3.60
"	2	"	"	15.89	17.91	12.06	15.06	13.86	15.57	3.83	2.85
"	3	"	"	14.53	13.93	12.98	12.13	13.25	12.66	1.55	1.80
6	1	KCl, 0.0005 M	0.848	5.42	5.03	3.68	4.02	4.55	4.15	1.74	1.01
"	2	"	"	5.36	5.02	3.98	4.01	4.39	4.13	1.38	1.01
"	3	"	"	5.44	5.40	4.00	4.27	4.47	4.36	1.44	1.13
7	1	Na_2SO_4, 0.0005 M	1.17	5.72	5.52	4.25	4.51	4.89	4.71	1.47	1.01
"	2	"	"	5.90	5.65	4.51	4.69	4.91	4.81	1.39	0.96
"	3	"	"	5.68	5.45	4.60	4.56	4.82	4.72	1.08	0.89
8	1	Na_2SO_4, 0.001 M	2.37	17.12	15.31	10.41	11.52	13.13	11.81	6.71	3.79
"	2	"	"	18.82	17.33	12.39	13.57	14.58	13.97	6.43	3.76
"	3	"	"	19.89	18.00	13.55	14.88	15.32	15.18	6.34	3.12
9	1	Na_2SO_4, 0.0008 M	1.83	8.56	8.56	6.67	7.18	7.43	7.38	1.89	1.38
"	2	"	"	9.29	9.29	7.44	8.05	7.96	8.24	1.85	1.24
"	3	"	"	19.89	18.00	13.55	14.88	15.32	15.18	6.34	3.12

(1) Liquid height at 0.25 m; voltage drop fixed at 50 V

(2) Negative/positive signs above columns denote direction of current

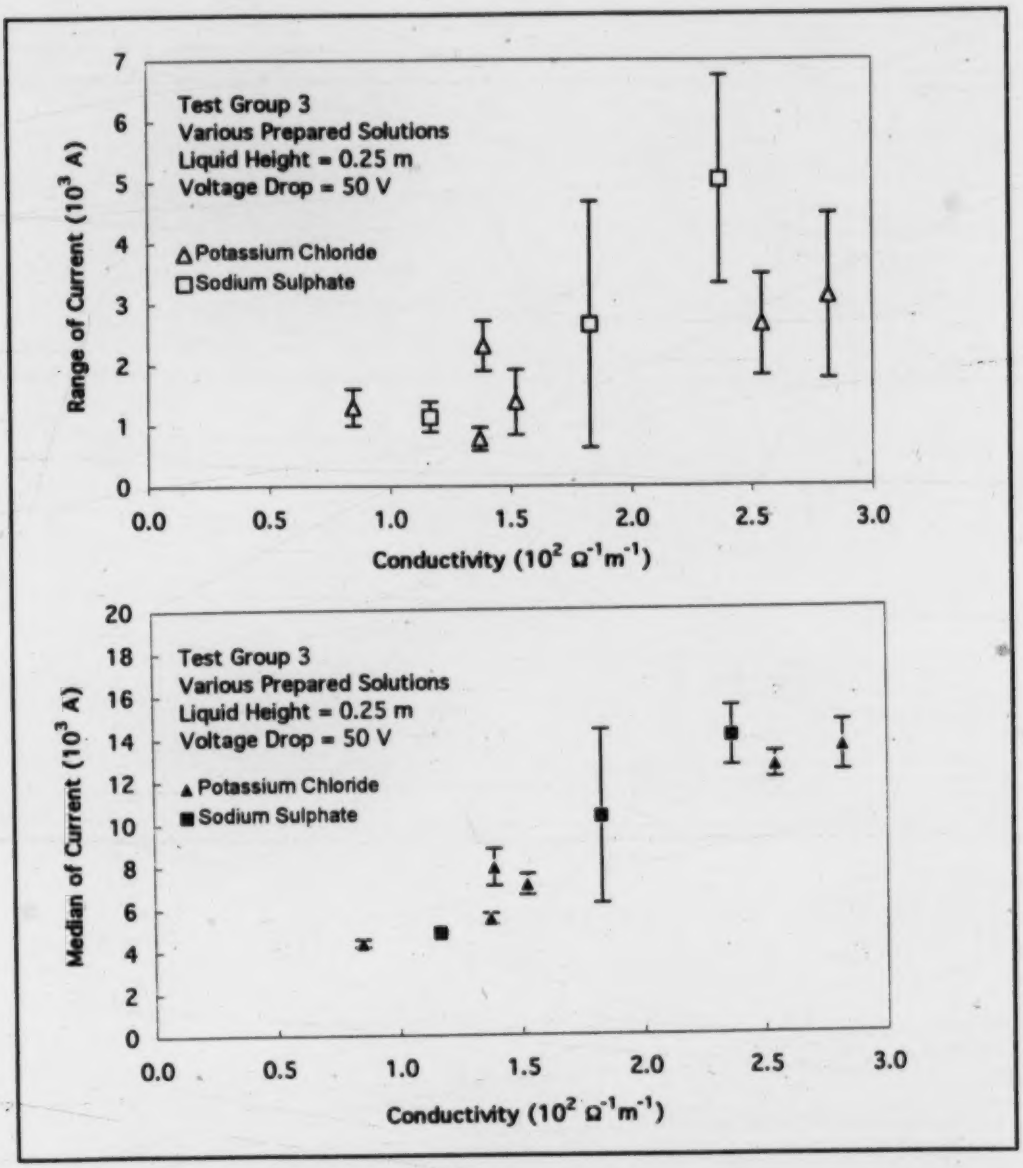

Figure 5.13 **Test Group 3: Variation of Current Range with Solution Conductivity**

Figure 5.14 **Test Group 3: Variation of Current Median with Solution Conductivity**

5.4 SUMMARY AND RECOMMENDATIONS

The hydrogen-charged palladium electrodes were able to provide an electric field within the magnitude range required for electrophoresis. The electrodes successfully suppressed bubbling and polarization, as indicated by the sustained current. However, the electric field did tend to vary over time. The degree of fluctuation increased with increasing voltage drop, liquid volume, and conductivity. It was also shown that fluctuations tended to increase with extended use in one constant voltage application. It is suspected that the variation could have occurred due to ohmic heating or volume changes of the palladium lattice. While the exact cause of the variation could not be isolated in this particular cell configuration, some operational rules of thumb were developed to limit the undesirable effects.

Firstly, it is recommended to limit the electrolyte concentration, such that the conductivity remains below $1.50\times10^{-2}\ \Omega^{-1}m^{-1}$. Secondly, extended use in any one constant voltage application should be avoided. Two minutes should provide ample time to make an electrophoretic measurement. Thirdly, the effects of ohmic heating can be minimized by reducing the solution temperature to about 278 K (Sirois and Millar, 1973), or by frequently introducing fresh solution.

There was no formal test completed to establish the useful life of an electrode for a given charging. The electrodes functioned adequately over periods of three to four hours. However, when left overnight in RO water, their bubble-suppressing capability was found to be highly diminished. Evidently, these electrodes have to be replenished with hydrogen at regular intervals. There was also no formal test done on the number of hydrogen absorption-depletion cycles that the electrodes can withstand. It is not unreasonable to expect that frequent cycling could eventually change the characteristics of the metal. Indeed, Neihof (1969) and Lewis (1967) did indicate that the palladium could be embrittled by overcharging.

There are several improvements that could be obtained by redesigning the cell and electrical system. Firstly, a constant current device should be implemented in place of a constant voltage supply (Seaman, 1975). Most commercial electrophoretic units do use a constant current supply, although in our case, a constant voltage supply was used because it was readily available.

Secondly, the electrode chambers and electrodes should be made larger, such that they extend beyond the front and back of the electrophoresis cell. The reason for this suggestion, is that there is no simple method to ensure that the electric field is uniform. Making the electrodes large is the simplest means to minimizing end effects. It might be advantageous to use thin foils, rolled into tubes, instead of purchasing large expensive

rods. There is also a safety issue to consider. Large pieces of palladium, freshly charged with hydrogen, can be highly reactive with the atmosphere (Plambeck, 1995).

Thirdly, porous glass barriers may be implemented to isolate electrode products away from the electrophoresis areas. Maintaining purity of solution was one issue that was not addressed in this first model because of the difficulties that would be incurred in the cell construction. The literature maintains that palladium is inert in most systems, except under acidic conditions, (Neihof, 1969; Pourbaix, 1974; Lewis, 1967). However, even in a neutral electrolyte solution, a local acidic environment is created in the vicinity of the anode. Thus the issue of electrode byproducts need not be a problem, so long as acidic media is avoided, the solution is frequently replaced, and the polarity of current is frequently reversed. This does, unfortunately, limit the research abilities of the electrophoresis cell. As a result, the addition of semipermeable barriers could greatly increase the scope of its scientific applications.

Finally, current fluctuations due to ohmic heating may be minimized by a cooling water jacket. It would also be of benefit to add an on-line current recorder. In its present form, the occurrence of these electric field fluctuations make it necessary for the operator to continuously monitor the current. As a result, this system is awkward and difficult to operate.

CHAPTER 6 THE OPTICAL SYSTEM

6.1 EQUIPMENT CRITERIA

An optical system provides the means to view and record the electrophoretic bubble motion. In choosing the system, several criteria must to be considered. Firstly, the system must provide sufficient magnification to view electrophoretic movement, but not so much that the bubbles would race across the view field. Secondly, the system also has to record the observed motion and play it back in real time. Finally, the mountings must be stable, secure, and easy to position. Stability is especially important when operating at high magnifications, in which even the smallest oscillations are greatly exaggerated.

6.2 EQUIPMENT CONFIGURATION

A schematic diagram of the optical components is shown in Figure 6.1. The system consisted of a Melles Griot fine focusing microscope, connected by an adapter to a Hitachi KP-113 B&W CCTV Camera. The camera, in turn, relayed the image to a television monitor (Sony Trinitron). Observations were documented by a video cassette recorder (Sony EV-7000 Hi-8 Editing VCR).

During experiments, the microscope, adapter, and CCTV camera were positioned in tandem as shown in Figure 6.2. The position of the adapter sleeve on the microscope neck was marked in ink such that the adapter could be assembled consistently each and every time.

The microscope body was mounted on a Melles Griot Stablerod™ System, which consisted of an adjustable height platform, Stablerod™, and an optical rail and carrier. The platform and rail carrier respectively provided vertical and horizontal positioning, while the Stablerod ™ inhibited undue vibrations. The entire assembly was screwed firmly into the cell support stand. A detailed frontal view is shown in Figure 6.3.

The CCTV camera rested on a standard camera tripod. A special holder was designed to allow the camera and focusing mechanism to move back and forth smoothly in unison. The holder consisted of a rectangular plastic trough with a glass-lined base. The plate was coated with a low viscosity oil and a layer of 3 mm diameter lead spheres. When the camera was placed inside this trough, it could glide smoothly over these spheres. The camera base was fitted with a glass plate that protected the electronics from the oil. A detailed view of this holder is shown in Figure 6.4.

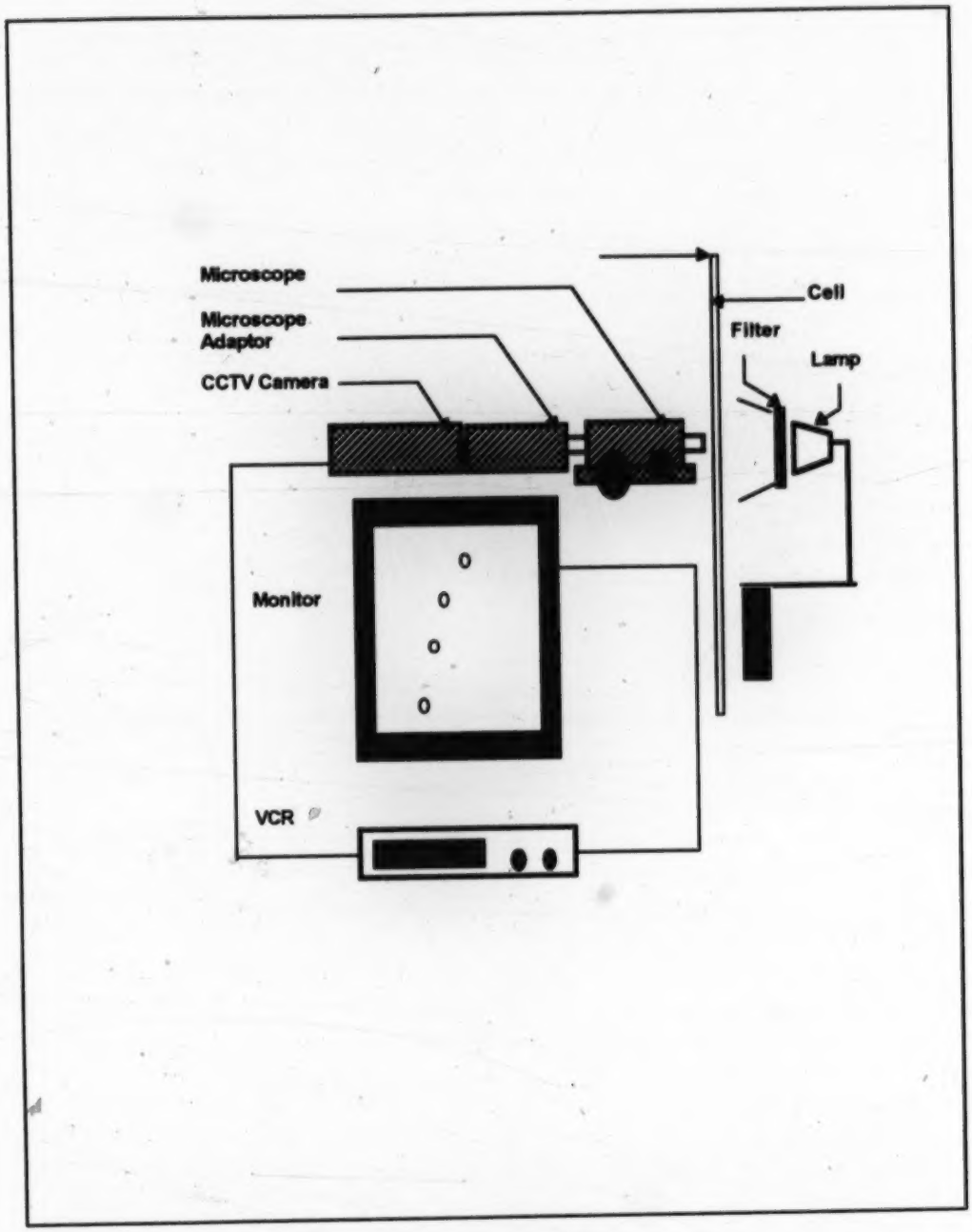

Figure 6.1 **Schematic View of Optical Components**

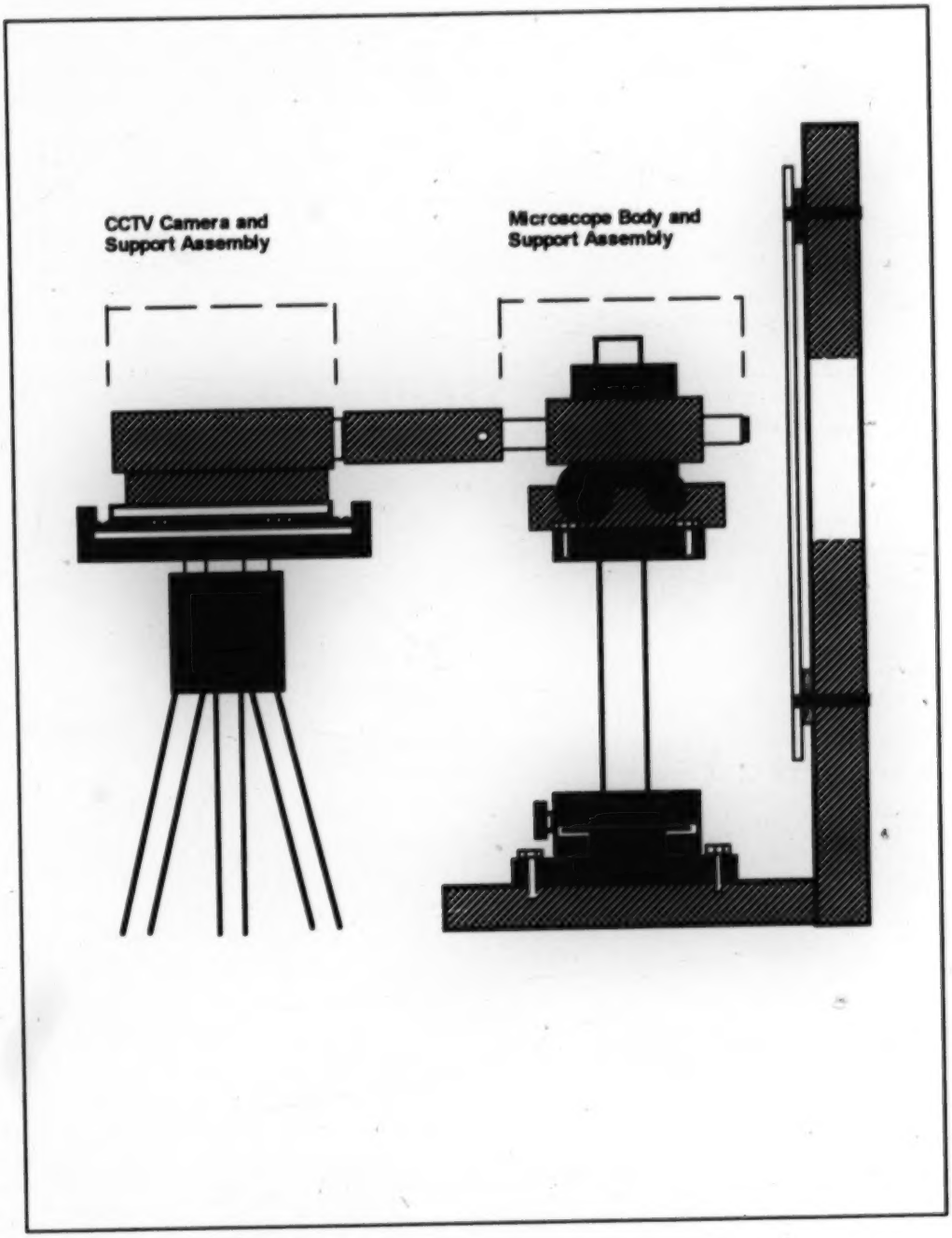

Figure 6.2 Arrangement of Microscope and CCTV Camera

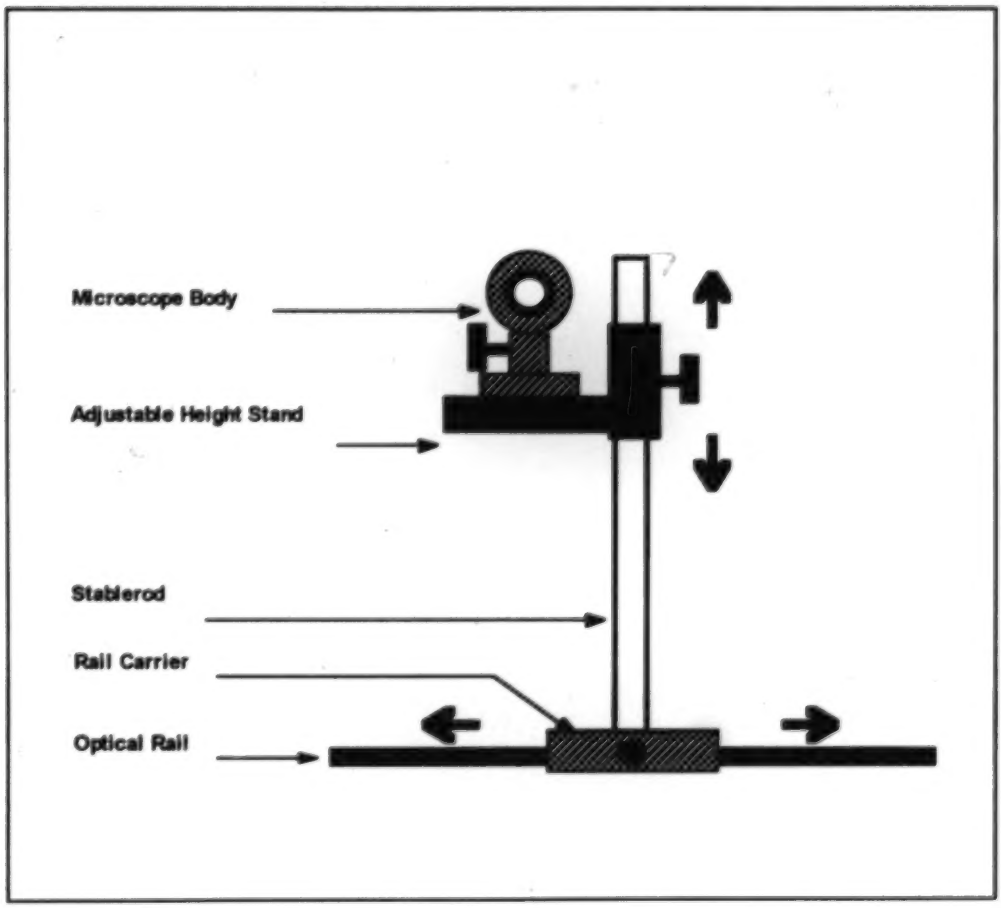

Figure 6.3 Front View of Microscope Mounting Assembly

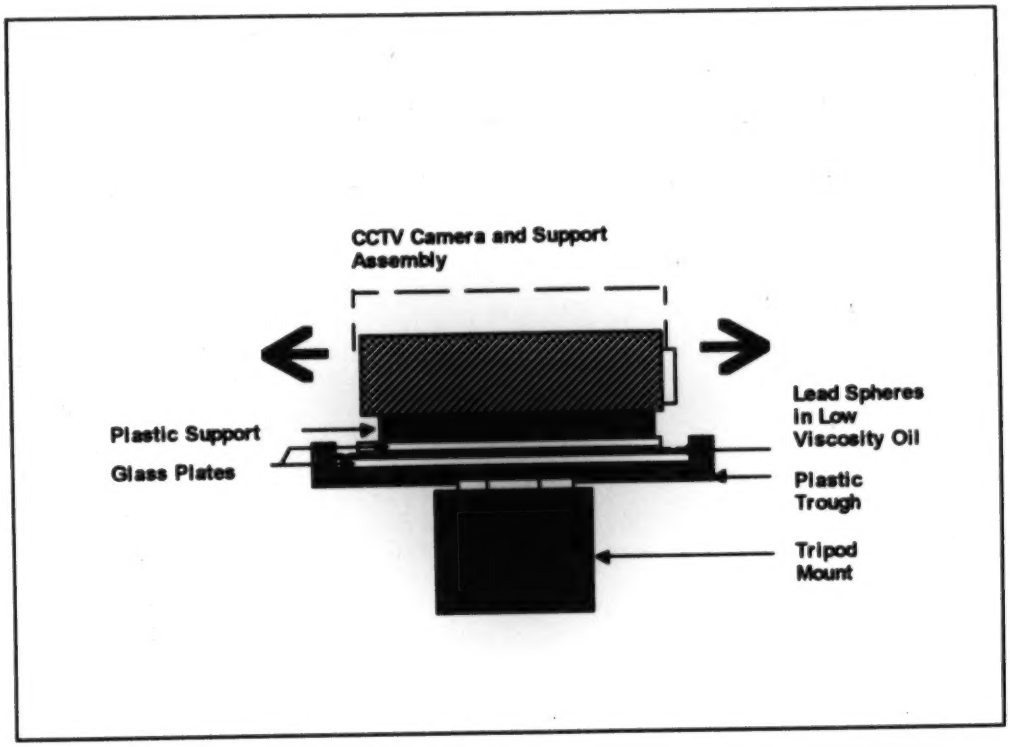

Figure 6.4 Detailed View of Camera Support Trough

6.3 MEASUREMENT OF CELL DEPTH

As described in Chapter 2 (Electrokinetic Theory), a bubble's electrophoretic velocity consists of electroosmotic and electrophoretic components. The electroosmotic component of the bubble's motion is a function of its distance from the cell walls. To distinguish between the electroosmotic and electrophoretic velocity vectors, it is necessary to:

1. determine the local depth of the electrophoresis cell, and
2. accurately pinpoint the position of the bubble in relation to this depth.

The bubble position was measured by a Mitutoya dial indicator, mounted as shown in Figure 6.5. This instrument was calibrated to read zero when the inner front wall of the cell was in focus. The cell depth was then measured by taking a reading at the inner back wall. The cell walls were easily identified due to small imperfections on the glass. Establishing the position of bubbles was then a simple matter of reading the position of the object plane from the dial indicator. Calibrations were made with a "wet" cell (filled with solution), to account for distortions caused by the liquid in the cell.

Precision of the dial indicator was tested by making nine sets of depth measurements. Each measurement consisted of taking readings at both the inner back and front cell walls, and the dial indicator was re-zeroed between consecutive trials.

Table 6.1 lists the results from these tests. The raw data are given in Appendix 6. Data sets 1 to 4 were made with a dry cell, whereby the camera and microscope were reassembled and positioned between sets. Sets 5a and 5b were taken at the same location, but with a dry and wet cell respectively. This was also the case with sets 6a and 6b. Here, "wet cell" refers to a cell filled with reverse osmosis water.

Table 6.1 Precision Testing of Dial Indicator Readings

Data Set	Number of Tests	Cell Condition	Readings at Front Wall			Readings at Back Wall		
			Average (mm)	Standard Deviation (mm)	Standard Deviation (% of Depth)	Average (mm)	Standard Deviation (mm)	Standard Deviation (% of Depth)
1	19	dry	19.7	10.8	0.6%	1795.4	12.3	0.7%
2	20	dry	2.9	10.0	0.6%	1772.9	15.7	0.9%
3	20	dry	-1.7	15.2	0.9%	1765.4	20.3	1.1%
4	20	dry	1.5	19.1	1.1%	1759.0	15.3	0.9%
5a	19	wet	-0.9	20.2	1.5%	1337.4	22.1	1.7%
5b	19	dry	-2.0	20.3	1.3%	1546.0	20.5	1.3%
6a	15	wet	19.3	80.6	6.0%	1334.1	17.6	1.3%
6b	15	dry	-10.4	98.2	5.6%	1762.1	25.9	1.5%

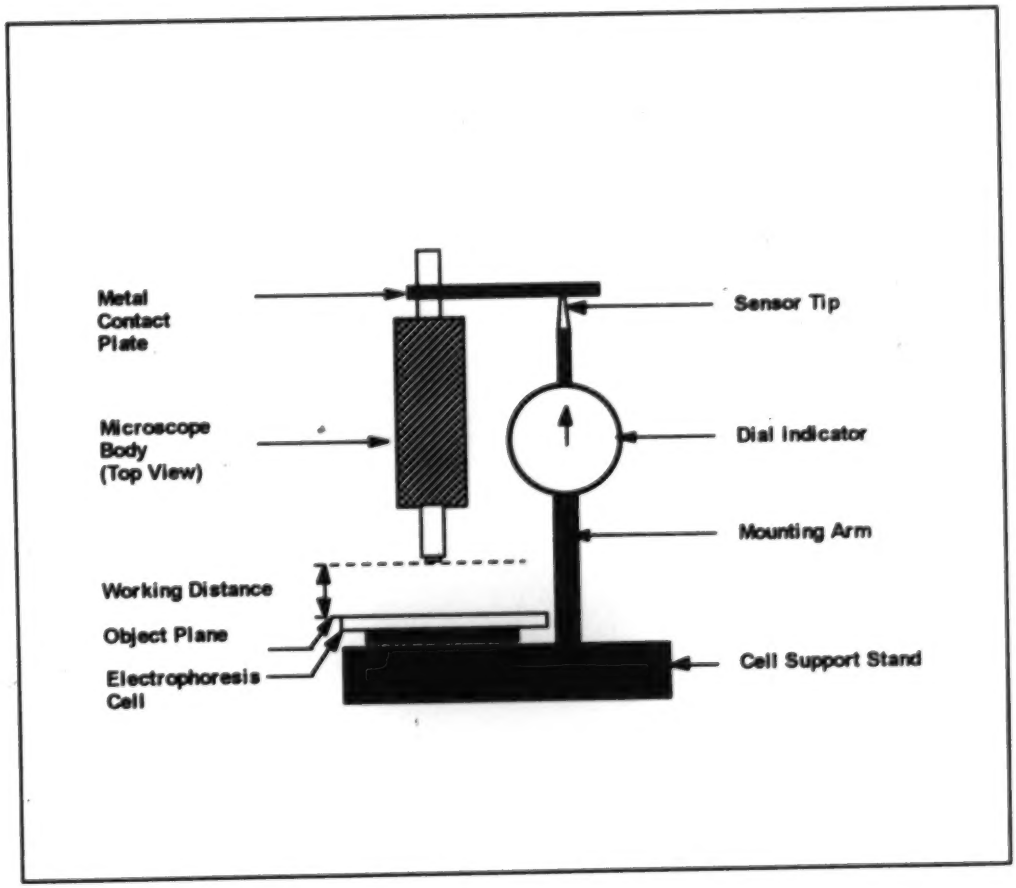

Figure 6.5 Top View of Dial Indicator Configuration

In general, there was no significant difference between the precision of measurements at the front and the back of the cell. The exceptions to this rule were series 6a and 6b, in which the camera rubbed against the sides of the holder. Otherwise, the standard deviation varied from 10 μm to 23 μm (0.6 to 1.5 percent of the measured cell depth). In addition, there were no significant differences in standard deviations between wet and dry measurements, or between measurements at the front and back walls

The precision was limited by the resolution of the video screen. It was challenging to verify when the cell walls were exactly in focus, and even more difficult to reproduce an exact image each time. There was also some slippage of the focus mechanism, particularly with the fine focus control knob. Ultimately, the fine focusing was dispensed with and only the coarse focusing was henceforth used.

6.4 CALIBRATION OF MAGNIFICATION

The overall magnification was determined in the following manner. The cell was filled with reverse osmosis water. A thin wire was then inserted into the cell. The diameter of this wire had been previously measured with a micrometer caliper at several locations along its length. The image of the wire on the screen was then traced onto a transparency, and the width of this tracing was determined by a ruler. Again, variability was taken into account by averaging several measurements along the length. The nonuniformity of the wire diameter produced the large uncertainty in the magnification. Table 6.2 summarizes the results.

Table 6.2 Calibration of Magnification

	Diameter of Wire	Diameter of Image		Magnification	
		Dry Cell	Wet Cell	Dry Cell	Wet Cell
Average (mm)	0.33	98.13	99.13	297	300
Standard Deviation (mm)	0.03	3.87	3.83		
Standard Deviation (percent of average)	8%	4%	4%		

6.5 IMAGE DISTORTION DUE TO SCREEN CURVATURE

There was some concern that the curvature of the video screen could distort the magnification. To assess this potential deformation, the microscope, was focused onto a standard reticle that was taped to the front of the cell. The scale of the reticle was 100 μm in length, divided into 10 μm divisions. These divisions, as viewed on screen, were traced onto an overhead transparency. Comparisons were then made between the magnification of the image and the position of the line segment on the screen. A

coordinate identification system was set up such that the abscissa spanned the screen from right to left, and the ordinate axis spanned from top to bottom.

Four sets of tracings were made. For each set, the scale image was moved to a new location on the abscissa. The adapter was disengaged and reassembled between every second data set. This procedure provided information on whether the repositioning of the adapter posed a significant source of discrepancy.

The tracings were analyzed by measuring the lengths of the line segments joining the 10 μm increments. The position of a segment was defined by the coordinates of its midpoint. In this manner, two plots were constructed. The first compared the magnification of each segment to the vertical location on the screen (y-coordinate). The second checked for a relation between magnification and horizontal position (x-coordinate). These plots are shown in Figures 6.6 and 6.7.

Figures 6.6 and 6.7 clearly show that precision of magnification was not related to the horizontal or vertical location of the image on the screen. Rather, uncertainty of magnification was a function of the actual length of the segment measured, as shown in Figure 6.8.

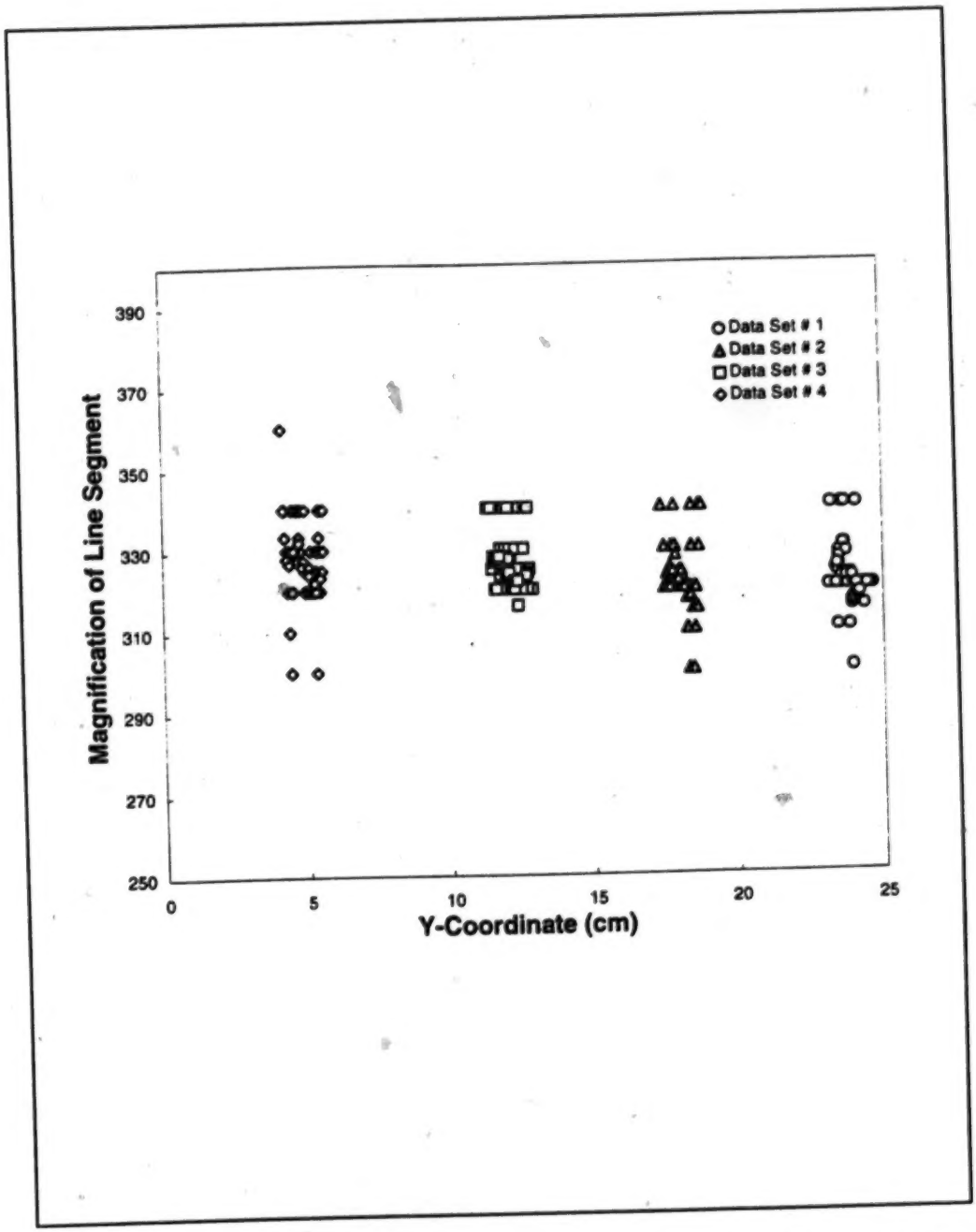

Figure 6.6 **Variation of Magnification with Vertical Position of Image on Video Screen (y-coordinate)**

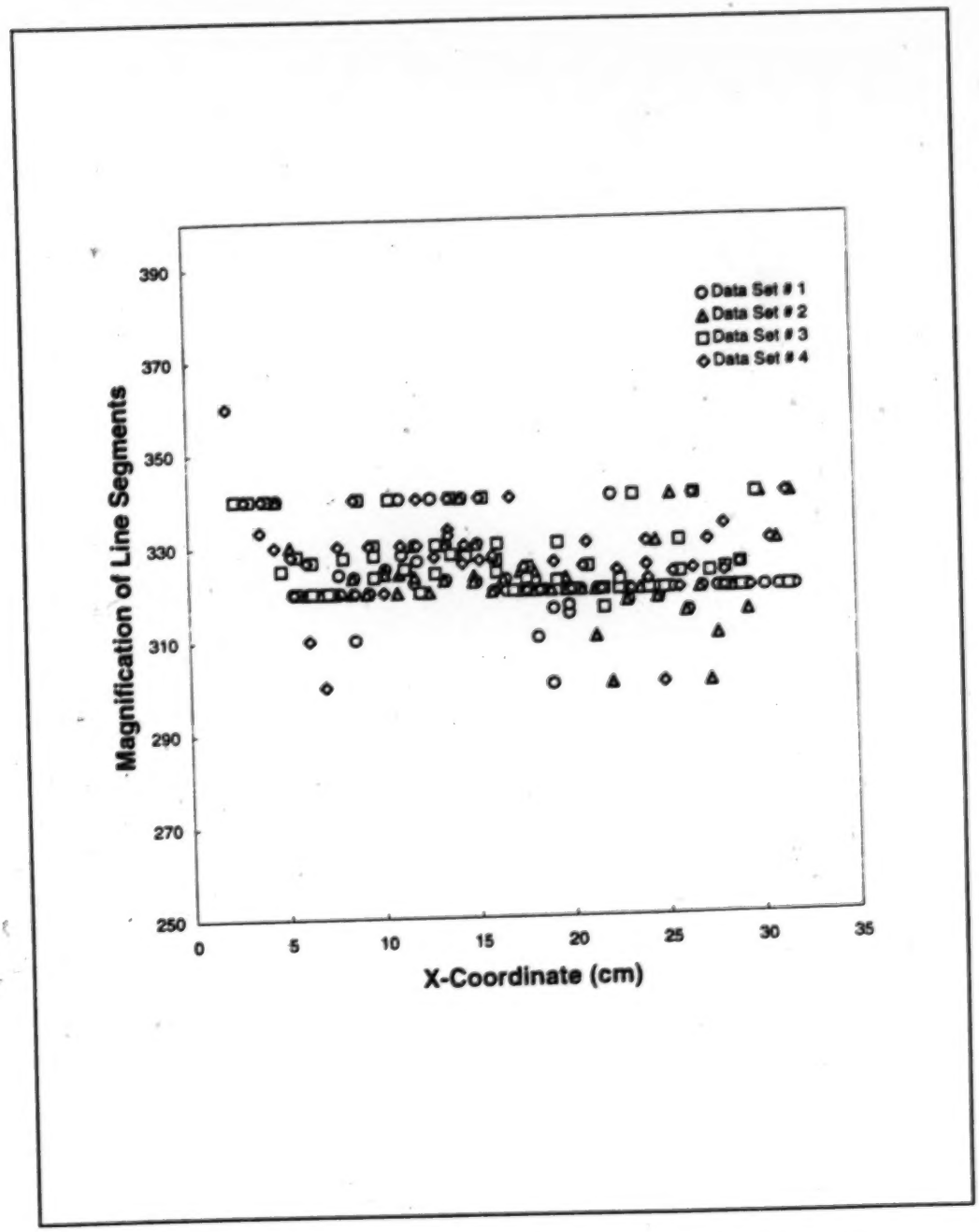

Figure 6.7 **Variation of Magnification with Horizontal Position of Image on Video Screen (x-coordinate)**

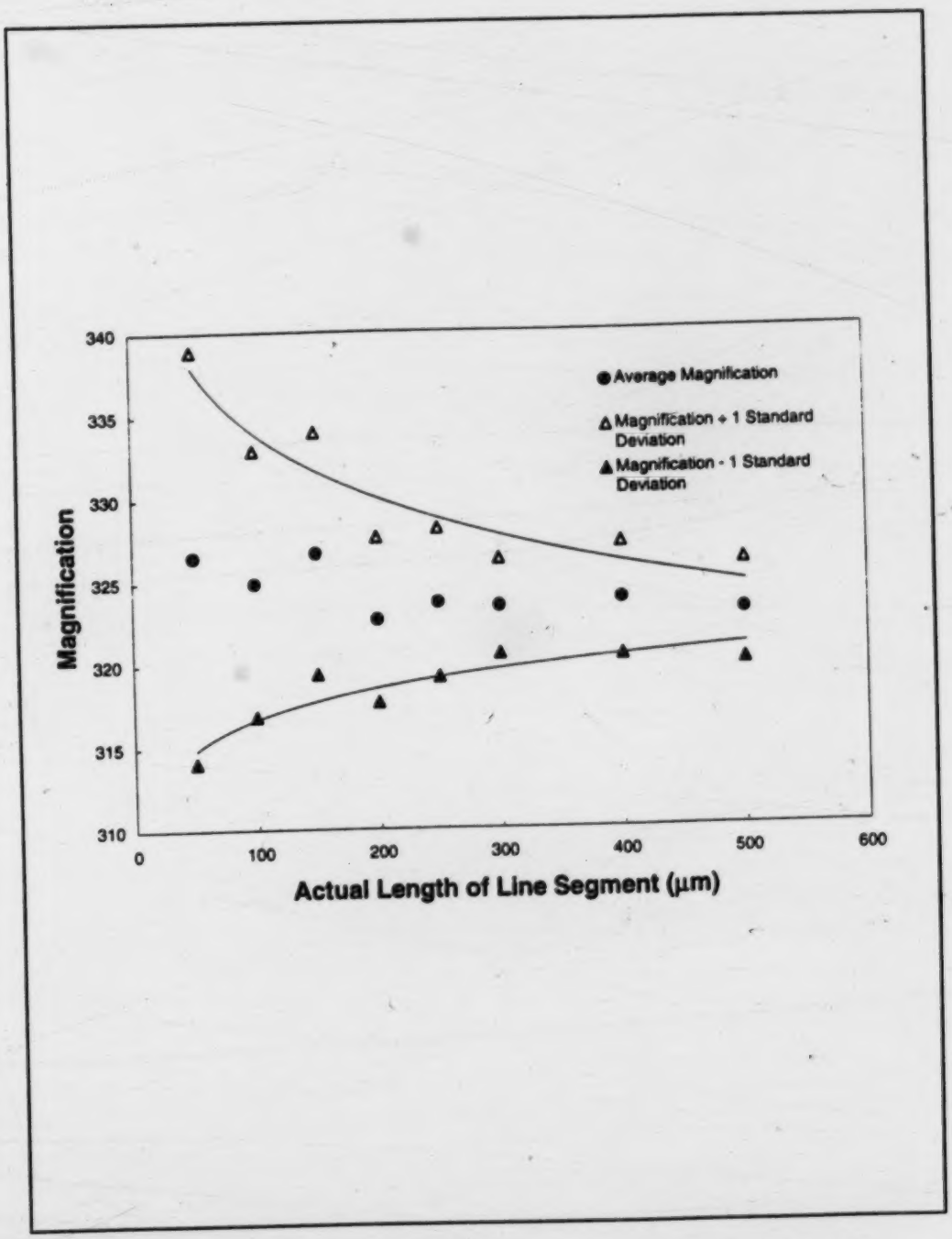

Figure 6.8 **Uncertainty of Magnification as a Function of Line Segment Length**

6.6 SUMMARY

An optical system was assembled to fulfill the listed equipment criteria. The apparatus could establish the depth-wise position of the objects with a maximum standard deviation of 20 μm. Uncertainty in locating the object plane was primarily limited by the quality of the monitor, and could greatly be improved by a high resolution screen.

The system provided an average magnification of 300 in a wet cell, with an expected standard deviation of four percent of the mean. The cell depth was measured to be about 1700 μm. Curvature of the monitor caused negligible distortion of the image.

CHAPTER 7 EXPERIMENTAL PROCEDURE (ELECTROPHORESIS TESTS)

7.1 PREPARATORY PROCEDURES

The cell mounting and preparation for electrophoretic experiments were elaborate procedures that consisted of the following steps:

1. preparation of the electrolyte solution,
2. mounting of the cell onto the platform,
3. attachment and testing of the bubble-producing electrode,
4. preparation and testing of the electric field-generating electrodes, and
5. positioning of the microscope, measurement of the cell depth, and location of the stationary planes.

7.1.1 Preparation of Electrolyte Solution

As determined in Chapter 3 (The Bubble-Producing System), the electrolyte solution had to be partially degassed in order to generate bubbles of a usable size. Reverse osmosis (RO) water was properly boiled for at least five minutes to drive off dissolved gases. One litre of the boiled water was transferred to a 2 L volumetric flask, which was then filled to the brim with untreated RO water. The flask opening was then quickly covered with several layers of wax "paper" (Fisher Scientific) to form an airtight seal. The contents were then cooled to room temperature. As the cooling took several hours, the water was usually boiled the evening before the solution was to be used, and allowed to cool overnight.

When the volumetric flask was sufficiently cooled, the seal was broken, and the contents were used to make up electrolyte solution of a desired concentration, either with KCl or with Na_2SO_4 salts. The chemicals were obtained from Fisher Scientific (reagent grade). The solutions were determined to have a limited shelf life of about one day. After one day, the solutions' ability to suppress bubble size was greatly reduced. In consequence, solutions were contained in volumetric flasks with tightly fitting stoppers, and every attempt was made to use solutions while they were still fresh.

7.1.2 Preparation and Mounting of the Electrophoresis Cell

The cell was thoroughly flushed for ten minutes with reverse osmosis water. The cell was then attached onto the stand and held in place by elastic bands. It was vital to mount the cell perfectly upright. Otherwise the bubbles would rise at an angle relative to the cell walls. This would present two problems. Firstly, the bubbles would impact the cell walls and never reach the viewing level, and secondly, the bubble trajectories would

not coincide with the stationary planes. The vertical positioning of the cell was a painstaking process, that involved the use of a level and adjustment screws at the base of the stand. As such, the cell was mounted only once during the entire electrophoresis test program. Once it was set up to satisfaction, it was not taken down from the stand. Cleaning and flushing cycles were henceforth completed in situ.

The next step was the attachment of the bubble-generating electrode manifold. Before this could be done, the manifold, including the bulb section that housed the counter-electrode, had to be filled with electrolyte solution. This was important so to ensure continuity of the bubble-generating electrical circuit. This task was not so simple, because the porous glass frit tended to trap air pockets in the bulb. It was finally necessary to attach a suction pump to force the liquid through the pores and to push the air out.

Once filled with solution, the manifold was now ready to be attached to the cell. The nozzle at the neck of the manifold was first wrapped with a thin layer of Teflon tape to form a leak proof fit between the male and female joints. An elastic sling helped to further reinforce the connection. The bubble-generating electrode and counter electrode were then connected to a power supply. The voltage was momentarily switched on to establish that the electrode was actually working. It was preferable to perform this test at this juncture, because trouble-shooting and parts replacement was simpler to complete before the entire assembly was put together. When the electrode was found to be not working, the cause was often attributed to a loose or broken electrical connection. It was prudent to keep several electrodes on hand, just in case. Finally, two coatings of waterproof silicon rubber were applied around the coupling and allowed to dry. The resulting connection was now airtight and leak-proof.

The final assembly step was to connect Tygon tubing between the bubble generating electrode manifold and the flow control valve network. There was difficulty in expelling trapped air from the tubing and piping system. Usually, this was counteracted by elevating the sump tank, thus forcing solution to flow backwards through the tubing and up into the cell. It was also helpful to "bounce" the cell up and down a few times to release small bubbles trapped in the nozzle area. However, this process was inefficient, time consuming, and the air pockets were never completely purged from the lines. Future designs of this cell system should incorporate some device to purge trapped air from the system.

Now that the cell was fully assembled, it was thoroughly flushed with RO water, then filled with electrolyte solution. To prevent inadvertent dilution of the electrolyte, the cell was completely filled and emptied three times, and then filled with solution once more. Filling took place from the top downward, using a beaker and microtubing, or an eyedropper.

7.1.3 Preparation of the Electric-Field Generating System

Prior to every electrophoresis session, the electric field-generating electrodes were charged rapidly with hydrogen and tested to ensure that they were properly working. The procedure and results of these tests are discussed in detail in Chapter 5 (The Electric Field-Generating System, under the subheading: "Electrode Tests: Group 3").

7.1.4 Measurement of the Local Cell Depth and Location of the Stationary Planes

The microscope, camera, and VCR were assembled as described in Chapter 6 (The Optical System), and aimed at the cell, roughly midway up its height. The bubble-generating electrode was switched on for a few minutes to produce a steady stream of bubbles. The microscope position was then adjusted until the bubbles appeared on the video screen. At this juncture, it became clear whether the partially degassed solution was working to keep the bubbles suitably small. If the solution was stale, then there was a larger proportion of unusable bubbles than if the solution was fresh. Care was also taken to watch for accumulations of bubbles on the inner walls. Such accumulations indicated a deviation of the cell posture from the vertical. In such cases, the cell mounting had to be readjusted, the cell had to be drained and refilled (to flush out accumulations of bubbles), and the bubble generator had to be tested again. Once it was ascertained that bubbles were rising properly without impediment, great care was taken not to disturb the cell assembly.

The system was now ready for measurement of the local cell depth and location of the stationary levels. The importance of this step is explained in Chapter 2 (Electrokinetic Theory). The method was similar to the procedure used to establish the precision of the dial indicator, as described in Chapter 6 (The Optical System). The depth was measured fifteen times, whereby the dial indicator was re-zeroed between measurements. The average was determined to be the depth of the cell in the region of focus (following adjustment for refraction of the liquid). The front and rear stationary levels were respectively calculated to be at 21% and 79% of the average measurement. The microscope was then focused on the front stationary plane.

This process was completed prior to every session of electrophoresis experiments, and was furthermore repeated if the cell or microscope were accidentally bumped or moved. At the completion of the this procedure, all components of the system were now in place to perform electrophoresis experiments.

7.2 ELECTROPHORETIC MEASUREMENTS

7.2.1 Procedure

The liquid height in the cell was initially adjusted to 25 cm. The electric field-generating power supply was switched on to "standby" mode. With the optical assembly focused on the front stationary plane, the bubble-generating electrode was switched on (at about 20 V) for a few minutes and then shut off. This practice allowed differences in buoyancy to separate the larger bubbles from the smaller ones. Once a promising bubble appeared, the video recording was commenced.

Much patience was needed when waiting for a bubble that was both in focus and of a suitable size. When such a bubble was found, the needle valve was opened slowly until the bubble rested at one height, or at least until its vertical ascent was significantly slowed. The most useful bubbles had diameters that ranged from 7 μm to 10 μm. Larger bubbles moved too quickly across the screen to be controlled. While their vertical motion could be slowed considerably, this required a counterflow that was too strong and which caused flow disturbances in the cell. Bubbles that were too small were too easily affected by flow disturbances caused by either the downcoming liquid, or by convection currents. With practice, the flow control mechanism was found to be highly effective at capturing the bubbles within the field of view. Once captured, a single bubble could be used to make several repeated electrophoretic measurements.

The motion of a captured bubble was first recorded in the absence of any electric field. This motion was referred to as the drift velocity. This observed drift was significant, and had to be accounted for in the data analysis. The magnitude of the drift tended to increase as time progressed. It was thought to be a product of heating from either the lighting, or from the repeated use of the palladium electrodes. The former cause was not likely because the lamp was shielded by a heat filter. When the drift velocity became too strong, the entire system was usually shut off for about twenty minutes, after which the cell was filled with fresh solution.

After the drift motion was recorded, the electric field was switched on. The initial voltage drop was set to 50 V, although this was not always enough force to counter the strong drift. Whenever feasible, the electrophoretic velocity of a bubble was measured in both directions of applied current. This was not always possible though. Sometimes a bubble would move out of focus or beyond the edge of the viewing screen before a measurement could be taken.

The direction of the electric field was picked at random. Most often, the direction was chosen to maximize the time which the bubble would remain on the screen. For example, if a bubble was located close to the left edge of the screen, it was logical to choose the field direction that would propel the bubble to the right. Assuming that the

bubbles were located exactly at the stationary level, and that they were probably negatively charged (Li and Somasundaran, 1991), it was expected that the bubbles would most likely move toward the anode. With the precise configuration of the electric field-generating circuit, this meant that the bubbles were expected to move in the same direction as the voltage directional control switch. Figure 7.1 illustrates this concept. However, the bubbles did not always move in the direction that was expected.

The greatest difficulty incurred by the system was in simultaneously keeping track of the electrical current, the location of the bubble, and the height of the liquid. Because the power supply could not maintain a constant current, it was necessary to monitor the fluctuations as time elapsed. It was impossible to do this and keep an eye on everything else at the same time. As a result, the current, voltage drop, and liquid height were noted at regular time intervals rather than continuously. This necessitated the use of interpolation in the analysis of the results. Future models, however, can be designed to avoid this problem. For example, an automatic data recorder would greatly ease the task of the operator.

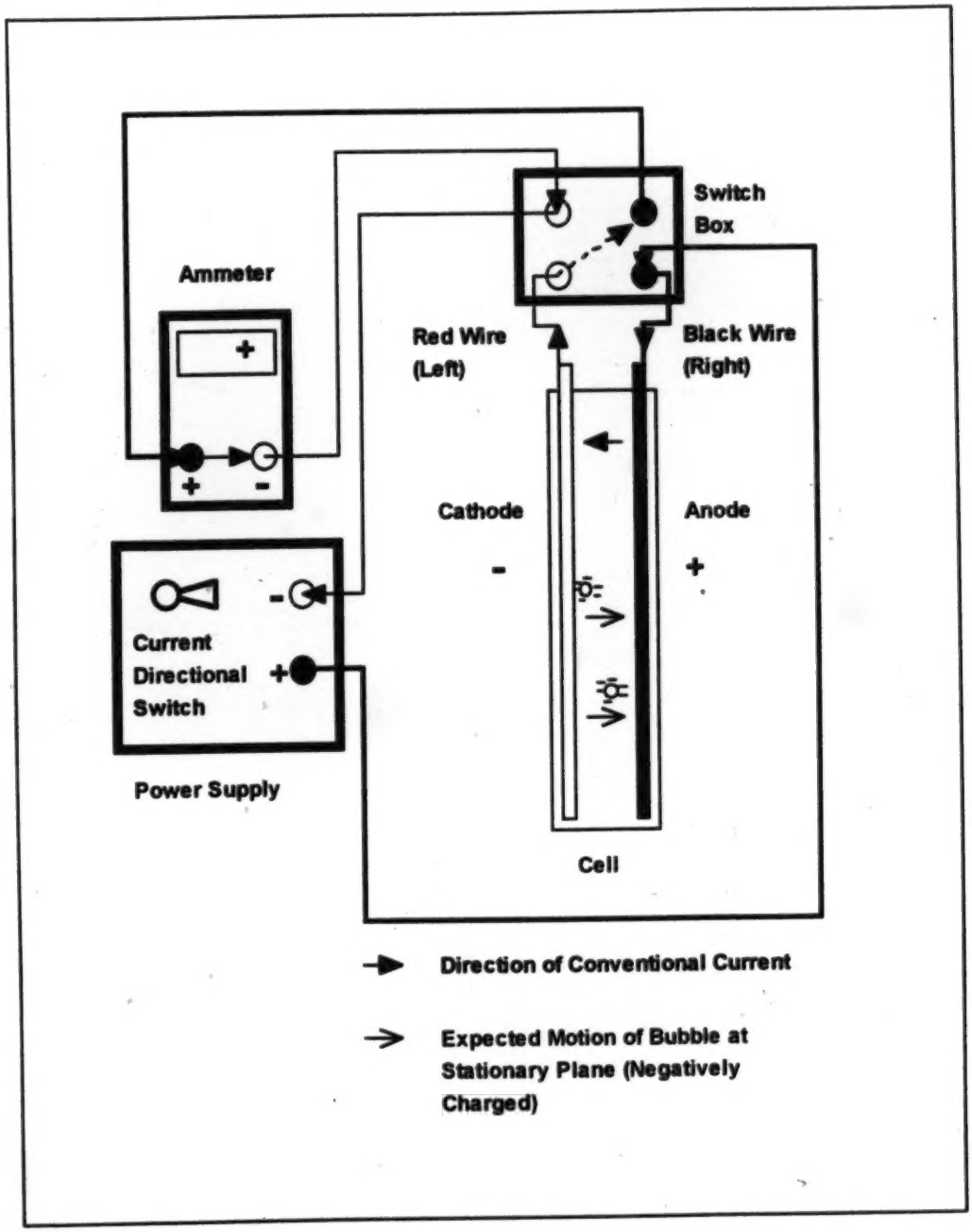

Figure 7.1 **Expected Direction of Bubble Motion Resulting from the Configuration of the Electric-Field Producing Circuit**

7.2.2 Collection of Data

Each recorded event was analyzed to yield an electrophoretic mobility. To calculate this value, the following parameters had to be acquired:

1. the local depth of the cell,
2. the electric current during the electrophoretic interval,
3. the height of solution in the cell,
4. the horizontal velocity of the bubble, and
5. the conductivity of the solution.

7.2.2.1 Local Depth of the Cell

The local depth of the cell was measured as part of the preparatory procedure. The procedure is described in detail in Chapter 6 (The Optical System).

7.2.2.2 Electric Current

The electric current was measured by an ammeter (Fluke 77 Multimeter) connected in series with the field-generating electrodes. Each time the electrical supply was turned on, a lag period of five seconds was allotted to allow the current to stabilize. The current was then recorded by hand every five or ten seconds for the duration of the electrophoretic event.

7.2.2.3 Height of Solution in the Electrophoresis Cell

Unlike a conventional cell, the effective height of the "Flow-through" cell does not stay constant during an electrophoretic event. Because the bubble must be captured by downcoming liquid, the height of the liquid, and thus also the effective cell cross section, are changed as the experiment proceeds. This facet requires that the operator must record the change of liquid height in addition to the changes in current.

The prototype cell was configured in such a manner that it was difficult to monitor both the height and the current at the same time. Consequently, the height was only noted at the beginning and end of each recorded event, (whereas the current was monitored at regular intervals throughout the electrophoretic event).

7.2.2.4 Horizontal Velocity of the Bubble

The electrophoretic motion of bubbles was recorded on video and played back in slow time. This particular cassette recorder was equipped with a time code adapter that

imprinted the elapsed time directly on the tape. This feature enabled the analyst to correlate any time frame on the tape with the real time data collected by hand (electric current and liquid height).

Only the horizontal trajectories of the bubbles were required for the calculations. Inherent to this approach was the assumption that the electric field lines were also straight and horizontal. To aid in the velocity measurements, a Cartesian grid was printed on a transparent sheet, which was then taped to the screen. The trajectory of the bubbles were traced onto the transparency, and the electrokinetic vectors were resolved into vertical and horizontal components. The drift velocity vectors were also resolved in this manner.

7.2.2.5 Conductivity of the Solution

Solution conductivity was measured with a Fisher Scientific conductivity meter (Dabros, 1995). The meter was first calibrated in standard solution to determine the instrument cell constant (not to be confused with the electrophoretic cell constant). It should be noted here that the value measured was that of the solution before the liquid was poured into the cell The construction of the cell did not allow for a sample to be removed for such an analysis. of the apparatus. As a result, changes to the solution that occurred in situ could not be accounted for.

7.3 SUMMARY

Prior to making electrophoretic measurements, an elaborate preparatory procedure was required to be carried out. The procedure consisted of making the electrolyte solution, mounting the cell, attaching the bubble-producing electrode and its housing, hydrogen-charging and testing the electric field-generating electrodes, and positioning the microscope.

Once the preparations were complete, the electrophoretic experiments could proceed. The experiments entailed measuring several parameters, including the local depth of the cell, the electric current magnitude and direction, the height of solution in the cell, the horizontal velocity of the observed bubble, and the conductivity of the solution. The experiments were challenging to run because there were many items that had to be looked after simultaneously. Despite this difficulty, the electrophoretic velocities of forty-five useful bubbles were measured and analyzed. The results are discussed in the next chapter.

CHAPTER 8 RESULTS AND DISCUSSION

8.1 ORGANIZATION OF DATA

The electrophoretic velocities of forty-five usable bubbles were recorded and analyzed. The results were organized according to bubble number. In some cases, a single bubble was used for repeated electrophoretic measurements. For such cases, each electrophoretic event was analyzed as a separate data set. For example, Bubble #19 was used for three consecutive measurements, denoted as Data Sets 19a, 19b, and 19c.

8.2 ANALYSIS OF THE DATA

The electrophoretic mobility, U_M, was calculated using the following equations:

(8-1) $$U_M = \frac{U_P}{E_\infty}$$

(8-2) $$\frac{U_P}{E_\infty} = \frac{L}{\mathrm{MF}} \times \frac{1}{\Delta t} \times \frac{\sigma}{I} \times 2HY$$

where U_P is the electrophoretic velocity of the bubble (m/s),
E_∞ is the electric field strength, far from the bubble (V/m),
L is the horizontal distance traversed by the bubble, as seen on the video screen (m),
Δt is the time interval (s),
σ is the electrical conductivity of the solution, ($\Omega^{-1}m^{-1}$),
I is the electrical current (A),
H is the height of the solution at any given time (m),
2Y is the local cell depth (m), and
MF is the overall magnification of the optical system.

Since the microscope was focused on the front stationary plane, the electroosmotic component of the bubbles' velocities was assumed to be negligible. However, drift velocity vectors could not be neglected. Therefor, the observed horizontal trajectories were "corrected" as follows:

(8-3) $$L = L_{obs} - L_D$$

where L_{obs} is the observed distance travelled by the bubble (m), and
L_D is the observed drift trajectory (horizontal distance traversed in the absence of an electric field) (m).

The ideal objective was to make at least two measurements for every captured bubble; one in either polarity of current. However, the drift velocity often interfered with this goal. Often, the electric current could only be applied in one direction; whichever direction that ensured that the bubble remained within the view field.

The problem with drift velocity was aggravated as the solution conductivity was increased. Figure 8.1 illustrates this observed trend. Other factors were also thought to contribute to the drift velocity, as illustrated by the anomalies in Figure 8.1. For example, the first few tests run at $0.85\times10^{-2}\ \Omega^{-1}m^{-1}$ had an almost negligible drift velocity. As more measurements were taken, the electric field was applied for progressively longer periods, and the drift velocity was observed to increase. Similarly, the tests run at $2.52\times10^{-2}\ \Omega^{-1}m^{-1}$ included many aborted runs, during which the electric field was applied for extended periods. For tests run at $2.82\times10^{-2}\ \Omega^{-1}m^{-1}$, the drift velocity was so severe, that the apparatus had to be shut down to cool within five to ten minutes of application. It is believed that the drift velocity was caused by ohmic heating of the field-producing electrodes. The heat from the back-lighting may have also contributed to convection currents, but that is unlikely, as the lamp was covered by an infra-red filter.

The zeta-potentials were calculated using the Helmholtz-Smulochowski equation (see Chapter 2, Electrokinetic Theory):

(8-4) $$\zeta = \frac{U_p \mu}{E_\infty \varepsilon \varepsilon_o} \qquad \text{for } \kappa a >> 1$$

The following equations were applied to confirm that κa was indeed much greater than unity (Hiemenz, 1986):

(8-5) $$\kappa(m^{-1}) = 3.29\times10^{9} M^{\frac{1}{2}} \qquad \text{for a 1:1 electrolyte}$$

(8-6) $$\kappa(m^{-1}) = 2.32\times10^{9}[6M]^{\frac{1}{2}} \qquad \text{for a 2:1 electrolyte}$$

Table 8.1 lists the calculated values of κa determined for the potassium chloride and sodium sulphate systems that were studied. Details on the Debye length are given in Chapter 2 (Electrokinetic Theory).

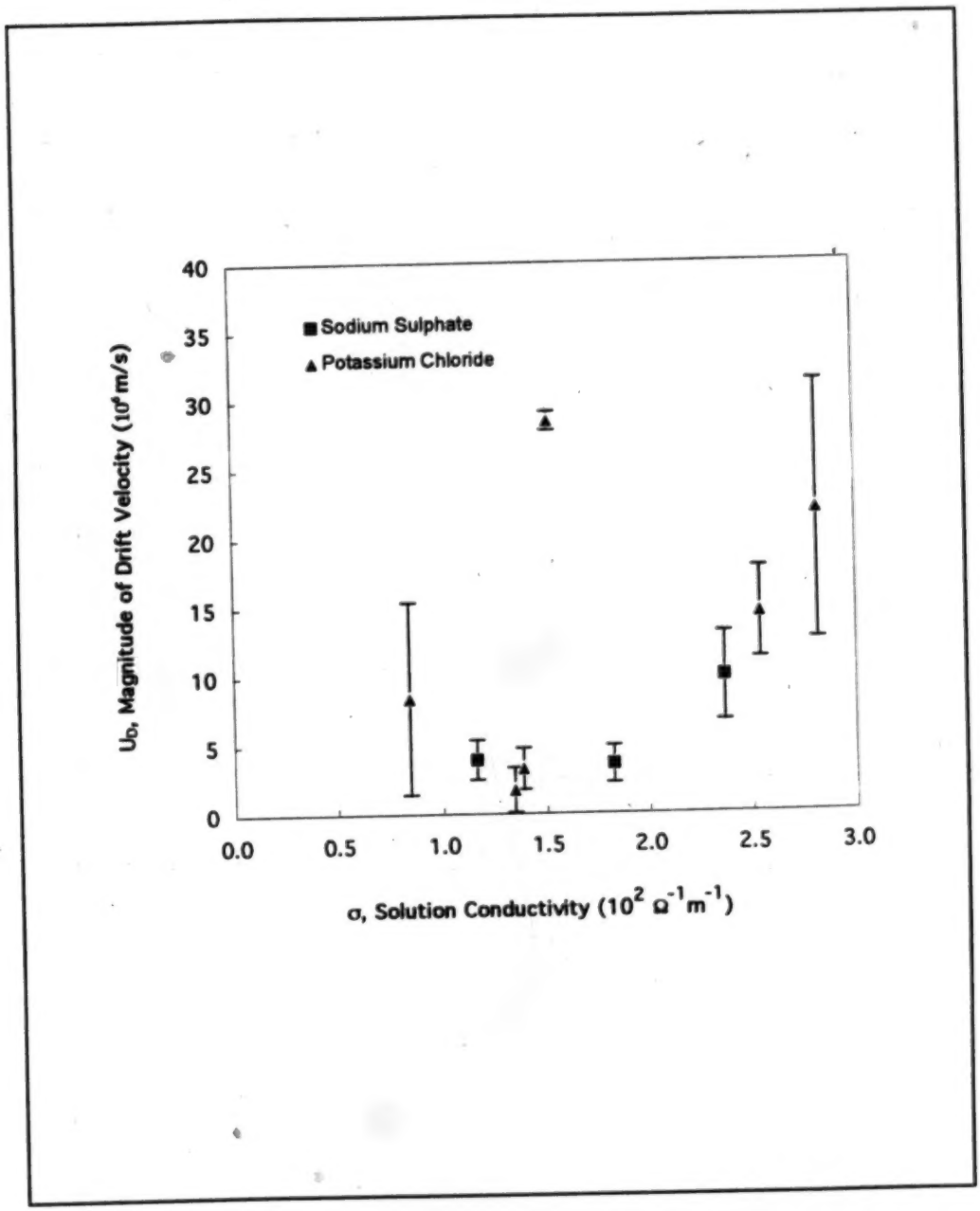

Figure 8.1 **Variation of Drift Velocity with Solution Conductivity (Error Bars Denote Upper and Lower Limits of the 90 % Confidence Interval)**

Table 8.1 Calculated κa Values for Aqueous KCl and Na_2SO_4 Solutions and Various Bubble Radii

Electrolyte	Concentration (M)	κa		
		$a = 2\times10^{-4}$ m	$a = 5\times10^{-4}$ m	$a = 15\times10^{-4}$ m
KCl	0.0005	150	370	1100
"	0.0009	200	490	1500
"	0.001	200	520	1560
"	0.002	290	740	2200
Na_2SO_4	0.0005	250	640	1900
"	0.0008	320	800	2400
"	0.001	360	900	2700

The calculations confirmed that indeed κa was much greater than unity. However, this did not necessarily mean that the Helmholtz-Smulochowski equation was applicable. The Helmholtz-Smulochowski, Hückel, and Henry equations were all developed to describe rigid non-conducting spheres (Wiersema et al., 1966; Hunter, 1981). Recently, Brandon et al. (1990) demonstrated that the electrophoretic mobility can vary with the bubble size. This deviation from classical theory was attributed to charge separation around the bubble. This separation was, in turn, attributed to either hydrodynamic flow around the bubble or polarization of surface charge by the electric field.

Brandon et al.'s results were apparently in conflict with those obtained by Okada et al. (1988), which showed that the bubble diameter was not a relevant factor. However, there were two principle differences between Brandon et al.'s studies and those of Okada et al. Firstly, Okada's team was studying bubbles with diameters that ranged from 14.4 μm to 33.1 μm. In contrast, the bubbles that Brandon's team studied ranged from 30 μm to 200 μm in diameter. The discrepancy between Okada's team and Brandon's team may have been caused by this difference in bubble sizes. One could argue that the smaller the bubble becomes, the closer it would resemble a point charge, and thus the less it would be prone to charge separation. The second fundamental difference was that Okada et al. studied systems that contained surfactants, whereas most of Brandon et al.'s systems were surfactant-free. Brandon et al. argued that adsorption of surfactant molecules onto a bubble would rigidify the surface, and suppress the separation of charge. Experimentally, Brandon's team showed that, with increasing concentration of surfactant (sodium dodecyl sulphate) in solution, the electrokinetic behaviour of oxygen bubbles did approach that of solid spheres.

If the findings of Brandon and his colleagues were in fact a function of the hydrodynamics, this could seriously impact the results obtained by the "Flow-Through" cell. In this study, most of the useful bubbles had diameters ranging from 7 μm to 10 μm. The scatter of data, however, was large, and no conclusions could be drawn about whether bubble size was an influencing factor.

In assessing the data, a convention was adopted whereby movements from left to right were considered to be positive (and vise versa). This convention applied to the true direction of motion. Since the optical system produced an inverted image, the true direction of motion was actually opposite to the observed direction. The same convention was applied to the direction of the electric field. The field direction coincided with the direction of conventional current across the cell. With the stringent configuration of the electrical system, the direction of field was the inverse of the direction of the polarity switch. Thus, when the switch pointed to the left, the electric field would in fact be pointing from left to right, and would thus be designated as positive. Consequently, the left electrode would act as a positive terminal, and the right electrode as a negative terminal. In such a case, a negatively charged bubble would naturally move from right to left; in the direction opposite to that of the electric field.

Initial viewing of the recorded trajectories showed that the electrophoretic velocity did not necessarily remain constant throughout the period in which the recording was made. This was no surprise, given that the magnitude of the electric field was also not constant. To compensate, each data set was divided into shorter time intervals. The electric field strength was calculated at the beginning and end of these subdivisions. To do so, the current and the liquid height data sometimes had to be interpolated to coincide with the interval endpoints. The average electrophoretic mobility was calculated for each sub-interval. Then these values were averaged again over the entire data set.

8.3 RESULTS

Tables 8.2 and 8.3 list the experimental results. The data are reported both as electrophoretic mobilities and zeta-potentials.

The principal problem with the results from this study was that the scatter was unacceptably large. It is, however, enlightening to compare the magnitude of error with that of others. Of all the research papers that were reviewed, only three authors divulged information regarding the error analysis of their results. Collins et al. (1978) reported their standard deviation to be 10 % of the mean of individual electrophoretic mobilities. Fukui and Yuu (1982), argued that Collins et al.'s results seemed "too good, considering their troublesome operation and the number of bubbles to be measured to determine each electromobility". Fukui and Yuu themselves reported typical standard deviations of at least 20 % of the averaged electrophoretic mobilities. Their work involved at least 80 measurements per concentration of electrolyte. Okada et al. (1990) reported their results in terms of zeta-potentials instead of electromobilities. Typical standard deviations ranged from 1.8 mV to 18.2 mV above and below the mean zeta-potentials. While the standard deviation in this study exceeded these values considerably, it is apparent that reproducibility problems are very common to particle electrophoresis.

The scatter of data was apparently unsystematic, being neither a function of solution conductivity nor of the bubble diameter. The random nature of the results alludes that the centers of the bubbles were not actually located at the stationary plane. The steep gradient of the electroosmotic velocity near the stationary planes would account for such large differences in measurements (see Chapter 2; Electrokinetic Theory). The prevalence of both positive and negative electrophoretic mobilities suggests that the focal plane was at least very near to the stationary level, but that the depth of field was not narrow enough to exclude bubbles on other planes. Bubble Numbers 2 and 3, for example, appeared to be simultaneously in focus, yet they moved in opposite directions when the electric field was applied (see Table 8.2).

As shown in Tables 8.2 and 8.3, there were not only deviations between the various bubbles, but also differences between electrophoretic measurements taken from individual bubbles. For example, Bubble Number 30 yielded electromobilities of -1.4×10^{-8} and -0.4×10^{-8} m^2/V s in two separate, consecutive measurements. This trend shows that the bubbles were probably moving back and forth along the y-axis (across the cell depth). It was also possible that the electric field was not spatially uniform. On a few occasions, a bubble was even observed to move in one direction for a period, then switch direction and move in the opposite direction. This motion was not accompanied by any changes in the focal quality of the object. Thus, either the optical system's depth of field was inadequate, or the bubble was moving through an electric field gradient.

Table 8.2 Results from Tests Conducted with KCl Solutions

Bubble Number	Data Set	Solution Conductivity $10^2\ \Omega^{-1}m^{-1}$	Bubble Diameter 10^6 m	Direction of Electric Field	Direction of Electrophoretic Motion	Electrophoretic Mobility $10^8\ m^2/V$ s	ζ 10^3 V
1	1a	1.35	10	←	←	-1.3	-19.1
"	1b	"	"	←	←	-0.9	-12.8
"	Average	"	"			-1.1	-16.0
2	2	1.53	13	←	→	2.0	28.8
3	3	"	10	←	←	-2.2	-31.7
4	4	"	8	←	←	-2.2	-31.2
5	5	1.39	13	←	←	-1.2	-16.8
6	6	"	7	←	→	1.4	20.0

Table 8.2 (Continued) **Results from Tests Conducted with KCl Solutions**

Bubble Number	Data Set	Solution Conductivity $10^2\ \Omega^{-1}m^{-1}$	Bubble Diameter 10^6 m	Direction of Electric Field	Direction of Electrophoretic Motion	Electrophoretic Mobility $10^9\ m^2/V\ s$	ζ 10^3 V
7	7a	1.39	13	←	→	0.5	6.5
"	7b	"	"	→	←	0.9	12.2
"	Average	"	"			0.7	9.4
8	8a	"	10	←	→	0.7	9.5
"	8b	"	"	→	←	1.5	21.5
"	Average	"	"			1.1	15.5
9	9a	2.54	7	←	←	-4.7	-67.3
"	9b	"	"	←	←	-5.2	-73.5
"	Average	"	"			-4.9	-70.4
10	10	"	13	←	←	-4.6	-65.2
11	11	"	10	←	→	0.5	6.7
12	12	"	7	←	→	0.8	12.1
13	13	"	5	←	→	0.5	7.1
14	14a	"	7	→	→	-0.9	-13.5
"	14b	"	"	←	←	-0.2	-3.0
"	Average	"	"			-0.6	-8.2
15	15	2.82	10	←	→	0.1	1.2
16	16	"	7	←	←	-1.4	-20.4
17	17	"	8	→	→	-0.2	-4.2
18	18	"	10	←	←	-2.3	-32.7
19	19a	0.848	7	→	→	-2.5	-35.6
"	19b	"	7	←	←	-2.6	-35.3
"	19c	"	7	→	→	-2.9	-40.3
"	Average	"	7			-2.7	-37.1
20	20	"	10	←	→	0.7	9.5
21	21	"	27	→	←	1.8	25.5
22	22	"	27	←	←	-0.3	-4.0
23	23a	"	7	←	←	-3.1	-43.9
"	23b	"	7	←	←	-2.4	-34.1
"	Average	"	7			-2.8	39.0
24	24	"	10	←	←	-0.9	-12.5

Table 8.3 Results from Tests Conducted with Na_2SO_4 Solutions

Bubble Number	Data Set	Solution Conductivity $10^2\ \Omega^{-1}m^{-1}$	Bubble Diameter 10^6 m	Direction of Electric Field	Direction of Electrophoretic Motion	Electrophoretic Mobility $10^8\ m^2/V\ s$	ζ 10^3 V
25	25	1.17	10	→	→	-3.7	-53.3
26	26a	"	10	←	←	-2.9	-41.4
"	26b	"	"	→	→	-2.7	-38.5
"	Average	"	"			-2.8	-39.9
27	27a	"	10	←	→	0.5	7.6
"	27b	"	"	→	←	0.2	2.4
"	Average	"	"			0.4	5.0
28	28a	"	7	←	←	-1.9	-27.5
"	28b	"	"	→	←	-0.9	-13.0
"	Average	"	"			-1.4	-20.3
29	29a	"	7	←	←	-1.2	-17.4
"	29b	"	"	→	→	-0.1	-1.2
"	Average	"	"			-0.7	-9.3
30	30a	"	10	←	←	-1.4	-19.4
"	30b	"	"	→	→	-0.4	-5.7
"	Average	"	"			-0.9	-12.6
31	31	"	8	←	←	-1.0	-14.7
32	32	"	8	←	←	-0.5	-7.4
33	33	2.37	7	←	←	-1.5	-21.7
34	34	"	7	←	←	-0.9	-12.6
35	35	"	7	←	←	-0.5	-7.3
36	36	"	7	←	←	-0.7	-10.4
37	37	1.83	8	←	←	-0.7	-9.7
38	38	"	8	←	←	-2.0	-28.1
39	39	"	10	←	←	-3.4	-48.5
40	40	"	7	←	←	-2.4	-34.7
41	41	"	12	→	→	-1.1	-15.7
42	42a	"	8	→	→	-1.2	-16.9
"	42b	"	"	→	→	-0.9	-13.4
"	Average	"	"			-1.1	-15.1
43	43a	"	7	←	←	-1.2	-16.3
"	43b	"	"	→	→	-1.0	-14.5
"	Average	"	"			-1.1	-15.4
44	44	"	8	←	←	-0.2	-2.7
45	45	"	7	←	←	-2.7	-37.8

The results from this study were compared to those obtained by Brandon et al. (1985). In both studies the bubbles were produced electrolytically from aqueous solutions of KCl and Na_2SO_4 with no surfactants present. The principle difference between the two studies was the size of the bubbles. In this study, most of the bubbles had diameters of 7 μm to 13 μm, whereas in Brandon et al.'s work, the bubble diameters ranged from 30 μm to 180 μm.

Figure 8.2 shows a plot of the electrophoretic mobilities of bubbles in 0.001 M KCl solution as functions of the solution pH, for bubble diameters of 30 μm, 100 μm, and 150 μm. Brandon et al.'s results showed the magnitude of the electrophoretic mobility to be an increasing function of both the pH and the bubble size. Given the trend observed in Brandon et al.'s results, the data from this study were expected to fall below the 30 μm curve, which indeed they did. The error bars denote upper and lower limits of the 90% confidence interval. In Figure 8.3, the results from Figure 8.2 were replotted against the bubble diameters. Brandon et al.'s data were fitted by linear regression, giving three separate lines representing pH 3.3, 6.2, and 6.8. To fit with the observed trends, the electrophoretic mobilities from this work should have almost coincided with the pH 6.8 line, but their magnitudes were actually considerably lower than expected.

A similar analysis was applied to the Na_2SO_4 system. The results are shown in Figures 8.4 and 8.5. Once more, Brandon et al.'s showed the electrophoretic mobility to vary linearly with the bubble diameter. To fit the observed trends, the data from this work were expected to fall in between the regressed pH 6 and pH 8 lines, which in fact, they did.

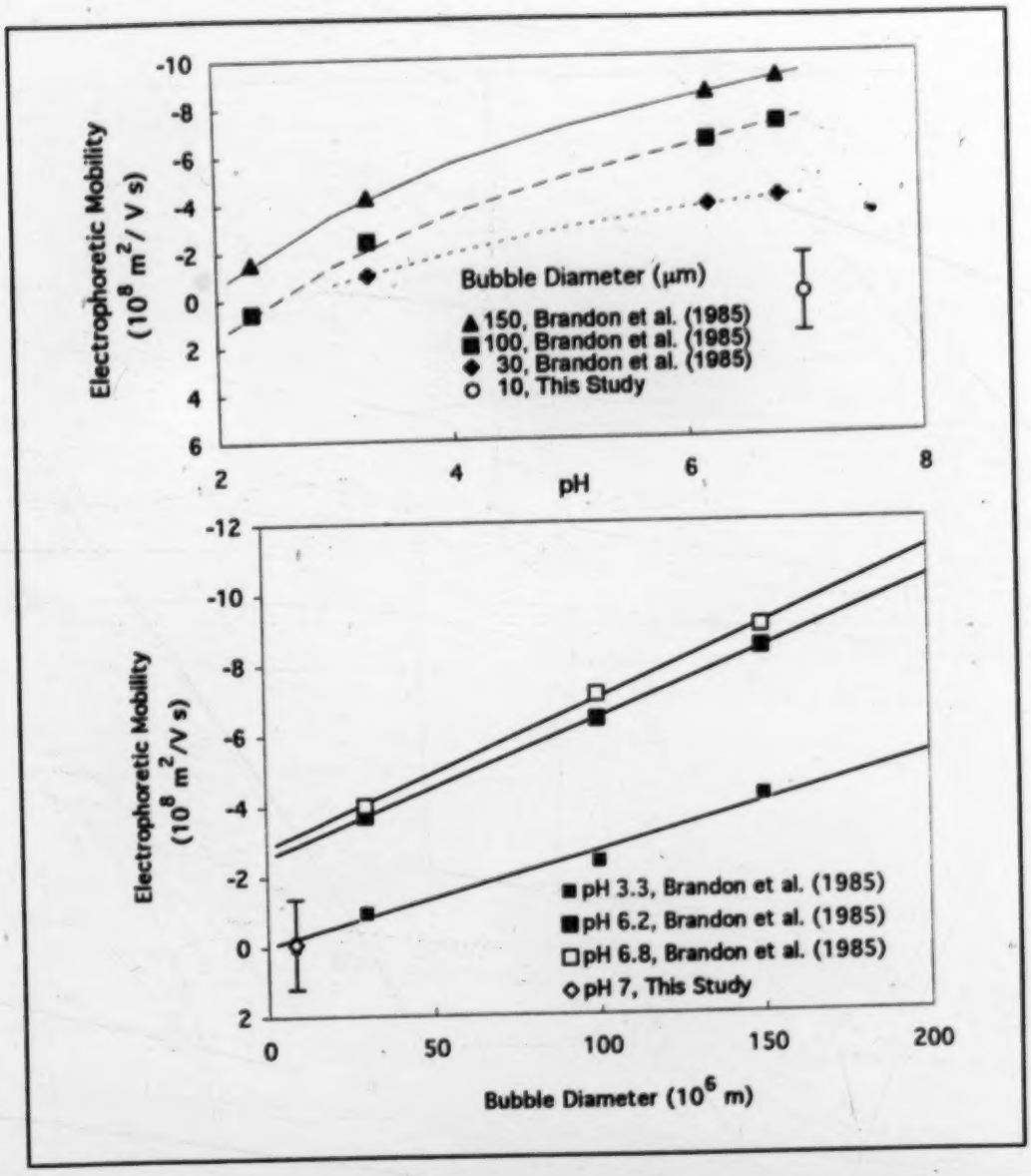

Figure 8.2 (above) **Comparison of Data from This Work to Results from Brandon et al. (1985): Effect of pH on the Electrophoretic Mobility of Chlorine Bubbles in Aqueous 0.001 M KCl Solution (Surfactant-Free)**

Figure 8.3 (below) **Effect of Bubble Diameter on the Electrophoretic Mobility of Chlorine Bubbles (Same System as Figure 8.2)**

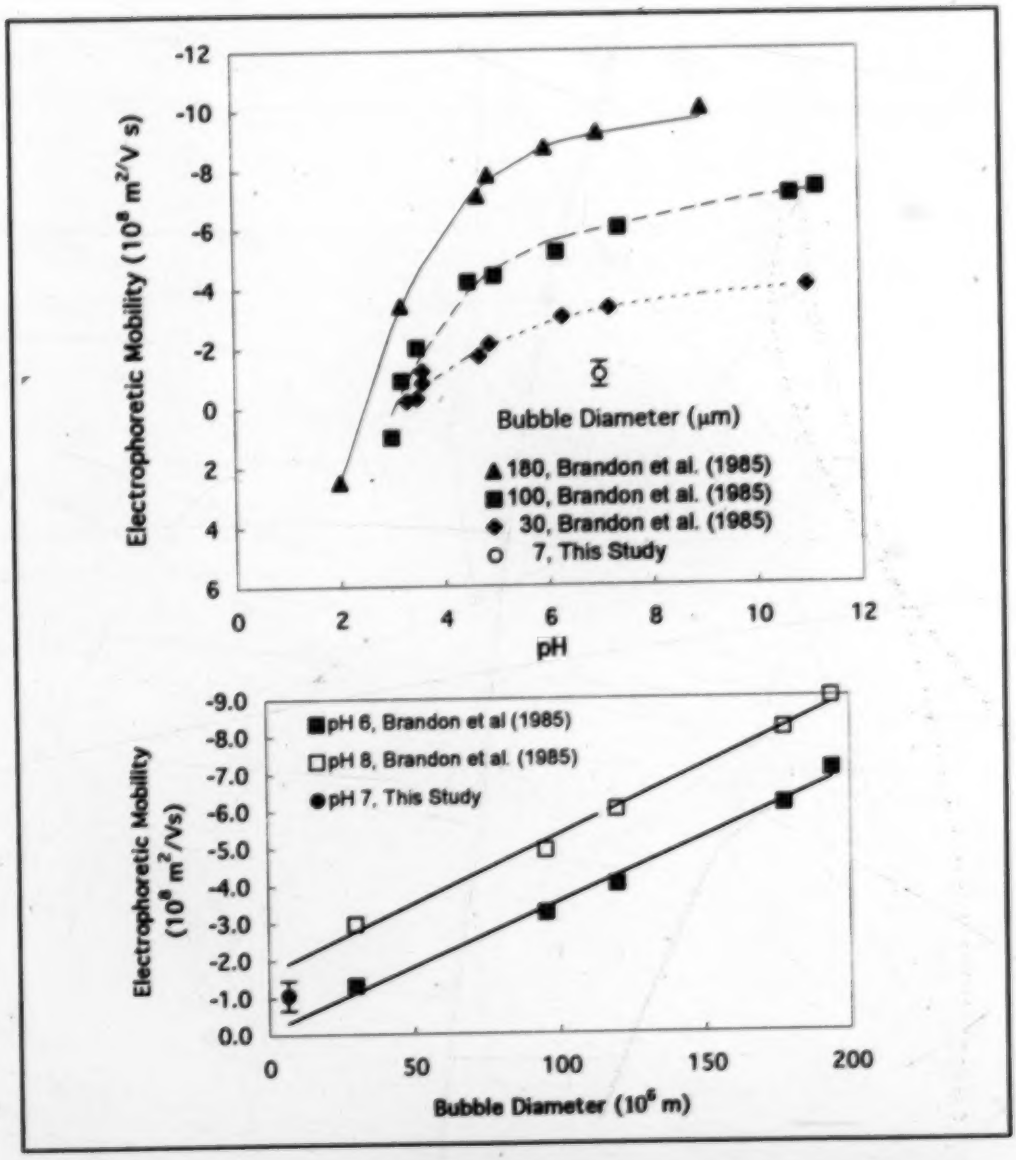

Figure 8.4 (above) **Comparison of Data from This Work to Results from Brandon et al. (1985): Effect of pH on the Electrophoretic Mobility of Oxygen Bubbles in Aqueous 0.001 M Na_2SO_4 Solution (Surfactant-Free)**

Figure 8.5 (below) **Effect of Bubble Diameter on the Electrophoretic Mobility of Oxygen Bubbles (Same System as Figure 8.4)**

8.4 RECOMMENDATIONS

The discussion now turns to methods by which the "Flow-Through" electrophoresis cell can be improved. Suggestions may be categorized into those which aim to improve the reproducibility of the data and those which aim to ease in the operation of the system. Ultimately, both would improve the credibility of the device.

8.4.1 METHODS OF IMPROVING THE REPRODUCIBILITY AND ACCURACY OF DATA

The dominant problem with these preliminary results was that the scatter of data is unacceptably large. The cause of the scatter may be attributed to three causes:

1. steep gradient of the electroosmotic velocity profile in the region of the stationary plane,
2. spatial non-uniformity of the electric field, and
3. movement of the bubbles along the y-axis of the cell.

The first cause may be alleviated by changing the optical devices to a system with a narrower depth of field. This option is, unfortunately, expensive. The more viable option is to change the procedure. The stationary plane method that was used is flawed on several counts. Firstly, the stationary level was determined theoretically rather than experimentally. Thus, deformities in the electroosmotic profile were not taken into account. Secondly, electromobilities were only measured at one stationary level, again not accounting for possible asymmetry in the elctroosmotic profile (Fukui and Yuu, 1982; Spitzer et al., 1981). Finally, the steep electroosmotic gradient in the vicinity of the stationary planes exacerbated any focusing errors.

An alternative approach is the depth-profile method, which avoids the direct use of any theoretical equation for the location of the stationary levels (Spitzer et al., 1981). The rationale behind the method is described in Chapter 2 (Electrokinetic Theory).

The drawback to this approach is that it was developed specifically for a closed cell. To apply this equation to the "Flow-through" cell, it would have to be proven that the flowing liquid would not alter the requirement of zero net horizontal flow. Furthermore, it would need to be determined where the estimate of one-directional flow is valid. Thus, it is evident that, despite the simplification to a one-dimensional flow expression, the method of depth-profile would require a very large number of electrophoretic measurements.

There was no simple way to actually measure local variations in the electric field. The usual practice in avoiding this problem is to avoid this problem altogether by making

the electrodes very large relative to the cell depth. Ideally this would eliminate the interference of end effects. This approach was difficult to adapt to the unusually tall "Flow-Through" cell. The electrodes used were the widest available palladium wires that could still fit into the electrode compartments. While thicker wires would have been preferable, they would have also drawn more current, thus limiting the usable solutions to very dilute electrolytes. The height of this particular cell was arrived with the assumption that the cell would be operated on a continuous flow basis (see Chapter 4: The Electrophoresis Cell). As it turned out, the cell was operated in an "outflow-only" mode. Consequently, the expected expansion disturbances at the flow intake were avoided altogether. Therefore, future cells may not have to be as tall as the prototype. Shorter cells would, in turn, require shorter electric-field generating electrodes, that would draw less current. Furthermore, future cells should be built with wider electrode chambers; such that they extend beyond the width of the cell. In place of palladium wire, foil, could then be curled to fit into the chambers.

The problem of bubbles moving along the y-axis may be the most difficult of the three to correct. By adopting the depth-profile method, however, the results may simply be less sensitive to such bubble migrations. That is; the electroosmotic gradient away from the stationary levels is not so steep, so the bubble motion back and forth would not be such a significant source of error.

If it is assumed that the bubble motions are caused in part by convective currents, then changes to the cell itself may help to minimize them. Firstly, the cell should be encased in a water jacket, so as to dissipate ohmic heating. In addition to a water jacket, it would be beneficial to add a sample outlet, possibly at the neck of the bubble inlet manifold. This addition would allow direct sampling of the temperature and conductivity of the solution.

Secondly, the conductivity of solutions should be kept low, so as to minimize the current being drawn. As a rule of thumb, the current should not exceed 20 mA. Operation was troublesome when the concentration of KCl and Na_2SO_4 were 0.002 M and 0.001 M, respectively. These concentration limits correspond to a conductivity limit of about $1.50\times10^{-2}\ \Omega^{-1}m^{-1}$. Unfortunately, this restricts the number of chemical systems for which this cell would be capable of handling.

Thirdly, the electrical current should not be left on in any one application for too long. What time period is "too long" is difficult to assess from this work, as the field was applied many times that were not recorded (chasing bubbles that turned out to be unusable). It was observed that the scatter associated with the sodium sulphate systems was somewhat less than the scatter obtained from the KCl systems. The tests performed with Na_2SO_4 were conducted after the latter, and as such, the operator was more deft at handling the controls. This may have been a factor in reducing the scatter.

The precision and accuracy of the results may have also been affected by the presence of impurities in the system. Several authors have cited the cleanliness of their cell to be of prime importance (Collins et al., 1978; Spitzer et al., 1981; Brandon et al., 1985). Options for cleaning this cell were limited, due to the nature of its construction. More specifically, the glue that held the cell together would have been eroded by the solvents. Clearly for sensitive work, the cell would have to undergo more rigorous cleaning procedures. To accommodate harsh cleaning requirements, a new cell should be constructed of fused glass, an option that was not available to us when this prototype was built. As an added bonus, the fused glass would allow the cell to be used with a wider range of solution pH (whereas the glue on this cell would be eroded by acids).

Impurities may have also entered the system as electrode reaction by-products. Although this has been determined to be unlikely in neutral and basic pH (Neihof, 1969; Pourbaix, 1974), some byproducts may have formed at locally acidic regions near the cathode. It is thus recommended that in future models, the electric field-generating electrodes should be isolated from the cell by porous glass, or any other method mentioned in the literature (Neihof, 1969).

8.4.2 METHODS OF EASING THE OPERATION OF THE CELL

Finally, there are some design alterations that would ease the operation of the system, and therefore reduce systematic errors. One of the key problems with the prototype was that it was awkward to work with. The addition of an automatic data-gathering system could record the time, electrical current, and liquid height, thus freeing the operator to concentrate on the bubble itself. A more subtle problem existed with the liquid flow control valve network. The metal tubing was set horizontally, and this caused bubbles to be entrapped in the tubes. A simple tilting of the valve network could have alleviated this difficulty.

8.5 SUMMARY

Preliminary tests were conducted on the prototype "Flow-Through" cell, using electrolyte solutions of potassium chloride and sodium sulphate. The results obtained coincided with the range of results obtained by other researchers. However, the scatter of the data was unacceptably large, indicating that there are still improvements to be made. Specifically, the performance of the electric field-generating electrodes, and the presence of horizontal drift need to be addressed. Regardless, the resulting electromobilties were not unreasonable. With some improvements, this device could indeed be a viable new method for measuring the electrophoretic mobilities of bubbles.

LITERATURE CITED

Brandon, N.P., and Kelsall, G.H. (1985a), *Growth Kinetics of Bubbles Electrogenerated at Microelectrodes*, Journal of Applied Electrochemistry, **Volume 15,** 475-484.

Brandon, N.P., Kelsall G.H., Levine, S., and Smith, A.L. (1985b), *Interfacial Electrical Properties of Electrogenerated Bubbles*, Journal of Applied Electrochemistry, **Volume 15,** 485-493.

Collins, G.L. and Jameson, G.J. (1977), *Double-Layer Effects in the Flotation of Fine Particles*, Chemical Engineering Science, **Volume 32,** 239-246.

Collins, G.L., Motarjemi, M., and Jameson, G.J. (1978), *A Method for Measuring the Charge on Small Gas Bubbles*, Journal of Colloid and Interface Science, **Volume 63 (1),** 69-75.

Dibbs, H.P., Sirois, L.L., and Bredin, R. (1974), *Some Electrical Properties of Bubbles and Their Role in the Flotation of Quartz*, Canadian Metallurgical Quarterly, **Volume 13 (2),** 395-404.

Dai, Q. (1994), Private conversation, CanMet, Devon, Alberta.

Fukui, Y. and Yuu, S. (1980), *Collection of Submicron Particles in Electro-Flotation*, Chemical Engineering Science , **Volume 35,** 1097-1105.

Fukui, Y. and Yuu, S. (1982), *Measurement of the Charge on Small Gas Bubble*, AIChE Journal, **Volume 28 (5),** 866-868.

Hiemenz, Paul C. (1986), *Principles of Colloid and Surface Chemistry, Second Edition*, Marcel Dekker Inc., New York

Hunter, Robert J. (1988), *Zeta Potential in Colloid Science: Principles and Applications*, Academic Press Limited, London, Great Britain.

Kubota, K., Hayashi, S., and Inaoka, M. (1983), A Convenient Method for Measurement of Zeta-Potentials Generated on the Bubble Suspended in Aqueous Surfactant Solutions, Journal of Colloid and Interface Science, **95 (2),** 362-369.

LITERATURE CITED (CONTINUED)

Kubota, Katsuyuki and Jameson, G.J. (1993), *A Study of the Electrophoretic Mobility of a Very Small Inert Bubble Suspended in Aqueous Inorganic Electrolyte and Cationic Surfactant Solutions*, Journal of Chemical Engineering of Japan, **Volume 26 (1)**, 7-12.

Laskowski, J.S., Yordan, J.L, and Yoon, R.H. (1989), *Electrokinetic Potential of Microbubbles Generated in Aqueous Solutions of Weak Electrolyte Type Surfactants*, Langmuir, **5**, 373-376.

Lewis, F.A. (1967), *The Palladium-Hydrogen System*, Academic Press, London.

Li, C. and Somasundaran, P. (1991*), Reversal of Bubble Charge in MultivalentInorganic Salt Solutions-Effect of Magnesium*, Journal of Colloid and Interface Science, **Volume 146 (1) October 1**, 215-218.

Li, C. and Somasundaran, P. (1992), *Reversal of Bubble Charge in Multivalent inorganic Salt Solutions-Effect of Aluminum*, Journal of Colloid and Interface Science, **Volume 148 (2), February**, 215-218.

Masliyah, J.H. (1994), *Electrokinetic Transport Phenomena*, AOSTRA Technical Publications, Edmonton.

Metcalf and Eddy (1979), *Wastewater Engineering: Treatment, Disposal, Reuse*, McGraw-Hill, Boston, 875-876.

Neihof, Rex, (1969), *Microelectrophoresis Apparatus Employing Palladium Electrodes*, Journal of Colloid and Interface Science, **Volume 30 (1), May**, 128-133.

O'Brien, R.W. and White, L.R. (1978), *Electrophoretic Mobility of a Spherical Colloidal Particle*, Journal of the Chemical Society Faraday Transactions, **II, 74**, 1607-1626.

Okada, K. and Akagu, Y., (1987*) Method and Apparatus to Measure the Zeta-Potential of Bubbles*, Journal of Chemical Engineering of Japan, **Volume 20 (1)**, 11-15.

Okada, K., Akagi, Y., and Yoshioka, N. (1988*), Effect of Zeta Potentials of Oil Droplets and Bubbles on Flotation of Oil-in-Water Mixtures*, The Canadian Journal of Chemical Engineering, **Volume 66 (4)**, 276-281.

Okada, K., Akagi, Y., Kogure, M., and Yoshioka, N., (1990*), Effect on Surface Charges of Bubbles and Fine particles on Air Flotation Processes*, The Canadian Journal of Chemical Engineering, **Volume 68 (6)**, 393-399.

LITERATURE CITED (CONTINUED)

Plambeck J.A., (1995), Private conversation, Department of Chemistry, The University of Alberta, Edmonton.

Perry, Robert H., (1973), *Perry's Chemical Engineer's Handbook, Fifth Edition*, McGraw-Hill Book Company, Toronto.

Pourbaix, Marcel, (1974) *Atlas of Electrochemical Equilibria, Second Edition*, **Section 13.3 (Palladium),** Publication of the National Association of Corrosion Engineers, Houston.

Seaman, G.V.F., (1975), *Electrokinetic Behaviour of Red Blood Cells*, The Red Blood Cell, Second Edition, **Volume 2** Surgenor, D.M. (editor), 1162-1166.

Sebba, F., (1971) *Microfoams-An Unexploited Colloid System*, Journal of Colloid and Interface Science, **Volume 35 (4), April**, 643-646.

Somasundaran, P., Chandar, P., and Chari, K., (1983), *A Study of the Interactions Between Particles and Bubbles in Surfactant Solutions*, Colloids and Surfaces, **Volume 8**, 121-136.

Spitzer, Jan J., Danielson, Laurie J., and Hepler, Loren G. (1981), *Electrophoretic Mobilities Determined by the Velocity-Depth Profile Method and Use of Hydrolyzed Potassium Chromium Sulphate Sol as a Reproducible Test Substance for Microelectrophoresis*, Colloids and Surfaces, **Volume 3**, 321-328.

Treybal, Robert E., (1980), *Mass Transfer Operations, Third Edition*, McGraw-Hill Inc., Toronto.

Usui, S. and Sasaki, H., (1978), *Zeta-Potential Measurements of Bubbles in Aqueous Surfactant Solutions*, Journal of Colloid and Interface Science, **Volume 65 (1), June 1**, 36-45.

Usui, S., Sasaki, H., and Matsukawa, H., (1981), *The Dependence of Zeta Potential on Bubble Size as Determined by the Dorn Effect*, Journal of Colloid and Interface Science, **Volume 81 (1), May**, 36-45.

Welty, J.R., Wicks, C.E., and Wilson, R.E., (1976), *Fundamentals of Momentum, Heat, and Mass Transfer, Third Edition*, John Wiley and Sons, Toronto.

LITERATURE CITED (CONTINUED)

Wiersema, P.H, Loeb, A.L, and Overbeek, J.T., (1966), *Calculation of the Electrophoretic Mobility of a Spherical Colloid Particle*, Journal of Colloid and Interface Science, **Volume 22**, 78-80.

Yoon, R.H. and Yordan, J.L., (1986), *Zeta-Potential Measurements on Microbubbles Generated Using Various Surfactants*, Journal of Colloid and Interface Science, **Volume 113 (2), October**, 430-438.

Zeta-Meter Inc. (Editors), (1980), Zeta-Meter (Zm-80) Manual, Fifth Edition, New York, 9-12, 27,45, 3-3.

APPENDIX 2-1 ELECTRICAL POTENTIAL DISTRIBUTION NEAR A FLAT, STATIONARY SURFACE

The treatise outlined in this section is adapted from similar cases described in Hunter (1981) and Masliyah (1994). We consider a flat, stationary surface, in contact with an electrolyte, as shown in Figure A-2-1.1. (Figure A-2-1.1 actually shows two parallel surfaces so as to keep the geometry consistent with subsequent sections). The electrical potential, ϕ, due to the double layer at any distance, (y), from the wall is given by:

(A-2-1.1) $$\phi = \psi(y)$$

where $\psi(y)$ is the potential due to the double layer, assuming no fluid motion and no applied electric field.

The Poisson equation defining the potential in rectangular coordinates is given by:

(A-2-1.2) $$\frac{\partial^2 \phi}{\partial w^2} + \frac{\partial^2 \phi}{\partial y^2} = -\frac{\rho^{(f)}}{\varepsilon \varepsilon_O}$$

where $\rho^{(f)}$ is the free charge density (C/ m^3),
ε is the dielectric constant of the electrolyte solution (dimensionless), and
ε_O is the permittivity in a vacuum (8.854×10^{-12} C/ V m).

As there is no fluid flow, and no external electric field, the potential is not a function of the axial (w) direction. Thus, substituting Equation A-2-1.1 into A-2-1.2, we get:

(A-2-1.3) $$\frac{d^2 \psi}{dy^2} = -\frac{\rho^{(f)}}{\varepsilon \varepsilon_O}$$

The free charge density is defined to be:

(A-2-1.4) $$\rho^{(f)} = \sum e z_k n_k$$

where e is the elementary charge (1.602×10^{-19} C),
z_k is the valence of the kth species (dimensionless), and
n_k is the ionic number concentration of the kth species (m^{-3}).

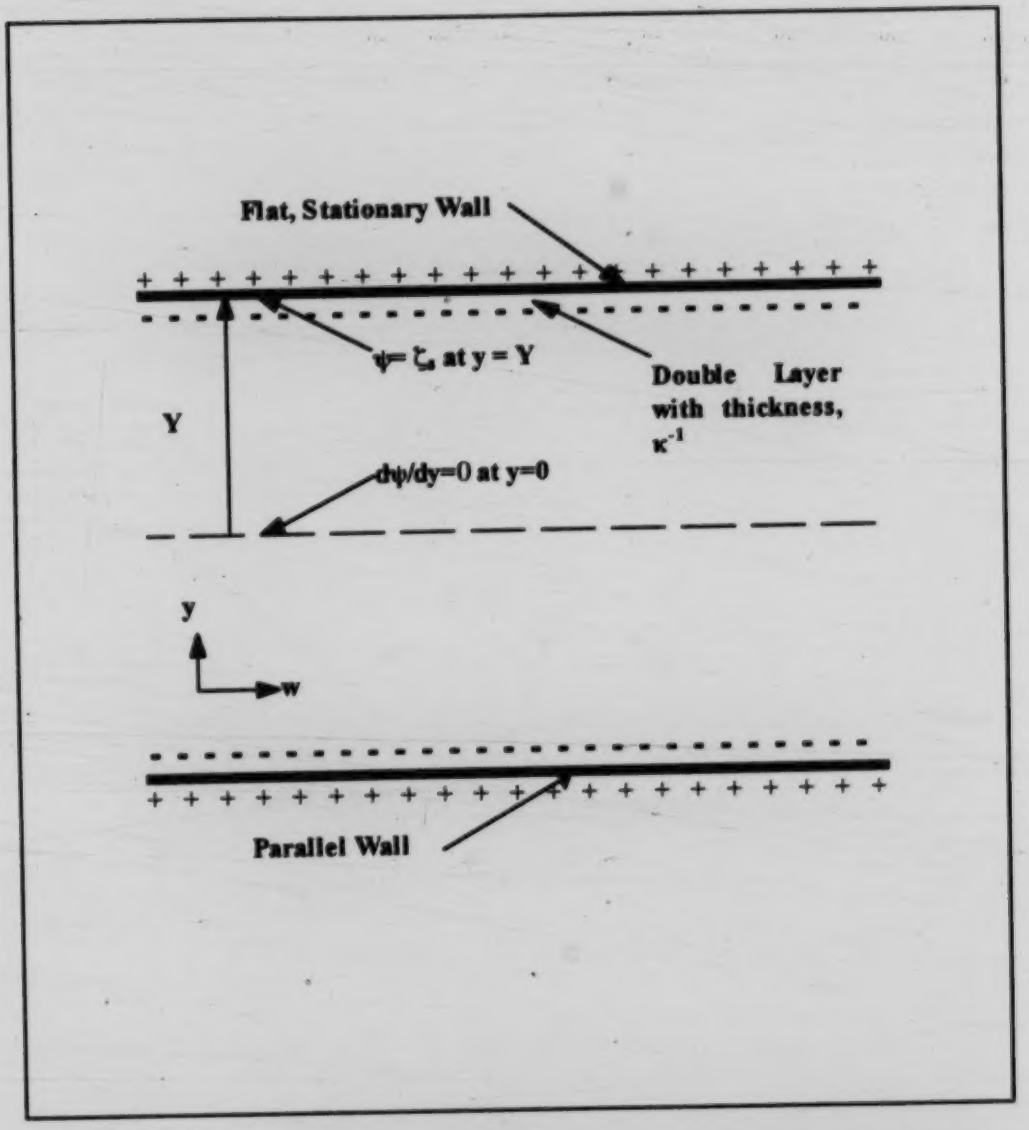

Figure A-2-1.1 **Geometry for Distribution of Electrical Potential for Two Parallel Flat Stationary Surfaces in Contact with an Electrolyte Solution**

The ionic number concentration of the k^{th} species can be approximated by the Boltzmann distribution, such that:

(A-2-1.5) $$n_k = n_\infty \exp\left[-\frac{z_k e\psi}{kT}\right]$$

where n_∞ is the ionic number concentration of all species in the bulk phase (m^{-3}),
k is the Boltzmann constant (1.381×10^{-23} J/ K), and
T is the temperature (K).

We now assume the special case of a 1:1 electrolyte. In this case, $z = z_+ = z_- = 1$, and n_∞ is the cation or anion number concentration in the neutral electrolyte. As a result, the free charge density becomes:

$$\rho^{(f)} = e(n_+ - n_-) = en_\infty\left\{\exp\left[-\frac{e\psi}{kT}\right] - \exp\left[\frac{e\psi}{kT}\right]\right\}$$

(A-2-1.6) or

$$\rho^{(f)} = -2en_\infty \sinh\left[\frac{e\psi}{kT}\right]$$

Now, if $\psi \ll 0.025$ V, then the term $e\psi/kT$ becomes very small. For $e\psi/kT \ll 1$, we can make the following approximations:

(A-2-1.7) $$\sinh\left[\frac{e\psi}{kT}\right] \approx \left[\frac{e\psi}{kT}\right]$$

and

(A-2-1.8) $$\rho^{(f)} \approx -2en_\infty\left[\frac{e\psi}{kT}\right]$$

This latter expression is referred to as the Debye-Hückel approximation.

Combining Equation A-2-1.8 with Equation A-2-1.3, we arrive at the Poisson-Boltzmann equation for a 1:1 electrolyte solution:

(A-2-1.9) $$\frac{d^2\psi}{dy^2} = \frac{2en_\infty}{\varepsilon\varepsilon_o}\left[\frac{e\psi}{kT}\right]$$

For a 1:1 electrolyte, we define the inverse Debye length, κ, to be:

(A-2-1.10) $$\kappa = \left[\frac{2n_\infty e^2}{\varepsilon\varepsilon_o kT}\right]^{\frac{1}{2}}$$

Thus, Equation A-2-1.9 simplifies to:

(A-2-1.11) $$\frac{d^2\psi}{dy^2} = \kappa^2\psi$$

for which the solution is given by:

(A-2-1.12) $$\psi(y) = C_1\cosh(\kappa y) + C_2\sinh(\kappa y)$$

where C_1 and C_2 are constants.

For the geometry shown in Figure A-2-1.1, the solution to Equation A-2-1.12, subject to the boundary conditions:

(A-2-1.13a) $$\psi = \zeta, \quad at \quad y = Y$$

and

(A-2-1.13b) $$\frac{d\psi}{dy} = 0 \quad at \quad y = 0$$

is given by:

(A-2-1.14) $$\psi(y) = \zeta, \frac{\cosh(\kappa y)}{\cosh(\kappa Y)}$$

Equation A-2-1.14, then, describes the equilibrium distribution of electrical potential in the vicinity of a flat, stationary surface. Substituting Equation A-2-1.14 into Equation A-2-1.8, we arrive at a new expression describing the free charge density:

(A-2-1.15) $$\rho^{(y)} = -\kappa^2\varepsilon\varepsilon_o\zeta_s\frac{\cosh(\kappa y)}{\cosh(\kappa Y)}$$

APPENDIX 2-2 ELECTROOSMOTIC FLOW IN A CLOSED RECTANGULAR DUCT

This analysis is similar to an analysis found in Masliyah (1994), but is derived in rectangular instead of cylindrical coordinates. We consider a closed rectangular duct, of the geometry shown in Figure A-2-2.1. The geometry is similar to that of Appendix 2-1, but now a uniform electric field is applied in the axial (w) direction. The electrical potential, ϕ, is assumed to be a sum of the potential due to the double layer, and the potential due to the electric field.

(A-2-2.1) $$\phi = \psi(y) - [\phi_o - wE_\infty]$$

where $\psi(y)$ is the potential due to the double layer assuming no fluid motion and no applied electric field (V), and
E_∞ is the uniform electric field, far from the walls of the duct, and pointed in the axial (w) direction (V/m).

As in Appendix 2-1, the Poisson equation defining the potential in rectangular coordinates is given by:

(A-2-2.2) $$\frac{\partial^2\phi}{\partial w^2} + \frac{\partial^2\phi}{\partial y^2} = -\frac{\rho^{(f)}}{\varepsilon\varepsilon_o}$$

where $\rho^{(f)}$ is the free charge density (C/ m^3),
ε is the dielectric constant of the electrolyte solution (dimensionless), and
ε_O is the permittivity in a vacuum (8.854×10^{-12} C/ V m).

Applying the second derivative of Equation A-2-2.1 with respect to the y-direction, and substituting the solution into Equation A-2-1.2, we get:

(A-2-2.3) $$\frac{d^2\psi}{dy^2} = -\frac{\rho^{(f)}}{\varepsilon\varepsilon_o}$$

This equation is identical to the expression derived in Appendix 2-1. We can apply the same assumptions and analysis as in Appendix 2-1, to arrive at the expression describing the free charge density:

(A-2-2.4) $$\rho^{(f)} = -\kappa^2\varepsilon\varepsilon_o\zeta_s\frac{\cosh(\kappa y)}{\cosh(\kappa Y)}$$

The modified Navier-Stokes equation for electroosmotic flow in the w-direction is given by:

(A-2-2.5) $$\mu\frac{d^2U_E}{dy^2} = \frac{dp}{dw} + \rho^{(f)}\frac{d\phi}{dw}$$

We define the pressure gradient as follows:

(A-2-2.6) $$-P_w = \frac{dp}{dw}$$

and, by definition, the electrical potential gradient is given by:

(A-2-2.7) $$-E_\infty = \frac{d\phi}{dw}$$

Substituting Equations A-2-2.4, A-2-2.6, and A-2-2.7 into the modified Navier-Stokes equation, we get:

(A-2-2.8) $$\mu\frac{d^2U_E}{dy^2} = -P_w + E_\infty \varepsilon\varepsilon_o\kappa^2\zeta_s\frac{\cosh(\kappa y)}{\cosh(\kappa Y)}$$

Applying the boundary conditions:

(A-2-2.9a) $$U_E = 0 \quad at \quad y = Y$$

and

(A-2-2.9b) $$\frac{dU_E}{dy} = 0 \quad at \quad y = 0$$

we arrive at the general expression for the electroosmotic velocity profile in a rectangular duct:

(A-2-2.10) $$\mu U_E = -\frac{P_w}{2}\left(y^2 - Y^2\right) - E_\infty\varepsilon\varepsilon_o\zeta_s\left[1 - \frac{\cosh(\kappa y)}{\cosh(\kappa Y)}\right]$$

To determine the axial volumetric flow, Equation A-2-2.10 is integrated across the cross-sectional area of the duct, whereby:

(A-2-2.11)
$$V = 2\int_0^Y U_E dy = \frac{(2Y)Y^2 P_w}{3\mu} - \frac{(2Y)\varepsilon\varepsilon_o\zeta_s E_\infty}{\mu}\left[1 - \frac{\sinh(\kappa Y)}{(\kappa Y)\cosh(\kappa Y)}\right]$$

For the special case of a closed duct, the net volumetric flow is zero. Thus, V=0, and:

(A-2-2.12)
$$\frac{P_w}{E_\infty} = \frac{3\varepsilon\varepsilon_o\zeta_s}{Y^2}\left[1 - \frac{\sinh(\kappa Y)}{(\kappa Y)\cosh(\kappa Y)}\right]$$

Finally, substituting Equation A-2-2.12 back into Equation A-2-2.10, we arrive at the electroosmotic velocity profile for a closed rectangular duct:

(A-2-2.13)
$$\frac{U_E}{E_\infty} = \frac{\varepsilon\varepsilon_o\zeta_s}{\mu}\left\{\frac{3}{2}\left[1 - \frac{y^2}{Y^2}\right]\left[1 - \frac{\sinh(\kappa Y)}{(\kappa Y)\cosh(\kappa Y)}\right] - \left[1 - \frac{\cosh(\kappa y)}{\cosh(\kappa Y)}\right]\right\}$$

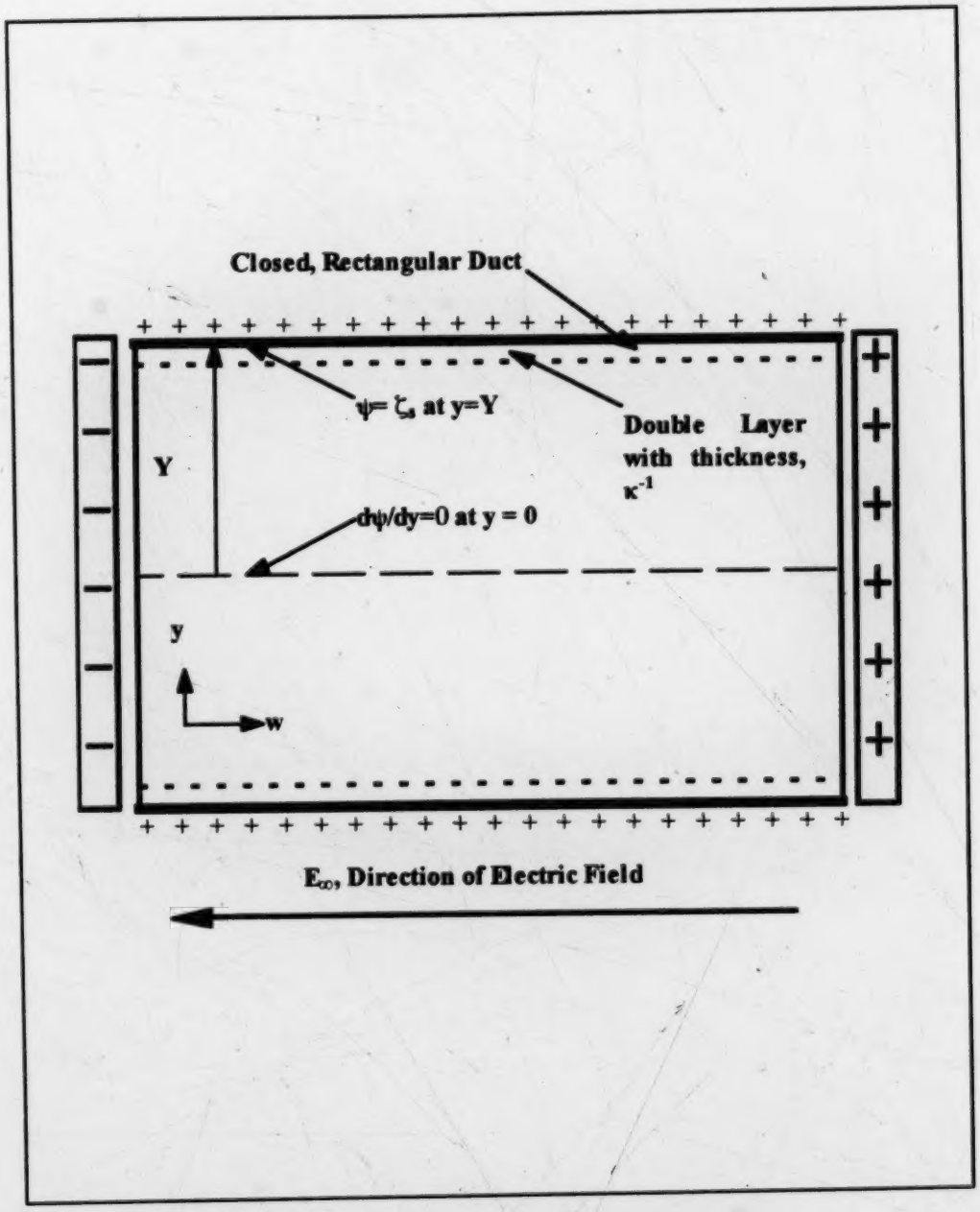

Figure A-2-2.1 Geometry of a Closed Rectangular Duct (Top View)

APPENDIX 3-1 CALCULATION OF A BUBBLE'S TERMINAL AND ELECTROPHORETIC VELOCITIES

The objective of this analysis is to estimate the range of bubbles diameters for which the (vertical) terminal velocity and (horizontal) electrokinetic velocity have comparable magnitudes. The following conditions are assumed to exist:

Table A-3-1.1 Assumed Parameters and Constants

Parameter	Symbol	Magnitude	Reference
Temperature	T	298 K	
Density of water	ρ_w	997.0 kg/m^3	Metcalf and Eddy , 1979
Viscosity of water	μ_w	0.00089 Pa s	Metcalf and Eddy , 1979
Electric permeability of water	ε	78.5	Masliyah, 1994
Dielectric Constant	ε_O	8.854 x10^{-12} C/Vm	Masliyah, 1994
Density of air bubble	ρ_G	0 kg/m^3	
Gravitational constant	g	9.81 m/s^2	Masliyah, 1994
Electric field strength	E_∞	1000 V/m	
Zeta-potential of bubble	ζ	0.025 V	
Avagadro's Number	N_A	6.022×10^{23}	
Boltzmann Constant	k	1.381×10^{-23} J/K	
pH		7	
Elementary Charge	e	1.602×10^{-19} C	
Diameter of bubble	d_B	1 to 30$\times10^{-6}$ m	

The bubble diameter, d_B, is varied from 1 to 50 μm. For each bubble diameter, the terminal velocity, U_T, is calculated by Stokes Law:

(A-3-1.1) $$U_T = \frac{d_B^2 \rho_w g}{18\mu_w}$$

(A-3-1.2) $$\mathrm{Re} = \frac{\rho_w U_T d_B}{\mu_w} \leq 1$$

Here, "Re" refers to the Reynolds number of the bubble. The electrophoretic velocity is estimated by the Helmholtz-Smulochowski Equation:

(A-3-1.3) $$U_P = \frac{\varepsilon\varepsilon_O \zeta E_\infty}{\mu_w}$$

According to this prediction, the electrophoretic velocity is independent of the bubble diameter. (A discussion on this issue is given in Chapter 8). For the Helmholtz-Smulochowski Equation to be valid, κa must be much greater than unity. The inverse Debye length, κ, is calculated as follows.

$$\kappa = \left[\frac{2n_\infty e^2}{\varepsilon\varepsilon_O kT}\right]^{\frac{1}{2}} \qquad \textbf{(A-3-1.4)}$$

For this calculation, water is considered to be a 1:1 electrolyte of H^+ and OH^- ions. The water is assigned a pH of 7, and thus the molar concentration of both ions is 1×10^{-7} M. The number concentrations are determined by using Avagadro's number, whereby Equation A-3-1.5 can be re-arranged as follows:

$$\kappa = \left[\frac{2\times 1000 N_A (C_{H^+} + C_{OH^-}) e^2}{\varepsilon\varepsilon_O kT}\right]^{\frac{1}{2}} \qquad \textbf{(A-3-1.5)}$$

where C_{H^+} is the concentration of hydronium ions (M), and
C_{OH^-} is the concentration of hydroxide ions (M).

Applying Equation A-3-1.5 to the conditions in listed in Table A-3-1.1, it is determined that $\kappa = 2.2\times10^{12}$ m^{-1}. Thus, κa is much greater than unity for the given range of bubble diameters, and the Helmholtz-Smulochowski Equation is applicable.

APPENDIX 3-2 SHRINKING SPHERE MODEL OF GAS TRANSFER FROM A BUBBLE TO ITS SURROUNDING LIQUID

A stepwise shrinking sphere model is applied to estimate the rate of gas transfer from a bubble to its surrounding liquid, and consequently to estimate the rate of change of bubble diameter, and the vertical velocity. These calculations are useful for several aspects of the bubble-producing system design. For example, the analysis can help to establish the proper position of the bubble-producing electrode below the cell. In the following equations, all subscripts noted with "G" refer to the gas bubble (hydrogen or oxygen), and all subscripts denoted by " W" refer to the surrounding medium (water).

The following conditions are assumed:

Table A-3-2.1 Assigned Parameters and Constants

Parameter	Symbol	Magnitude	Reference
Temperature	T	298 K	
Pressure	P	1 atm	
Viscosity of water	μ_w	0.00089 Pa s	Metcalf and Eddy, 1979
Surface Tension	γ_{gw}	0.0720 N/m[(1)]	Metcalf and Eddy , 1979
Density of water	ρ_W	997.0 kg/m^3	Metcalf and Eddy , 1979
Density of hydrogen	ρ_H	0.082 kg/m^3	Welty, Wicks, and Wilson, 1976
Density of oxygen	ρ_O	1.25 kg/m^3	Welty, Wicks, and Wilson, 1976
Molar mass of water	M_W	18.0 kg/kmol	Perry's, 1973
Molar mass of H_2	M_H	2.016 kg/kmol	Perry's, 1973
Molar mass of O_2	M_O	32.00 kg/kmol	Perry's, 1973
Diffusivity of H_2 in water	$\mathcal{D}_{Hw}$	5.85×10^{-9} m^2/s	Perry's, 1973
Diffusivity of O_2 in water	$\mathcal{D}_{Ow}$	0.77×10^{-9} m^2/s	Perry's, 1973
Henry's constant for H_2	He_H	7.06×10^4 atm/mol fraction	Metcalf and Eddy , 1979
Henry's constant for O_2	He_O	4.38×10^4 atm/mol fraction	Metcalf and Eddy , 1979
Gravitational constant	g	9.81 m/s^2	Masliyah, 1994
Initial diameter of bubble	$d_{B,i}$	100×10^{-6} m	

(1) Surface tension for water in contact with air at 298 K

The time is initialized to time, t, and the initial bubble diameter, $d_{B,1}$,is set to 1×10^{-4} m. Assuming a completely spherical bubble, the initial volume of the bubble is given by:

(A-3-2.1) $$V_{B,1} = \frac{4}{3}\pi\left(\frac{d_{B,1}}{2}\right)^3$$

where $V_{B,1}$ is the volume of the bubble at time, t, (m^3).

Calculations can be made for both oxygen and hydrogen bubbles. In either case, it is assumed that the bubble is made up entirely of the chosen gas. The number of moles of gas in the bubble is determined by:

(A-3-2.2) $$m_{G,1} = \frac{V_{B,1}\rho_G}{M_G}$$

where $m_{G,1}$ is the number of moles of the given gas at time, t, (kmol),
ρ_G is the density of the given gas (kg/m^3), and
M_G is the molar mass of the given gas (kg/kmol).

The mass transfer of gas from the bubble to the liquid is calculated using the relation:

(A-3-2.3) $$m' = k_L\left(C_{G,S} - C_{G,B}\right)\pi\, d_{B,1}^{\,2}$$

where m′ is the rate of mole transfer of gas from the bubble to the bulk solution (kmol/s)
k_L is the mass transfer coefficient (m/s),
$C_{G,S}$ is the molar concentration of gas at the bubble surface ($kmol/m^3$), and
$C_{G,B}$ is the molar concentration of gas in the bulk solution ($kmol/m^3$).

It is inherently assumed that the gas is being lost uniformly around the sphere. The concentration of the gas in the bulk phase is assigned some fraction of its saturation concentration at the given temperature and pressure. The saturation bulk concentration and the concentration of the gas on the bubble surface are both estimated by Henry's Law:

(A-3-2.4) $$C_{G,S} = \frac{P}{He} \times \frac{\rho_W}{M_W}$$

where He is Henry's constant for the given gas (atm/ mol fraction of gas),
ρ_W is the density of the liquid (kg/m^3)
M_W is the molar mass of water (kg/kmol), and
P is the pressure acting on gas/liquid interface (atm).

For the bulk concentration, the pressure, P, is presumed to equal the atmospheric pressure. At the bubble surface, the pressure, P_s, is assumed to be the sum of the atmospheric pressure and the Laplace pressure:

(A-3-2.5) $$P_S = P_{Atm} + \frac{4\gamma_{G/W}}{d_{B,t}} \times \frac{1}{101.32}$$

where P_s is the pressure acting on the bubble surface (atm),
P_{Atm} is the contribution of atmospheric pressure (atm), and
γ_{GW} is the surface tension at the gas-liquid interface (N/m).

The mass transfer coefficient, k_L, is estimated by empirical correlation. The following set of correlations are taken from page 144 of Mass Transfer Operations (Treybal, 1980):

(A-3-2.6) $$k_L = \frac{Sh\,\mathcal{D}_{G/W}}{d_{B,t}}$$

where Sh is the Sherwood Number (dimensionless), and
$\mathcal{D}_{GW}$ is the diffusivity of the gas in the liquid (m^2/s).

The Sherwood Number, Sh, is in turn calculated by the correlation:

$$Sh = 2 + \left(b_1 \, \mathrm{Re}^{0.779}\right)\left(Sc^{0.546}\right)\left(\frac{d_{B,1}\, g^{\frac{1}{3}}}{\left(\mathcal{D}_{G/W}\right)^{\frac{2}{3}}}\right)^{0.116} \qquad \textbf{(A-3-2.7)}$$

where b_1 is a dimensionless constant,
Re is the Reynolds Number of the bubble (dimensionless), and
Sc is the Schmidt Number (dimensionless).

The constant, b_1, is given by Treybal (1980) to be 0.061 for a single bubble, and 0.0187 for a swarm of bubbles. (In this treatise, only the case of single bubble is considered). For the Reynolds Number, Re, the terminal velocity must first be estimated by Stokes Law:

$$U_T = \frac{d_{B,1}^{\,2} g \rho_W}{18 \mu_W} \qquad \textbf{(A-3-2.8)}$$

From whence:

$$\mathrm{Re} = \frac{\rho_W U_T d_{B,1}}{\mu_W} < 1 \qquad \textbf{(A-3-2.9)}$$

For Stokes Law to be valid, Re has to be less than unity.

The Schmidt Number, Sc, is given by:

$$Sc = \frac{\mu_W}{\rho_W \mathcal{D}_{G/W}} \qquad \textbf{(A-3-2.10)}$$

Having determined the mole transfer rate from Equation A-3-2.1 and the listed correlations, the moles lost for a given time step are calculated by:

(A-3-2.11) $$\Delta m = m' \Delta t$$

From which the new bubble diameter is given by:

(A-3-2.12) $$d_{B,t+\Delta t} = \left[d_{B,t}^{\,3} - \left(\frac{6}{\pi} \frac{\Delta m \, M_G}{\rho_G} \right) \right]^{\frac{1}{3}}$$

and the increment of height traversed in this time step is given by:

(A-3-2.13) $$\Delta H_B = U_{T,t} \Delta t$$

Finally, the bubble diameter and surface gas concentration are reinitialized:

(A-3-2.14) $$d_{B,t} = d_{B,t+\Delta t}$$

and

(A-3-2.15) $$C_{GB,t} = C_{GB,t+\Delta t} - \frac{\Delta m}{V_w}$$

The volume of the liquid, V_w, is assigned the volume of the container (presumably the electophoresis cell). At any rate, the change of the bulk gas concentration is very small relative to the total concentration.

This algorithm has several important flaws that should be mentioned at this point. Firstly, the calculation fails when $C_{G,S}$ reaches zero (the bubble disappears). Secondly, both the surface concentration and the bulk concentration of gas are estimated by Henry's Law. Consequently, the bubble is predicted to shrink, even in a completely saturated liquid. Finally, for simplicity, the model assumes that the liquid contains one dissolved gas only, specifically the same gas as in the bubble. In reality, the liquid would contain a mixture of dissolved gases.

APPENDIX 5-1 ESTIMATION OF REQUIRED ELECTRIC FIELD STRENGTH

Consultation of the literature determined that electrophoretic bubble mobilities could reasonably range from 1×10^{-9} to 1×10^{-7} $m^2/V\,s$. (Kubota and Jameson, 1993; Brandon et al., 1985). It is assumed that the electrophoretic mobility was inversely proportional to the electric field strength, whereby:

(A-5-1.1) $$U_P = \frac{U_{obs}}{E_\infty} \times \frac{1}{MF}$$

where U_p is the bubble electrophoretic mobility ($m^2/V\,s$),
U_{obs} is the observed bubble electrophoretic velocity on the video screen (m/s)
MF is the magnification factor between the true velocity and the velocity observed on the monitor (dimensionless), and
E_∞ is the magnitude of the electric field (V/m).

A series of desired U_{obs} is chosen. With an assumed magnification factor of 300×, the given equation is then manipulated to isolate E_∞. Tables A-5-1.1 to A-5-1.3, below, present the results of these calculations for three values of U_{obs}. These values of U_{obs} represent travel distances of 5, 10, and 20 cm (on the video screen) over a period of 2 minutes.

Table A-5-1.1 Electric Field Required to Give $U_{obs} = 4.17\times10^{-4}$ m/s [1]

U_P ($m^2/V\,s$)	U_{obs} (m/s)	MF	E_∞ [2] (V/m)	E_∞ (V/cm)
1×10^{-9}	4.17×10^{-4}	300	1390.0	13.9
5×10^{-9}	"	"	277.8	2. 8
1×10^{-8}	"	"	138.9	1.4
5×10^{-8}	"	"	27.8	0.3
1×10^{-7}	"	"	13.9	0.1

(1) At the given velocity (U_{obs}) and magnification factor (MF), the bubble will appear to traverse 5 cm across the screen in two minutes

(2) $E_\infty = U_{obs}/(U_P \times MF)$.

Table A-5-1.2 Electric Field Required to Give $U_{obs} = 8.33\times10^{-4}$ m/s [1]

U_P (m^2/V s)	U_{obs} (m/s)	MF	E_∞ [2] (V/m)	E_∞ (V/cm)
1×10^{-9}	8.33×10^{-4}	300	2780.0	27.8
5×10^{-9}	"	"	555. 6	5. 6
1×10^{-8}	"	"	277.8	2. 8
5×10^{-8}	"	"	55.6	0. 6
1×10^{-7}	"	"	27.8	0.3

(1) At the given velocity (U_{obs}) and magnification factor (MF), the bubble will appear to traverse 10 cm across the screen in two minutes.

(2) $E_\infty = U_{obs}/(U_P \times MF)$

Table A-5-1.3 Electric Field Required to Give $U_{obs} = 1.67\times10^{-3}$ m/s [1]

U_P (m^2/V s)	U_{obs} (m/s)	MF	E_∞ (V/m)	E_∞ (V/cm)
1×10^{-9}	1.67×10^{-3}	300	5555.6	55.6
5×10^{-9}	"	"	1111.1	11.1
1×10^{-8}	"	"	555.6	5.6
5×10^{-8}	"	"	111.1	1.1
1×10^{-7}	"	"	55.6	0. 6

(1) At the given velocity (U_{obs}) and magnification factor (MF), the bubble will appear to traverse 20 cm across the screen in two minutes.

(2) $E_\infty = U_{obs}/(U_P \times MF)$